T-PM-Min1 LINKAGES OF H^+ AND Ca^{++} TO THE DIMER-TETRAMER EQUILIBRIUM OF CONCANAVALIN A. David C. Teller and Donald F. Senear. Department of Biochemistry, University of Washington, Seattle, WA. (Intr. by J. M. Schurr).

We have studied the influence of H^+, $CaCl_2$, NaCl and α-methylmannoside on the dimer-tetramer equilibrium of Concanavalin A. The equilibrium is not affected by NaCl (0-6.3m) or by saccharides which bind to the protein. The pH dependence of the association constant indicates that a histidine residue is linked to the equilibrium. The dimer-tetramer equilibrium is shifted toward dimer when calcium chloride is the added electrolyte. This is due to weak binding of the Ca^{++} by the dimeric enzyme form. In no case of these linked function relations could the binding of water be detected, in spite of the calculated release of 100-200 molecules of water in the reaction. We conclude that Tanford's [C. Tanford, J. Mol. Biol. 39, 539-544 (1969)] linkage equation does not properly express the effect of preferential hydration on protein self association equilibria. (Supported by NIH grant GM-13401).

T-PM-Min2 ACTIVE-SITE LIGAND INTERACTIONS WITH GLUTAMINE SYNTHETASE FROM *E. COLI*. A. Ginsburg, J. B. Hunt, A. Shrake, E. G. Gorman, and M. R. Maurizi, NHLBI, NIH, Bethesda, MD 20205

Glutamine synthetase from *E. coli* is a dodecamer; each subunit contains a catalytic site with 2 essential Me^{2+} sites (n_1 and n_2) and a tyrosyl residue that is the site of regulation by adenylylation. Kinetic studies of Mn^{2+} release from high-affinity n_1 sites have shown that 1 H^+/subunit binds at the fast rate of Mn^{2+} dissociation (presumably to a group within the Mn^{2+} binding cluster) and another H^+/subunit binds after Mn^{2+} release as the protein undergoes a slow conformational transition. Kinetic and equilibrium data indicate that Mn^{2+} binds to n_1 sites of the enzyme in 2 states (a low- and a high-affinity conformation); active-site ligands stabilize additional conformations of the enzyme which have decreased rates of Mn^{2+} dissociation. Calorimetric studies of the interactions of the substrate analog L-methionine-S-sulfoximine with unadenylylated and adenylylated enzymes have shown that binding enthalpies and proton effects markedly differ, indicating conformational differences between these enzyme forms. Also, L-methionine-S-sulfoximine produces different spectral perturbations on binding to unadenylylated and adenylylated enzymes. Cooperative protein interactions in glutamine synthetase are revealed by the extremely tight but reversible binding of L-met-S-sulfoximine phosphate, ADP, and 2 Mn^{2+} formed on each enzyme subunit at pH 7 by phosphorylation of the substrate analog with ATP ($K'_A > 10^{12}$ M^{-1} for ADP). Disruption of the enzyme complex depends on the protonation of 3-4 carboxylate groups per subunit and on structural perturbations produced by increasing temperature and KCl concentration. At neutral pH, the tight synergistic binding of ligands to the active site of each subunit strengthens both intra- and inter-subunit bonding domains in the dodecamer.

T-PM-Min3 SUBUNIT INTERACTIONS IN ALLOSTERIC ENZYMES. James C. Lee, Lyndal K. Hesterberg, and Robert W. Oberfelder. Dept. of Biochemistry, St. Louis Uni. Sch. of Med., St. Louis, Mo. 63104.

The role of subunit interactions in the regulation of enzyme activity for two rabbit muscle enzyme systems (pyruvate kinase, PK, and phosphofructokinase, PFK) was examined. PK exhibits allosteric properties in the presence of phenylalanine (Phe). The effects of Phe concentration, pH and temperature on the allosteric properties were examined by steady state kinetics and equilibrium ligand binding studies. Results from these studies were further analyzed by the linked-function derived by Wyman leading to a conclusion that PK can exist in an activated or an inactivated state. These results further infer that these states are characterized by significant structural changes, a conclusion substantiated by evidence provided by results from differential sedimentation velocity experiments.

Results from sedimentation and electron microscopic studies reveal that the tetrameric form of PFK is the only detectable active species under all the experimental conditions tested, thus, implying that smaller oligomeric species of PFK are inactive. The effects of ligands on the self-asso-ciation of PFK was, therefore, investigated by velocity sedimentation at pH 7.0 and 23° C. The simplest mode of association is $M \rightleftharpoons M_2 \rightleftharpoons M_4 \rightleftharpoons M_{16}$. Ligands and temperature would perturb the various equilibrium constants without altering the mode of association. The equilibrium constants determined as a function of ADP and citrate concentrations were further analyzed by the linked-function theory, leading to the conclusions that the formation of a tetramer involves the binding of two additional molecules of ADP per monomer whereas the formation of dimer involves one additional citrate molecule per PFK subunit.

T-PM-Min4 LINKED FUNCTIONS IN E. COLI ASPARTATE TRANSCARBAMYLASE. N.M. Allewell and D.S. Burz, Department of Biology, Wesleyan University, Middletown, CT 06457.

Quantitative information on linkages between ligand binding, conformational transitions and subunit association will be analyzed using linked function theory. Observations to be considered include the following: Substrate binding is ordered (1), cooperative (2), and linked to nucleotide binding (2,3). Both substrate and nucleotide binding induce conformational transitions (cf.4) and alter subunit association constants (5,6,7). Since the Hill coefficient is highly pH dependent (8), particular attention will be paid to linkages to protons. Substantial changes in proton equilibria accompany substrate analog binding, nucleotide binding to catalytic (c_3) and regulatory (r_2) subunits and subunit association. The maximal effects are between pH 7.8-9.5 for PALA and c_6r_6, at pH 7.4 for nucleotides and c_3, at pH 6.6 and 7.8 for nucleotides and r_2, and at pH 9.5 for association of c_3 with r_2. Proton uptake effects accompanying ATP binding to both subunits are approximately three times greater than those for CTP. Supported by USPHS grant AM 17335.

(1) Jacobson, G.R., and Stark, G.R., J. Biol. Chem., 249, 8003 (1973).
(2) Changeux, J.-P., Gerhart, J.C., and Schachman, H.K., Biochemistry 1, 531 (1968).
(3) Gray, C.W., Chamberlin, M.J., and Gray,D.M., J. Biol. Chem., 249, 6071 (1973).
(4) Wang, C.-M., Yang, Y.R., Hu, C.Y. and Schachman, H.K., J. Biol. Chem., 256, 7028 (1981).
(5) Chan, W. W.-C., J. Biol. Chem., 250, 660 (1975).
(6) Subramani, S., Bothwell, M.A., Gibbons, I., Yang, Y.R. and Schachman, H.K., Proc. Natl. Acad. Sci. USA, 74, 3777 (1977).
(7) Knier, B.L. and Allewell, N.M., Biochemistry, 17, 784 (1978).
(8) Pastra-Landis, S.L.,Evans, D.R. and Lipscomb, W.N., J. Biol. Chem., 253, 4624 (1978).

T-PM-Min5 DIMER - TETRAMER KINETICS FOR OXYHEMOGLOBIN A

Herbert Halvorson and William Johnston, Henry Ford Hospital, Detroit, MI., 48202

Pressure-jump relaxation experiments on dilute solutions of hemoglobin partially saturated (ca. 90%) with oxygen show a time-dependent change in deoxyhemoglobin concentration. The rate, nominally 20/sec, is a strong function of both oxygen and hemoglobin concentrations. The signal arises from elementary linkage between ligand binding and subunit dissociation: elevated pressure enhances the dissociation of oxy tetramers to oxy dimers with no optical signal; dimers bind oxygen more tightly than tetramers, hence the overall oxygen affinity has been increased; and the resulting decrease in deoxyhemoglobin concentration, which provides the optical signal, is sufficiently rapid to track the kinetics of subunit dissociation. Assuming the equivalence of α and β chains, the kinetic linkage scheme still contains 12 reactions. The relaxation spectrum is highly degenerate, with only one normal relaxation for subunit interactions. The expression for this relaxation takes a particularly simple form under conditions of ligand buffering. Analysis of data taken at pH 7.4, 0.1 M Tris-HCl, 0.1 M KCl, 1 mM EDTA, 21.5°C, and 1-10 μM heme leads to estimates of 9.3 ± 0.5/μM sec and 12.9 ± 0.5 /sec for the association and dissociation rate constants of fully liganded hemoglobin A. Increasing the pH to 8.0 decreases the relaxation rate; hence, it is the dissociation rate constant that is affected and protonation of the tetramer occurs prior to the subunit dissociation. The effect of chloride ion concentration is currently being studied. The significance of these findings to the overall linkage relations will be discussed. Supported by NIH GM 23302.

T-PM-Min6 LINKED FUNCTIONS IN MACROMOLECULES. S. J. Gill, Department of Chemistry, University of Colorado, Boulder, CO., 80309

Basic ideas describing ligand binding reactions and linked-functions will be reviewed. The reactions are of the form $M + iX + jY = MX_iY_j$, where M is the macromolecule and X and Y are the ligands. Evaluation of the equilibrium constant β_{ij} is accomplished by experimental binding curves, which measure $\bar{X}$ (moles of X bound/mole of macromolecule) versus ligand activity a_x. The binding partition function Q, $\sum_{i=0} \sum_{j=0} \beta_{ij} a_x^i a_y^j$ for tX and rY sites, is determined by the integral of the binding curve, $\bar{X}$ versus $\ln a_x$ at various a_y.

Cooperativity is expressed by derivatives of the binding curves: homotropic by $(\partial\bar{X}/\partial \ln a_x)_{ay}$ and heterotropic by $(\partial\bar{X}/\partial \ln a_y)_{ax}$. Heterotropic effects, related by thermodynamic relations known as linkage equations, show the reciprocal effects of X upon Y. Molecular insights comes from factorization of the binding partition function and the use of specific models such as the allosteric model. Ligand binding can effect the distribution of macromolecular forms (allosteric), the degree of aggregation (polysteric) and the amount of phase formation (polyphasic(1)). The precipitation of sickle-cell hemoglobin upon deoxygenation is a striking example of the last case.(Supported by HL22325)

1. Wyman, J., and Gill, S. J. (1980), Proc. Natl. Acad. Sci. USA 77,5239

T-PM-A1 IDENTIFICATION OF HIGH pH FORMS OF CYTOCHROME OXIDASE - IMPLICATIONS FOR THE NEUTRAL ENZYME. Patricia M. Callahan and Gerald T. Babcock, Department of Chemistry, Michigan State University, East Lansing, MI 48824.

Resonance Raman spectra of cytochrome oxidase at various pH values have been obtained with both Soret and visible excitation. At neutral pH, the visible excitation Raman spectrum of reduced cytochrome oxidase can be attributed entirely to cytochrome $\underline{a}^{2+}$ vibrations, in accord with the greater α-band extinction coefficient of $\underline{a}^{2+}$ compared to $\underline{a}_3{}^{2+}$. However, low spin heme $\underline{a}^{2+}$ model compounds do not reproduce all the features of the enzyme spectrum at pH 7.4. On raising the pH of reduced cytochrome oxidase to pH 9.5 the Soret and α band maxima occur at 436 and 598 nm, respectively, typical of a low spin, heme $\underline{a}^{2+}$ model. Moreover, the Raman spectrum of this species corresonds well to that of heme $\underline{a}^{2+}$ $(NMeIm)_2$ in a hydrophilic environment, thereby indicating that the pH effects are a manifestation of changes of the cyt $\underline{a}$ chromophore. With Soret excitation at pH 9.5, we observe a decrease in intensity of the 1610 cm^{-1} vibration and an increase at 1627 cm^{-1} relative to the enzyme at neutral pH. The 1627 cm^{-1} band corresponds to a hydrogen bonded carbonyl vibration of a reduced, low spin heme which implicates the carbonyl of cyt $\underline{a}$ in these pH dependent spectral changes. A new oxidase species is formed at $\sim$pH 12 which results from Schiff base formation at the heme $\underline{a}$ carbonyl. The imine linkage shifts the α band of the reduced enzyme to 575 nm and the Raman spectrum is mimicked well by the Schiff base complex of heme $\underline{a}^{2+}$ $(NMeIm)_2$. These results indicate that a pH dependent chemical linkage or special environment of the cytochrome $\underline{a}$ carbonyl is responsible for the red shift of the absorption spectrum of cytochrome oxidase relative to heme $\underline{a}^{2+}$ $(NMeIm)_2$ and for some major features of the resonance Raman spectra of the reduced, neutral enzyme. (Supported by NIH Grant GM 25480).

T-PM-A2 ON THE DETERMINATION OF ZERO FIELD SPLITTINGS FROM THE TEMPERATURE DEPENDENCE OF MAGNETIC SUSCEPTIBILITY. B.S. Gerstman and A.S. Brill, Dept. of Physics, U. of Virginia, Charlottesville, VA 22901.

The zero field splitting (ZFS) of the ground spin manifold, in a system such as the iron in heme proteins, can be described by an interaction of the form $\mathcal{H} = DS_z{}^2$ where D is the ZFS parameter. For such a system the magnetic susceptibility χ versus 1/temperature is a function which exhibits negative curvature as it passes from one constant slope limit to another. In considering the possible influence of a distribution in D upon χ, we were led to the following results.

Calculations show that D will determine, with a minimal effect arising from a distribution, the location and magnitude of the minimum in a plot of $\partial^2\chi/\partial(1/T)^2$ vs. 1/T. Furthermore, a thermal equilibrium between high and low spin states also has little effect within the temperature range of interest unless the energy difference between these spin states is <100 cm^{-1}. For a range of D from 7 to 20 cm^{-1}, the minimum in $\partial^2\chi/\partial(1/T)^2$ falls between $.012 < 1/T < .034$. To determine D to within $\pm.5$ cm^{-1} when measurements are made at increments in 1/T of .001 K^{-1}, the error in $\partial^2\chi/\partial(1/T)^2$ must be less than 5%. If $\partial^2\chi/\partial(1/T)^2$ is to be numerically determined from measurements of χ at these 1/T increments, then the measurements must have a high accuracy (better than one part in 10^4). It is possible to measure $\partial\chi/\partial(1/T)$ directly, in which case the required experimental accuracy would be 0.5%. It would be worthwhile to devise a means of measuring $\partial^2\chi/\partial(1/T)^2$ directly because this would reduce the required experimental accuracy by another order of magnitude.

T-PM-A3 STUDIES ON THE MAGNETIC ENVIRONMENT OF [1-^{13}C] OLEIC ACID BOUND TO BOVINE SERUM ALBUMIN. John S. Parks, Donald M. Small and James A. Hamilton, Biophysics Institute, Boston Univ. Sch. Med., Boston, MA 02118 and Department of Comparative Medicine, Bowman-Gray Sch. Med., Wake Forest Univ., Winston-Salem, NC 27103. (Introduced by Moseley Waite)

Mixtures of 0.5-10 moles of 90% isotopically enriched [1-^{13}C] oleic acid (FA)/mole of bovine serum albumin (BSA) were studied by ^{13}C NMR spectroscopy at 50.3 MHz. Samples were prepared by adding BSA to FA in its acid or soap form; similar results were obtained with both methods. At low FA/BSA ratios (0.5-2.0), two narrow FA resonances were detected at chemical shift (δ) values of 182.0 ppm and 180.5 ppm. At FA/BSA ratios $\geq$3, four distinct narrow resonances (183.5, 182.5, 182.0, and 180.5 ppm) were observed. The δ differences are a result of differences in the electrostatic and/or hydrogen bonding character of the FA carboxyl environments. The total integrated intensity of the FA peaks increased in proportion to the FA/BSA mole ratio; however, individual peak intensities increased differentially; most notably, at FA/BSA ratios >4, the intensity of the 182.0 ppm peak exhibited a disproportionately large increase. At any FA/BSA ratio, the δ's of the FA resonances were nearly invariant ($<.5$ ppm) from pH 5.5 to 10, which suggests that the carboxyls are protected from the bulk aqueous environment, since large carboxyl δ changes accompany bulk pH changes in aqueous fatty acid systems not containing BSA. Linewidth and spin lattice relaxation data showed that motions of the FA carboxyl group are rapid relative to tumbling of the BSA molecule. Thus, there are at least four fatty acid binding sites of BSA which (1) are magnetically distinct and in slow exchange, (2) are invariant in their magnetic environment over a wide range of pH values and FA/BSA ratios and (3) do not greatly restrict the motions of the fatty acyl carboxyl group.

T-PM-A4 DYNAMICAL DEDUCTIONS FROM THE FIELD DEPENDENCE OF PROTON NMR RELAXATION OF WATER AT THE WATER-PROTEIN INTERFACE. Robert, G. Bryant, Department of Chemistry, University of Minnesota, Minneapolis, MN 55455.

NMR relaxation has long been used to characterize molecular motions in liquids and solids. The interfacial regions pose unique problems in that one portion of the sample falls in the extreme narrowing limit while the other does not. In addition the coupling of independent spin baths provides complication in extracting a clear characterization of the molecular dynamics at the macromolecule surface. A careful analysis of the temperature dependence of proton relaxation of water on lysozyme has suggested that the motion of the water is adaquately explained by a simple model of anisotropic motion which leads to the prediction of a low frequency dispersion in the proton NMR longitudinal relaxation rate. We have examined this relaxation in several systems including protein solutions, protein crystals, and protein powders. In all cases a low frequency dispersion is found, though its origins must differ in detail in these different systems. The implications of these measurements will be discussed in terms of a dynamical model for the interfacial region that accounts for the known relaxation data.

This work is supported by the National Institutes of Health; GM-18719, GM-29428.

T-PM-A5 FLUORESCENCE AND PHOSPHORESCENCE QUENCHING OF PROTEINS AT ROOM TEMPERATURE. J.M. Vanderkooi, D.B. Calhoun and S.W. Englander, Department of Biochemistry and Biophysics, School of Medicine, University of Pennsylvania, Phila PA

Molecules which interact with the singlet and triplet excited states of tryptophan were used to examine the ability of small molecules to penetrate to tryptophan sites in alkaline phosphatase and liver alcohol dehydrogenase at room temperature. The bimolecular rate constant for oxygen quenching of fluorescence and phosphorescence and phosphorescence agreed within an order of magnitude indicating that oxygen can penetrate to the buried tryptophan responsible for phosphorescence. Organic molecules, including acrylamide, bisacrylamide, N-isopropylacrylamide, cinnanamide, acetone, methylethyl ketone, methylvinyl ketone and mesityl oxide and nitrite quench fluorescence with efficiencies approximately related to the spectral overlap between the emission and absorption spectra and independent of their size. Forster's theory indicates that quenching could occur at distances around 1 nm; therefore quenching of protein fluorescence does not indicate that these molecules have to penetrate the protein interior. For the organic molecules the molecular rate constant for fluorescence quenching in proteins was around 10^{10} l/M/sec and for phosphorescence around 10^5 l/M/Sec for alcohol dehydrogenase and less for alkaline phosphatase. We conclude that, except for oxygen, small molecules are greatly restricted in their ability to penetrate the interior of proteins. (Supported by NIH GM 12202 and AM 11295)

T-PM-A6 ANALYSIS OF CALMODULIN FLUORESCENCE SPECTRUM. C.E. Swenberg, Radiation Sciences Dept., Armed Forces Radiobiology Research Inst., Bethesda, MD 20014; H.C. Pant, Lab. of Preclinical Studies, Nat'l. Inst. Alcohol Abuse & Alcoholism, Rockville, MD 20852; S. Shapiro, F. Wang and R. Cavanagh, Nat'l Bureau of Standards, Washington, D.C.

The calcium binding protein calmodulin is present in most eukaryotic cells and is known to be involved in numerous regulatory processes which it performs through its binding with calcium. Calcium binding to this protein is known to produce conformational changes. The technique of fluorescence spectroscopy offers a means of determining these structural alterations. Calmodulin (0.4 mg/ml in 10 mM Tris-HCl, pH=7.6) emission spectra were measured with a SPEX Fluorlog spectrofluorometer. Our measurements of the calmodulin fluorescence spectra revealed two intrinsic bands: one centered at 305 nm and a broader band at 343 nm in contrast to previous fluorescent measurements which reported only the 305 nm band. The band at the shorter wavelength was more sensitive to calcium ions than the 343 nm band and increased by more than a factor of two at high Ca^{2+} concentrations. The experimental data at all Ca^{2+} ion concentrations was adequately fit with two gaussians. An analysis of the deconvoluted emission spectra at various calcium ion concentrations suggests cooperativity among the four binding sites. Excitation spectra of the two bands supports the notion that the bands originate from tyrosine residues. Preliminary measurements of fluorescence lifetime of 343 nm band was 4 nsec. Because of the correspondence in the emission spectra of calmodulin with that of serum albumin reported by Longworth (N.Y. Acad. Sci. 237-245, 1981) the data suggests that the 305 nm emission is associated with a protonated tyrosine residue whereas the 343 nm band corresponds to the deprotonated species.

T-PM-A7 ACRYLAMIDE QUENCHING STUDIES WITH AZURIN B by Roger Mallinson, Roseann Carter and Camillo A. Ghiron, Department of Biochemistry, University of Missouri, Columbia, MO 65211.

The acrylamide quenching of holoazurin B was studied as a function of emission wavelength in order to investigate discrepancies in interpretation of previous fluorescence measurements. A red-fluorescing acrylamide-quenchable component, which may be an impurity, is observed, suggesting that prior studies need to be interpreted with great caution. The presence of this component is not detectable when the 6-fold more fluorescent apo form is studied. Significant acrylamide quenching of apoazurin B is observed. The quenching constant of 5 x $10^7 M^{-1}s^{-1}$ at 20°C and the activation energy of 17 kcal/mol obtained are the most extreme values yet reported for a single tryptophan-containing protein. Since azurin B's indole is definitely known to be buried in the hydrophobic interior of the molecule, these results provide additional support for the contention that light-excited proteins undergo structural fluctuations in the nanosecond time range.

T-PM-A8 4-aminobutyrate-aminotransferase. Microenvironment of the cofactor binding site and distance of the catalytic sites. Jorge E. Churchich. Dept. of Biochemistry, Knoxville, Tenn 37916. Supported by NIH-27639-02 grant.

The analogues P-pyridoxal-aminooxyacetate and 4-vinyl-Pyridoxal-5-P inhibit reduced 4-amino-butyrate aminotransferase reconstituted with Pyridoxal-5-P, but they don't affect the catalytic activity of the holoenzyme. The binding of the P-pyridoxal adducts to the holoenzyme was monitored by measuring the fluorescence properties of the protein and the ligands. The presence of nonequivalent binding sites in reduced samples of enzyme containing 1 and 1.8 moles of P-pyridoxyl residues/dimer was detected by steady and nanosecond fluorescence spectroscopy. The spectroscopic properties (fluorescence lifetime < 1 ns, polarization = 0.36 and quantum yield = 0.01) of the first molecule of P-pyridoxyl are different from the properties of the second molecule of P-pyridoxyl covalently bound to the enzyme (τ = 2.1 ns, p = 0.16, Q_T = 0.1). The spectroscopic properties of Pyridoxal-5-P and P-pyridoxal-aminooxyacetate bound to different sites on the holoenzyme can be used to deduce proximity relationship between the catalytic sites of 4-amino-butyrate aminotransferase. On the basis of resonance energy transfer measurements, it is proposed that a distance of 27Å separates the two catalytic binding sites.

T-PM-A9 THE INFLUENCE OF THE SIGMA SUBUNIT AND DNA TEMPLATE ON THE ACCESSIBILITY OF THE RIFAMYCIN BINDING SITE ON RNA POLYMERASE. By L. S. Rice and C. F. Meares, Chemistry Department, University of California, Davis, CA 95616.

The rifamycins are a family of antibiotics which specifically inhibit bacterial RNA polymerase. Complexes of rifamycin with RNA polymerase are stable even when they include the dissociable sigma subunit of the enzyme and also when they include the DNA template. Previous work has indicated that the rifamycin site on E. coli RNA polymerase lies in a cleft between enzyme subunits, but is readily accessible to small molecules in the solvent (C.F. Meares and L.S. Rice, Biochemistry 20, 610 (1981) and references therein). We have used lanthanide energy transfer in the "rapid-diffusion limit" to probe the accessibility of rifamycin bound to the RNA polymerase core enzyme, the holoenzyme (core + sigma), and the holoenzyme-DNA complex. The electrically neutral, approximately spherical terbium (III) hydroxyethyl-ethylenediaminetriacetate complex was used as an energy donor probe of rifamycin (acceptor) accessibility. From millisecond excited-state lifetime measurements, bimolecular rate constants for energy transfer from the terbium probe to each acceptor at 20°C were: (20±6)x10^6 $M^{-1}s^{-1}$ to free rifamycin, (3±0.3)x10^6 $M^{-1}s^{-1}$ to core enzyme-rifamycin complex, (9±2)x10^6 $M^{-1}s^{-1}$ to holoenzyme-rifamycin complex, and (4±0.5)x10^6 $M^{-1}s^{-1}$ to DNA-holoenzyme-rifamycin complex. The results imply that when rifamycin binds to the holoenzyme it occupies a very accessible position; removal of the sigma subunit from the enzyme makes the rifamycin site much less accessible to other molecules in solution. This suggests that, if the rifamycin is bound in a cleft on the enzyme, the sigma subunit holds that cleft open. The accessibility of bound rifamycin is also reduced when DNA is added to the holoenzyme complex.

T-PM-A10 LOW TEMPERATURE EFFECTS ON PLASMA FIBRONECTIN STRUCTURE. J. M. Mortillaro*, D. L. Amrani#, M. W. Mosesson# and N. M. Tooney*#. Contribution from the Department of Chemistry, Polytechnic Institute of New York, Brooklyn, NY (*) and the Department of Medicine, Mt. Sinai Medical Center, Milwaukee, WI (#).

The far uv circular dichroism (CD) spectrum of human plasma fibronectin undergoes temperature dependent changes. The CD spectrum of fibronectin at 37°C shows a positive ellipticity band near 227 nm, a negative band at 212-213 nm and another positive band near 198 nm. At 5°C, the intensity of these bands is altered by as much as 20 to 40%. This evidence, together with an observed 30-40% reduction in sedimentation coefficient, suggests that fibronectin undergoes shape changes at low temperatures.

Temperature also affects the macromolecular associations of fibronectin, as assessed by CD and ultracentrifuge data. Fibronectin has been shown to form insoluble complexes with heparin and with mixtures of fibrinogen/fibrin at 5°C (Stathakis, N. E. and Mosesson, M. W. (1977) J. Clin. Invest. 60, 855 and Stathakis, N. E., Mosesson, M. W., Chen, A. B. and Galanakis, D. K. (1978) Blood 51, 1211). Our CD and ultracentrifuge experiments support the idea that heparin may bind preferentially to the low temperature form(s) of fibronectin. Electron microscope observations of fibronectin have indicated that the molecule can assume a fibrillar form with an elongated shape under certain conditions (Vuento, M., Vartio, T., Saraste, M., Von Bonsdorff, C.-H. and Vaheri, A. (1980) Eur. J. Biochem. 105, 33). The low temperature form of fibronectin described here may be an intermediate related to the fibrillar form.

T-PM-A11 THERMODYNAMIC ANALYSIS OF PROTEIN-PROTEIN INTERACTIONS IN *E. COLI* ASPARTATE TRANSCARBAMYLASE. M.P. McCarthy and N.M. Allewell, Department of Biology, Wesleyan University, Middletown, CT. 06457.

Allosteric regulation of enzymatic activity in *E. coli* aspartate transcarbamylase depends upon protein-protein interactions within the native enzyme (c_6r_6) and its catalytic (c_3) and regulatory (r_2) subunits. We have begun to use potentiometry, microcalorimetry and analytical gel chromatography to examine the energetics of these interactions as a function of pH, ionic strength, and temperature. Over the pH range 7-10.2, formation of c_6r_6 from c_3 and r_2 is linked to the binding of protons. The maximum effect is at pH 9.5, where $\Delta\nu_{H^+} \approx 4$ mol H^+/mol c_6r_6 formed (μ=0.02 M, 25°). Under similar conditions, ΔH_{assoc}, corrected for proton effects, has a minimum value of -40 kcal/mol c_6r_6 formed at pH 7 and a maximum value of -105 kcal/mol c_6r_6 formed at pH 9.5. Analysis of reaction mixtures by microzone electrophoresis and analytical gel chromatography indicates that reassociation is complete up to pH 10, but incomplete at higher pH values. Increasing the ionic strength from 0.02 M to 1 M with KCl decreases ΔH_{assoc} by approximately a factor of 3; the extent of reassociation under these conditions has not yet been determined. Over the temperature range 15-35°C, ΔH_{assoc} becomes more negative with increasing temperature; at pH 8.3 and 25°C, ΔCp has a value of approximately -2 kcal $deg^{-1} mol^{-1}$. The source of this large, negative ΔCp remains to be identified. Supported by USPHS grant AM-17335.

T-PM-A12 INHIBITION OF ELECTRON TRANSFER REACTIONS IN PHYLOGENICALLY DIVERSE SPECIES BY HOMOLOGOUS 5-n-ALKYL-6-HYDROXY-4,7-DIOXOBENZOTHIAZOLES AND 3-n-ALKYL-2-HYDROXY-1,4-NAPTHOQUINONES WHICH BIND TO THE IRON-SULFUR PROTEIN OF THE CYTOCHROME *b*-c_1 COMPLEX. C.A. Edwards, P. Graff, D. Godde, and B.L. Trumpower, Department of Biochemistry, Dartmouth Medical School, Hanover, NH 03755

Homologous alkyl-hydroxydioxobenzothiazoles containing 7, 9, 11, 13, and 15 carbon alkyl sidechains (X-HDBT, were X = 7, 9, etc) and an analogous hydroxynapthoquinone containing an 11 carbon sidechain (11-HNQ) have been compared and found to inhibit electron transfer reactions in the *b*-c_1 complexes of bovine heart and *Neurospora* mitochondria, *Paracoccus denitrificans* membranes (see Abstract by Godde *et al.*), and spinach chloroplasts. With cytochrome *c* reductase complex from heart mitochondria 13-HDBT and 15-HDBT bind stoichiometrically to the *b*-c_1 complex ($K < 1 \times 10^{-9}$ M) and the titer for inhibition is one inhibitor per complex. The efficacy of inhibition of electron transfer reactions through the *b*-c_1 complexes by the X-HDBT's increases as the length of the alkyl sidechain increases and decreases as the pH is raised above pH 6.5. The pH dependence is less with the longer sidechain X-HDBT's, and the relative ineffectiveness of the shorter sidechain homologues is not due to a mediator effect. There are species dependent differences in the relative efficacy of the analogous 11-HDBT and 11-HNQ. In addition, in chloroplasts the X-HDBT's and 11-HNQ are more potent inhibitors of electron transfer from H_2O to methyl viologen than from durohydroquinone to methyl viologen, suggesting a site of higher affinity between photosystem II and plastoquinone than that in the *b*-*f* complex. At pH's where the X-HDBT's do not inhibit cytochrome *c* reductase activities the inhibitors remain bound to the *b*-c_1 complex, but can be removed by washing with serum albumin or phospholipid plus ubiquinone. (Supported by NIH Grant GM-20379)

T-PM-A13 SUBSTRATE BINDING BEHAVIOR OF ADRENAL CYTOCHROME P-450scc. N. J. Greenfield, B. Gerolimatos. Columbia University, College of Physicians and Surgeons, 630 W. 168 St., N. Y., N. Y. 10032

Cytochrome P-450scc has been isolated from bovine adrenal cortex by the method of Seybert et al (J. Biol. Chem. 254:12088-12098 (1979)). The binding of substrates to the cytochrome has been followed using difference spectroscopy. In the absence of detergents the affinity for cholesterol (C) and cholesterol sulfate (CS) are high (Kd's = 0.1-0.2 μM). The spin state changes caused by substrate addition are approxomately 45 and 27% respectively. Addition of adrenodoxin does not change the binding constants, however the changes in spin state increase to 66 and 40% respectively. In the presence of adrenodoxin only 0.5 moles of substrate apparently bind per mole of cytochrome P-450. This suggests that the minimal functional unit of the cholesterol side-chain cleavage enzyme contains at least two moles of cytochrome P-450 with non-equivalent substrate binding sites. In the presence of the non-ionic detergent, Emulgen 913, the binding affinities for C and CS decrease dramatically and the spin state changes are altered (Kd's = 90 and 250 μM respectively; spin state changes = 38 and 100% respectively). Addition of adrenodoxin increases the binding constants (Kd's = 6 and 45 μM respectively) and the spin state changes caused by substrate addition are 80 and 100% respectively. These results indicate that data obtained in the presence of detergents may not reflect accurately the mechanism of action of the enzyme in its native state.

T-PM-B1 THE INTERACTION OF BENZENE WITH LECITHIN BILAYERS. R.V. McDaniel, S.A. Simon, T.J. McIntosh, and V. Borovyagin. Depts. of Anatomy, Anesthesiology, and Physiology, Duke University Medical Center, Durham, N.C. 27710.

The interaction of benzene with saturated lecithins has been studied by DSC, light scattering, x-ray diffraction, freeze fracture, and partition experiments. At low mole fractions ($x<0.4$) of benzene, the main transition is only slightly decreased in temperature but significantly decreased in peak area. The peak area approaches zero at $x=0.4$. The pretransition peak disappears ($x\leq0.1$). The heat capacity, C_p, in the gel phase is about 1 kcal/mol^{o}K higher than the C_p of the liquid crystalline phase (LC). Benzene is in the nonpolar region both above and below Tm. As more benzene is added to DSPC ($0.4<x\leq0.9$) a new set of thermal events appears at about 300^{o}K. The enthalpy of these events increases with increasing benzene concentration. C_p in the LC phase increases by about 1 kcal/mol^{o}K to match that of the gel phase. For both sonicated and unsonicated benzene saturated bilayers of DPPC, a broad thermal event is detectable at 300^{o}K by light scattering but not by DSC. For both DPPC and DSPC, x-ray diffraction shows that these thermal events include a gel to LC transition. Freeze-fracture shows that benzene induces striations (with periodicities of 13nm and 26nm) on the bilayer hydrophobic surfaces at 290^{o}K. Lenses of benzene are not detected between monolayers. Cross fractures and x-ray diffraction show that benzene increases the fluid space between bilayers. At concentrations near $x=0.9$, the large liposomes have been replaced by smaller (0.5-1μm) vesicles which contain one to several striated bilayers. Our results indicate that benzene interacts differently with lecithin bilayers than do other hydrocarbons such as cyclohexane, n-hexane, and naphthalene. This work was supported in part by Grants 5T32GM07046-05 and GM27278.

T-PM-B2 MODIFICATION OF INTERFACIAL DIPOLE POTENTIALS IN BILAYER MEMBRANES. W. J. Kleijn,[+] L. J. Bruner,[+] M. Mark Midland,[*] and Janet Wiesniewski[*] (Intr. by David F. Bocian), Departments of Physics[+] and of Chemistry[*], University of California, Riverside, CA 92521

Hydrophobic anions of dipicrylamine (DpA^-) have been used to probe bilayer membrane dipole potential changes induced by aqueous phase addition of amine-boranes, as previously described.[1] In this study the additive, triphenyl-[4-trimethylphenylammonium]-borate (TTB), orients in the membrane/solution interface with its charge centers aligned as illustrated:

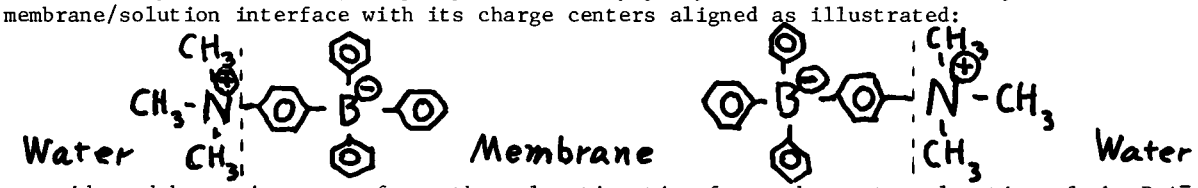

as evidenced by an increase of τ_o, the relaxation time for membrane translocation of the DpA^- probe, with increasing aqueous phase concentration of TTB. This dipole alignment is opposite to that previously reported for trialkylamine boranes,[1] and illustrates that the distribution of hydrophilic and hydrophobic groups relative to the charge centers of the amine-boranes can control the interfacial dipole orientation. Inferences relating to the adsorption isotherm for TTB will be discussed.

[1] This work was supported by NIH grant GM-27626.

[1] L. J. Bruner, et al. Biophysic. J. 33, 140a (1980).

T-PM-B3 MEMBRANES, ELECTROSTATIC POTENTIALS AND LARGE DIVALENT CATIONS. O. Alvarez, Universidad de Chile, Santiago; R. Latorre, Harvard Medical School, Boston, MA; G. Szabo and M. Brodwick, UTMB, Galveston, TX; A. Balasubramanian, S. Carnie and S. McLaughlin, SUNY, Stony Brook, N.Y.

In the classical Gouy-Chapman-Stern theory of the diffuse double layer it is assumed that the ions in the aqueous phase may be regarded as point charges. This theory describes adequately the effect of small divalent ions, such as the alkaline earth cations, on the surface and zeta potentials of bilayer membranes (J. Gen. Physiol. (1981) 77: 445-473; Biochim. Biophys. Acta (1981) 645: 279-292). Large divalent cations such as hexamethonium and decamethonium, however, exert a smaller effect on the zeta and surface potential of bilayer membranes than that predicted by the Gouy-Chapman theory. For example, when a phosphatidylserine membrane is exposed to a concentration of 0.1 M divalent cation, the Gouy-Chapman theory predicts that the zeta potential should be -31 mV; the experimental zeta potentials observed in 0.1 M decamethonium and hexamethonium are -44 and -48 mV respectively. We extended the Gouy-Chapman theory by considering the divalent cation to be either two point charges connected by a thin rigid rod or two non-interacting point charges connected by a thin flexible string. The string and the rod models predict that the zeta potentials of PS vesicles exposed to a concentration of 0.1 M divalent cation should be -42 and -45 mV respectively, in reasonable agreement with the experimental results. The rod and string models also predict that the discrepancy between the experimentally determined zeta potential and the zeta potential predicted by the Gouy-Chapman theory should decrease as the salt concentration is lowered and the Debye length increases. The experimental results agree with this prediction.

T-PM-B4 SPECIES DIFFERENCES IN BARRIER PROFILE OF THE GRAMICIDIN CHANNEL ARE REVEALED BY THE I-V SHAPES IN THE LIMIT OF LOW ION CONCENTRATION. G. Eisenman, J. Sandblom, and J. Hägglund. Dept. of Physiol., UCLA, L. A., CA 90024. (Supported by NSF (PCM 7620605) and USPHS (GM 24749)).

With two refinements (subtracting bare bilayer I's and using a spline) the I-V shape at the low ion concs. limit was measured as before (Uppsala J.Med.Sci.85:247) with the results at the right (3-D plots for Cs and Na exemplify conc. dependences). The I-V shape gives the V depend. of the entry step (F) and the ratio (R) of rate constants for leaving vs. crossing (ibid.). F and R for the theor. curves are: Li(10.8%, 0.7), Na(5.7%, 1.31), K(6.5%, 0.41), Cs(0.4%, 0.5), Tl(3.3%, 0.5), H(4.8%, 0.19), CH_3NH_3(4.6%, 2.0). The V depend. of entry decreases with size among the alkalis, Cs (0%), Li (11%). CH_3NH_3 has the most difficulty crossing relative to leaving, while H crosses easily, consistent with not having to displace a water plug. Species diff. in exit- vs. central-barriers must be considered to interpret selectivity, as well as to infer occupancy from flux-coupling. E.g. a major part of the 'selectivity filter' for Na is in the middle, while for K it is at the mouth; and for Na a flux ratio exponent of 1 is expected even for double occupancy.

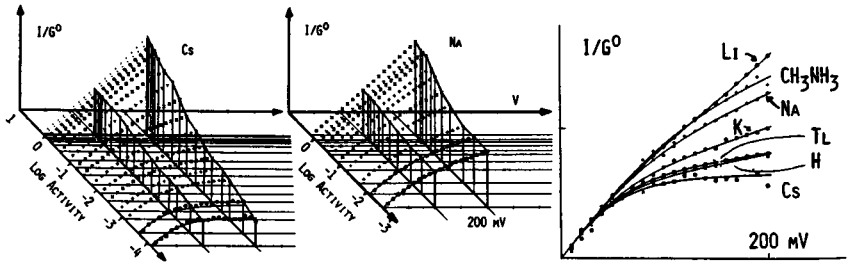

T-PM-B5 ION OCCUPANCY AND CHANNEL STABILITY IN THE GRAMICIDIN CHANNEL. D.W. McBride, Jr. and G. Szabo, (Intr. by R.B. Clark), Univ. of Texas Medical Branch, Galveston, Texas.

The stability of the dimeric gramicidin A channel is assumed to be related to the single channel lifetime. In order to test the hypothesis that the channel stability is related to ion occupancy of the channel, the conductances and lifetimes of single gramicidin channels were measured, as a function of both ion concentration (1 mM to 5 M) and voltage (10 to 250 mV). Membranes were formed from monoolein/hexadecane (50 mg/ml) in symmetrical solutions of either AgF or KF. From 1 to 300 mM the lifetime in either salt, at 10 mV, is found to increase with increasing concentration. However, above 300 mM the single channel lifetime, at 10 mV, decreases with increasing concentration. The voltage dependence of the lifetimes in these two regions is different. Increasing the voltage, increases the lifetime at high concentrations, but decreases the lifetime at lower concentrations. These trends cannot solely be attributed to surface tension, thickness or other membrane properties. Furthermore, these trends correlate with single ion occupancy of the channel predicted by a three-barrier, two-site model whose parameters are obtained by fitting the model to the conductance data of each salt. It is concluded that both zero occupancy and double occupancy destabilize the channel, while single occupancy stabilizes the dimeric channel structure.

Supported by Grant HL-24820.

T-PM-B6 RECTIFYING GRAMICIDIN A CHANNELS: ASYMMETRIC POTENTIAL ENERGY PROFILES. David Busath and Gabor Szabo, University of Texas Medical Branch, Galveston, Texas.

Gramicidin is generally considered to form symmetric channels of a single conductance state in lipid bilayers. Membrane current recordings in the presence of very small amounts of purified Gramicidin A demonstrate that gramicidin channels have a variety of conductance levels but that individual channels appear to remain in their initial state throughout their lifetime. By extending the average channel lifetime to 40-60 sec using monoolein/squalene bilayers, we have observed spontaneous changes in the conductance state of patent single channels. The state changes can be long-lived and reversible. The occurrence of state changes in single channels together with observations on the lifetime and turn-on frequency of low-conductance channels ("minis") imply that both the primary structure and the structure of the dimeric junction are the same for minis and standard channels. By using small bilayers and applying a continuous triangular voltage ramp to the membrane, we were also able to measure the I-V relation for single gramicidin channels. We find the channels of the most predominant conductance level to have symmetric I-V's as expected. Minis, however, have rectifying I-V's. We compared the I-V's of several minis to predictions of a three-barrier, two-site model. Starting with a set of parameters which adequately fit the I-V of the standard channels, we found that changing only the position and height of a single barrier and it's adjacent site adequately predicted the measured rectifying I-V's. Thus rectifying mini channels are likely to be the result of a localized asymmetric change in the channel.

Supported by NIH Grant GM-26897.

T-PM-B7 VARIATION OF ION SELECTIVITY IN THE GRAMICIDIN A CHANNEL. Gabor Szabo and David Busath, University of Texas Medical Branch, Galveston, Texas.

We have measured the current-voltage relationship for single channels formed in glyceryl-1-monoolein (50 mg)/hexadecane (1 ml) bilayers by HPLC-purified Gramicidin A, under biionic conditions. Several combinations of permeant ion pairs have been used including Na/K, Cs/Na, Cs/Li, Cs/H (.01 M), Cs/NH_4, NH_4/Na, NH_4/Li, and Ag/Na (.5 M). (Solutions were 1.0 M except where noted). Reversal potentials and limiting conductances were found to vary from channel to channel. This was neither due to electrode drift nor to variation in the concentration gradient across the membrane since channels formed in .01 M HCl/.001 M HCl did not vary in reversal potential. The range of variation of reversal potential was found to be greatest for the Cs/H (8 - 48 mV) and Cs/Li (58 - 69 mV) pairs. In other combinations, reversal potentials varied less than 6 mV from channel to channel. Previously reported data (Busath and Szabo, Nature, in press, also these abstracts) indicate that Gramicidin A forms β-helical channels with a conductance lower than that of typical channels. The measurements reported here indicate that these atypical channels also have altered ion selectivity.

Supported by NIH Grant GM-26897.

T-PM-B8 ALAMETHICIN'S STRUCTURE AFFECTS THE ASYMMETRY OF THE I-V CURVE IT INDUCES IN MEMBRANES. James E. Hall, Igor Vodyanoy, and T.M. Balasubramanian[+] (Univ. of Calif., Irvine, CA 92717 and [+] Washington University, St. Louis, MO 63110).

The major component of natural alamethicin (Fraction 4), obtained either from synthesis or purification, has the structure: Ac -Aib -Pro -Aib -Ala -Aib -Aib -Gln -Aib -Val -Aib -Gly-Leu-Aib-Pro-Val-Aib-Aib-Glu-Gln-Phol. It induces an asymmetric I-V curve in bacterial phosphatidylethanolamine (BPE) membranes. The conductance increases only when the voltage is positive in the compartment to which the alamethicin is added. We have also synthesized a derivative with the following structure: Boc-Pro-(same as fraction 4)-Glu-Gln-Phol, (Boc 2-20, for short). Boc 2-20 has a perfectly symmetric I-V curve in all symmetric membranes we have studied. In asymmetric membranes, its I-V curve shifts by the asymmetry potential regardless of whether it is added to one or to both sides or what its concentration is. Boc 2-20 is thus an ideal probe of membrane asymmetry potential. We have also synthesized the structure: + -Pro(same as fraction 4)-Glu-Gln-Phol, (BG-backgating, for short). BG induces an asymmetric I-V curve in BPE membranes, but the voltage must be negative in the compartment to which it is added to increase the conductance. Our results are consistent with alamethicin having a dipole moment pointing from the C to the N terminus. The positive end of fraction 4's dipole seems to cross the membrane in going from off to on state under the influence of a positive voltage. For BG, the negative end crosses under the influence of a negative voltage. Membranes of several compositions appear very permeable to Boc 2-20, but we cannot say at present whether the positive, negative, or either end of the molecule crosses the membrane under the influence of voltage. (Supported by HL23183 and AI16182 from NIH.)

T-PM-B9 MEMBRANE THICKNESS DEPENDENCE OF ALAMETHICIN CURRENT-VOLTAGE CURVE STEEPNESS. Igor Vodyanoy and James E. Hall. Univ. of California, Irvine, CA 92717.

The voltage-dependent conductance induced by alamethicin probably arises because of the interaction of electric field with the dipole moment of the alamethicin molecule. If molecules in the on state have dipole moment $\vec{P}on$ and those in the off state dipole moment $\vec{P}off$, the number of channels containing n molecules will vary with electric field as $\exp[n(\vec{P}on-\vec{P}off)\cdot\vec{E}/kT]$. In terms of applied voltage V, this can be written $\exp[n\Delta PV/dkT]$, where d is membrane thickness and constant field is assumed. Thus $V_e = dkT/n\Delta P$ is the voltage which will cause an e-fold change in conductance. If $n\Delta P$ is independent of membrane thickness, V_e should increase linearly with membrane thickness. We tested this prediction by measuring V_e in membranes formed from monoglycerides and squalene (Waldbillig and Szabo, 1979, BBA 597: 445). Our results are:

Chain length	14:1	16:1	18:1	20:1	22:1
Thickness (nm)	2.0	2.3	2.6	3.0	3.6
V_e (mV)	14.3	8.7	5.4	4.7	3.9

These data do not agree with the above prediction, but are consistent with the empirical formula $1/V_e = nq[d-M]/dkT = nq[1-M/d]/kT$, where q is the effective charge of the dipole (thus $\Delta P = q[d-M]$) and M is a distance independent of membrane thickness. Linear regression of $1/V_e$ vs. 1/d gives $nq = 12.5e$ and $M = 1.7$ nm with a regression coefficient of 0.994. One interpretation of our result is that the effective gating charge in the off state is at a fixed distance from the membrane surface. It moves across the membrane to the on state, which is a fixed distance from the opposite membrane surface. M is the sum of these two distances. (Supported by HL23183 from NIH.)

T-PM-B10 PRESSURE EFFECTS ON ALAMETHICIN CONDUCTANCE. L. J. Bruner[+] and James E. Hall.[*] Dept. of Physics[+], Univ. of California, Riverside, CA. 92521, and Dept. of Physiology and Biophysics[*], Univ. of California, Irvine, CA. 92717

The kinetics of alamethicin induced bilayer membrane conductance have been characterized at hydrostatic pressures ranging from ambient to 1,000 atm. The lipid used was bacterial phosphatidyl-ethanolamine bathed by unbuffered 1M KCl solutions. Membranes were formed by the Montal-Mueller method in a suitable pressure vessel. Principal observations are: (a) single channel lifetimes are lengthened with increasing pressure, (b) both the turn-on and turn-off of alamethicin conductance accompanying application of supra-threshold voltage pulses are slowed with increasing pressure, (c) the turn-on of alamethicin conductance at elevated pressure becomes distinctly signoidal, suggesting an electrically silent intermediate state of channel assembly, (d) single channel conductance is not affected by pressure, (e) the voltage threshold for onset of alamethicin conductance is not affected by pressure. Apparent activation volumes for both the formation and the decay of conducting channels are positive and of comparable magnitude, $\sim 100 \text{Å}^3$/event.

Observation (d) indicates that channel geometry and the kinetics of ion transport through open channels are not significantly modified by pressure. The remaining observations indicate that, while the relative positions of free energy minima characterizing individual conducting states are not modified by pressure, the heights of intervening potential maxima are increased.

This work was supported by NSF grant PCM-7926672 and by NIH grant HL-23183.

T-PM-B11 ELECTRICAL DETECTION BY MONAZOMYCIN OF NEUTRAL CALCIUM FLUXES THROUGH CHARGED PLANAR BILAYERS MEDIATED BY IONOPHORES A23187 AND X-537A. Mario M. Moronne and Joel A. Cohen, Laboratory of Physiology and Biophysics, University of the Pacific, San Francisco, CA 94115.

Monazomycin was used as a conductance probe to monitor shifts in the *trans* surface potential of phosphatidylserine:phosphatidylethanolamine (1:1) planar bilayers in NaCl solution. When Ca^{++} was added to the *cis* compartment in the presence of ionophore A23187 or X-537A, positive shifts of the *trans* surface potential were observed, resulting from accumulation of transported Ca^{++} at the *trans* interface, where Ca^{++} is trapped by the diffusion barrier of the aqueous unstirred layer. The steady-state concentration of Ca^{++} accumulated in the aqueous phase near the *trans* surface was determined from the observed surface-potential shift by use of separate calibration measurements, which established the dependence of the *trans* surface potential on $[Ca^{++}]$ added to the *trans* compartment. Ca^{++} flux through the *trans* unstirred layer was then calculated from the interfacial $[Ca^{++}]$, the unstirred-layer thickness, and the Ca^{++} aqueous diffusion constant. In the steady state, the ionophore-mediated transmembrane Ca^{++} flux is equal to this unstirred-layer Ca^{++} flux

Titrations of [A23187] at constant *cis* $[Ca^{++}]$, and of *cis* $[Ca^{++}]$ at constant [A23187], were performed. A plot of log (Ca^{++} flux) vs. log [A23187] yielded a slope of 2.1±0.1 at low [A23187] and showed saturation behavior at high [A23187]. With X-537A, the Ca^{++}/Mg^{++} specificity of the neutral fluxes was determined. Measurement of electroneutral fluxes of other multivalent cations is also possible with this technique, which is of particular value in the case of ions for which convenient radioisotopes do not exist. Supported by NIH (HL-16607).

T-PM-B12 INSERTION OF PROTEINS INTO PLANAR LIPID BILAYERS BY MEANS OF DETERGENT SOLUBILIZATION: COLICIN Ia ACTIVITY IN NEUTRAL LIPIDS. J. O. Bullock and F. S. Cohen* Department of Physiology, Rush Medical College, 1750 West Harrison, Chicago, Illinois.

The bacterial product colicin Ia is known to form voltage dependent channels in bilayer membranes made from monolayers of asolectin, which contains approximately 30% negatively charged lipids. While it is desirable to study the conductance of this channel in a neutral lipid, no activity is observed in membranes of the neutral lipid diphytanoyl phosphatidylcholine (DiPh-PC). We have obtained both single channel and macroscopic conductance activity in DiPh-PC membranes by prior solubilization of the protein with the negatively charged detergent Na cholate and the zwitterionic detergent octylglucoside at concentrations in the range 0.1-0.6%. The protein concentrations were approximately the same as those yielding comparable activity in asolectin. Preliminary characterization of the colicin Ia single channel behavior in asolectin revealed a heterogeneous population of channel sizes. Detergents appear to have no marked effect on this behavior; the qualitative behavior of the macroscopic conductance is also unaffected. In membranes of DiPh-PC the most prominent single conductance in 1M Na_2SO_4 is approximately 15 pS measured at potentials near 70 mV, and is independent of the identity and concentration of detergent. At approximately 5-fold higher protein concentration, some single channel activity was observed in dioleoyl-PC membranes with no detergent present. The single channel conductance was comparable to that in DiPh-PC with detergent. (Supported by USPHS Grants NS15741,NRSA T32 HL07320 and GM27367.)

T-PM-B13 DIPHTHERIA TOXIN FRAGMENT A CROSSES LIPID MEMBRANES AT ACIDIC pH. James Donovan, Melvin Simon, and Mauricio Montal. Depts. of Physics and Biology B-019, UCSD, La Jolla, CA 92093

Diphtheria toxin (DT) interacts with lipid bilayers at acidic pH but not at neutral pH, resulting in the formation of ionic channels[1]. It has not been previously shown, however, that this interaction is sufficient to transport fragment A (A) across the membrane, or if some other component, such as a membrane receptor or protease is required. We report here that A crosses lipid vesicle membranes under appropriate conditions. This was determined by measuring the appearance of the enzymic activity of A inside vesicles when DT was applied externally. A catalyzes the hydrolysis of NAD according to the reaction: NAD $\rightleftharpoons$ Nicotinamide + ADP-ribose. Vesicles containing C^{14}-NAD were exposed to DT under various conditions of pH for 15 minutes, and then incubated overnight at pH 7.8. Hydrolysis of NAD was measured by the appearance of C^{14}-Nicotinamide. NAD was hydrolyzed only when the vesicles were exposed to DT at acidic pH. Further, for A to be accessible inside the vesicle, the toxin molecule had to be both nicked and reduced, suggesting that A needs to be released inside the vesicle to be active. Hydrolysis of C^{14}-NAD occurred even in the presence of excess cold NAD in the extravesicular space, indicating that the nicotinamide did not arise from NAD which leaked out of the vesicle. The transport of A is voltage dependent, and is also affected by membrane composition.

It has been suggested that A crosses the membrane through the channel formed by the B fragment. Our results raise the possibility that this is not the case for our system, since 1) the pH profile for the appearance of A is different from that for channel formation, and 2) the NAD does not leak out of the vesicle, which would be expected if the channel were large enough to accomodate A.

This work supported by grants from the NIH and the ONR.

1) Donovan et al. Proc. Nat. Acad. Sci. (USA) 78:172-176(1981), Biophys. J. 33:139a (1981)

T-PM-B14 CHANNEL PROPERTIES OF COLICIN E1 IN LIPOSOMES. C. Kayalar, N. Düzgüneş, and G. R. Erdheim, Dept. of Chemistry, Univ. of California, Berkeley, CA 94720.

Large, unilamellar liposomes (d = 0.1 μm) were prepared containing carboxyfluorescein (CF) at a concentration where fluorescence was self-quenched (50 mM). The phopholipid composition of the membrane was 70% phosphatidylethanolamine (PE), 25% phosphatidylglycerol (PG), and 5% cardiolipin (CL). The channel formation of colicin E1 in these liposomes was followed by a fluorescence increase due to colicin-induced CF efflux and loss of self-quenching. Using this assay various kinetic parameters of colicin channel formation were measured. No positive cooperativity between colicin molecules was observed indicating that each channel was formed by a single molecule. We found that colicin E1 requires the presence of negatively charged phospholipids (phosphatidylserine, PG, CL) to spontaneously insert into membranes and form channels. Liposomes composed entirely of neutral phospholipids (phosphatidylcholine and PE) did not allow channel formation. At a constant colicin concentration the rate of CF release was strongly dependent on the percentage of negatively charged phospholipids in the membrane. We also attempted to investigate the possibility of voltage dependence in channel formation. We generated K^+ diffusion potentials by valinomycin addition to liposomes which were prepared from 70% PE and 30% PG. We monitored these potentials by ANS fluorescence. Addition of colicin E1 rapidly dissipated both negative and positive membrane potentials with rates that were indistinguishable. (Supported by a grant from Dreyfus Foundation).

T-PM-C1 OSMOTIC-SHOCK EFFECTS ON THE IMPEDANCE AND VOLTAGE-CLAMP CURRENTS OF SQUID AXON.

HR LEUCHTAG, HM FISHMAN, D POUSSART. Univ. of Texas, Galveston, Univ. Laval, Quebec.

The effects of osmotic shock on the external access paths to the axolemma were studied in squid axon by impedance and voltage-clamp measurements. The impedance $Z(j\omega)$ was determined from the response to pseudorandom current perturbations through FFT calculations. Since Z is most sensitive to the access pathways at high frequencies, measurements were made in a 100 kHz band. To suppress the effects of the Na and K systems, TTX was used in all test solutions and the axons were hyperpolarized during impedance measurements. On exposure to external hyperosmotic solutions (10% glycerol, 1 M urea, or 1 M sucrose), axons under microscopic observation showed diameter decreases of up to 30% and increases in light scattering of the outer borders, suggesting an expansion of the space between axolemma and Schwann cells. Exposure to hypoosmotic solutions (1/2 [NaCl] ASW) produced axon expansions. The hyperosmotic step-clamp data showed, probably due to an enlargement of the space, substantial reduction of the K^+ current droop and tail current and, at all but the largest depolarizations, a reversal of the direction of the tails. On return to isoosmotic solutions the tails reverted to the inward direction but increased in size. During hypoosmotic shock, the K^+ currents were reduced and tails enhanced. On return to isoosmotic solution, the K^+ currents increased and the tails reversed direction, initially. This effect was transient, lasting about 20 min. The contribution to the impedance due to access paths could not be accounted for by a series resistance, but could be fitted by a parallel RC circuit, with parameters depending on the osmotic conditions. The axolemma was modeled by an R_M in parallel with a constant-phase C_M.

Aided by Grants NS11764, NS13778 and CRC A-5274.

T-PM-C2 INTERNAL LOW IONIC STRENGTH (LIS) AND VOLTAGE DEPENDENCE OF Na AND K CHANNELS.

J. López-Barneo and C.M. Armstrong. Dept. of Physiology, Univ. of Pennsylvania, Philadelphia, Pa.

The effects of internal LIS solutions on the voltage dependent parameters of Na and K channels were examined. Na activation was measured by recording voltage-clamp currents, or, to minimize series resistance errors, by measuring dV/dt under current clamp. In the second method, the clamp was turned off after a 0.3 ms step from the holding potential, and a membrane action potential was recorded. dV/dt was measured 10-20 μs after clamp turn-off, and current calculated from the formula $INa=-C(dV/dt)$. Internal solutions contained 275 mM K + 20 mM TEA, or 10 mM K (LIS), with sucrose for isotonicity in all cases. Action potential threshold and the gNa-V curve were shifted 35-40 mV positive in LIS, and Na ON kinetics 30-35 mV positive. These effects did not change substantially after complete removal of inactivation by pronase. Steady-state Na inactivation was shifted by 35-40 mV in the same direction. Thus Na activation and inactivation are shifted in parallel by LIS.

K currents were measured using 110 mM K sea water in the external solution and 10 mM K + 200 mM TMA or 10 mM K (LIS) as internal solution. While LIS shifted the gK-V curve by only 10-20 mV toward more positive voltages closing kinetics were shifted by 40-60 mV in the same direction. ON kinetics have not been carefully measured but preliminary observations suggest they were much less affected than OFF kinetics. This strong effect of LIS on K channel closing can be explained if it is assumed that a negative charge appears at the inner surface of the membrane during activation. Lack of counterions in LIS would then destabilize the active state and thus speed channel closing.

T-PM-C3 DEPENDENCE OF RAPID MECHANICAL CHANGES IN SQUID AXON DURING PROLONGED ACTION POTENTIAL ON EXTERNAL CALCIUM CONCENTRATION

K. Iwasa and I. Tasaki, National Institute of Mental Health, Bethesda, MD 20205

Production of an action potentail in the squid giant axon is accompanied by rapid changes in the axon diameter and in the pressure inside the axon. These rapid mechanical changes are quite distinct from the slow change in the axon diameter induced by prolonged repetitive stimulation of the axon, as reported by D.K.Hill. The peak of a normal action potential coincides with the peak of swelling (pressure increase); the hyperpolarizing afterpotential is associated with shrinkage (pressure decrease) of the axon. The rapid mechanical changes associated with a prolonged action potential were examined using axons treated internally with tetraethylammonium (TEA) ion. In such axons, the swelling phase of the mechanical change was not prolonged. Instead, the second phase, a progressively increasing shrinkage of the axon was observed during the entire period of the action potential. Replacement of the external Ca-ion with Mg-ion decreased the magnitude of the shrinkage. These results obtained are explained by assuming that both the axolemma and the ectoplasm of the axon play a crucial role in producing mechanical chages.

T-PM-C4 THE EFFECT OF pH ON Ca EXTRUSION MECHANISMS IN INTERNALLY DIALYZED SQUID AXONS.
DiPolo, R. and Beaugé*; L. C.B.B., IVIC, Apartado 1827, Caracas 1010A, Venezuela. *Instituto M. y M. Ferreyra, Córdoba, Argentina.

The effect of internal and external pH, on the components of the Ca efflux, have been investigated in internally dialyzed squid axons. The internal dialysis solution had the following composition (mM): K^+, 310; Na^+, 40-50; Mg^{2+}, 4 in excess of the ATP concentration; Cl^-, 98; Aspartate, 310; EGTA, 1-2; Glycine, 310. The pH of both external and internal solutions was buffered from pH 6 to 8.8 with tris-maleate (50 mM). 1) Internal pH: A fall in intracellular pH (below 7.3) inhibited both the ATP-dependent uncoupled (Ca pump) (50% at pH_i 6.3) and the Na_o-dependent Ca efflux (forward Na/Ca exchange) (50% at pH_i 6.8) components. Internal alkalinization to pH 8.8 has no effect on the uncoupled component but markedly increased (4 fold) the Na_o-dependent Ca efflux. 2) External pH: Altering the external pH from 7.3 to 9.0 had no effect on the Na_o-dependent Ca efflux mechanism. In the absence of Ca_o^{2+}, alkalinization to pH: 8.8 causes a reduction in the magnitude of the uncoupled Ca efflux. This inhibition is markedly enhanced by the presence of Ca^{2+} ions in the external medium. As for the case of the sarcoplasmic reticulum Ca-ATPase, the combined inhibitory effect of high pH_o and Ca_o^{2+} is most probably related to a reversal of the cycle of the ATP driven Ca pump. The mark differences in the pH dependence of the components of the Ca efflux supports the model of two separate mechanism of Ca extrusion in squid axons, Ca pump and Na/Ca exchange.
(CONICIT S1-1144, Venezuela; BNS-80-25579, USA).

T-PM-C5 FORM BIREFRINGENCE AND THE BIREFRINGENCE RESPONSE OF THE SQUID AXON MEMBRANE
D. Landowne and E. Quinta-Ferreira Dept. of Physiology & Biophysics, Univ. of Miami, Miami, FL

We measured the birefringence response by placing axons between crossed polars and measuring a change in light intensity associated with a change in membrane potential. We used internally perfused voltage clamped axons. The change in intensity indicates a change in optical anisotropy which could arise from oriented molecules in or near the membrane or from a change in the form of the membrane. The membrane will have form birefringence because light polarized in the plane of the membrane will be retarded compared to light polarized perpendicular to the membrane. To distinguish between form and intrinsic birefringence we varied the index of refraction of the internal perfusion fluid by adding sucrose.

With 1.8 M sucrose (n=1.43) the response was about half the size seen with 0.3 M sucrose (n=1.36) 2.5 M sucrose (n=1.46) produced a very small inverted response. All changes were reversible and acted equally on depolarizations and hyperpolarizations. There was no dramatic alteration of time course although there was a slight slowing in high sucrose.

These results indicate a large contribution of form birefringence. Theoretical fits to the data suggest a minimum in the form birefringence curve at n=1.56. This implicates proteins rather than lipids which have n=1.48. The inversion of the response and the projected minimum imply there is also a contribution from intrinsic birefringence.

T-PM-C6 GIGANTIC CHARGE MOVEMENT IN THE SQUID GIANT AXON, J.M. Fernández, R.E. Taylor, F. Bezanilla, Dept. of Physiology, UCLA, Ca 90024; Lab. of Biophysics, NINCDS, NIH, Bethesda, MD 20205.

The charge movement induced by the lipophilic ion dipicrylamine was studied in the squid giant axon membrane under voltage clamp using the P/4 procedure, in the absence of ionic conductances, for membrane potentials between -150 mV and +100 mV. After perfusing internally and externally with solutions containing 10^{-6}M dipicrylamine, very large polarization currents could be obtained (about 2 mA/cm^2 or more), where the contributions from gating currents becomes negligible. The currents have an exponential decay in the whole potential range and the charge versus voltage curve is sigmoidal having its centerpoint at about -15 mV. The relaxation time constants follow a bell-shaped curve as a function of voltage with a maximum at about -15 mV and they range between 100 and 400 μs at 5° C. Frequency domain studies of the membrane admittance showed that the induced charge movement promotes very large changes in the membrane capacitance (about 8 μf/cm^2 or more at f=20 Hz), this capacitance is voltage and frequency dependent. The low frequency capacitance follow a bell-shaped curve as a function of voltage having its maximum at about -15 mV. In the presence of normal ionic conductances, the promotion of such large changes in the membrane capacitance do not affect the membrane resting potential. Membrane action potentials under these conditions become graded and prolonged with a much smaller maximum rate of rise. The possibility is suggested that many drugs or naturally occurring substances could act by promoting large changes in the cable parameters of a cell by modifying its membrane capacitance in a way similar to that induced by dipicrylamine. Supported by USPHS grant GM 30376 and a Grass Fellowship.

T-PM-C7 DIRECT MEASUREMENT OF ELECTROGENIC Na^+/K^+ PUMP CURRENT AND RESTING INWARD Na^+ CURRENT IN SQUID GIANT AXONS UNDER VOLTAGE CLAMP CONTROL. R.F. Rakowski and P. De Weer, Department of Physiology and Biophysics, Washington University School of Medicine, St. Louis, MO 63110.

The outward electrogenic Na^+/K^+ pump current and the inward passive Na^+ channel-mediated current have been measured in giant axons of the squid, Loligo pealei, using a low noise voltage clamp system. Measurements were made on freshly dissected axons placed in either natural or 10 mM-K^+ artificial sea water (pH = 7.4, T = 25°C). Steady-state inward Na^+ current was measured by the change in holding current produced by addition of 0.2 μM tetrodotoxin (TTX) to the bathing solution. At a resting potential of -60 mV the TTX sensitive holding current was 2.2 ± 0.3 $\mu A/cm^2$ (n = 4). The reversibility of TTX action allows repeated determinations of the steady state inward Na^+ current in the same axon at various holding potentials. The resting Na^+ conductance increased e-fold per 6.8 ± 0.5 mV change in membrane potential. The electrogenic Na^+/K^+ pump current was measured under voltage clamp conditions in axons pretreated with TTX by measuring the change in holding current produced by exposure to ouabain (100 μM) or by exposure to the reversible inhibitor dihydrodigitoxigenin (10 μM). If the pump current was blocked by either inhibitor, the addition of the second inhibitor produced no further change in holding current. This is consistent with the assumption that these two agents do not produce a change in membrane conductance. The magnitude of the Na^+/K^+ electrogenic pump current at a mean resting potential of -57.9 ± 0.6 mV was 1.55 ± 0.09 $\mu A/cm^2$ (n=22). This value is comparable to that expected from measurements of ouabain sensitive Na^+ efflux and a 3 to 2 Na^+/K^+ stoichiometry. Supported by NIH grants NS-11223, NS-14856 and the Muscular Dystrophy Association.

T-PM-C8 THE Na PUMP AND THE SPIKE OF VERTEBRATE ROD RESPONSES. K. N. Leibovic, Dept. of Biophysical Sciences, State University of New York at Buffalo, Buffalo, New York, 14214.

At high intensities, vertebrate photoreceptors exhibit a hyperpolarizing spike in response to a flash of light. It has been claimed that the spike involves voltage sensitive conductances, which are operative when a certain level of membrane hyperpolarization has been reached. If this is the case the question arises why the spike should be graded with light intensity. Moreover, the spike should be generated whenever the membrane is hyperpolarized to the appropriate threshold level. As an alternative to the postulate of voltage sensitive conductances, one may consider what contribution the Na pump could make to the response. It is known that this pump works at a high rate. Computer simulation demonstrates that the sudden reduction of membrane conductance following a light stimulus produces a spike at high intensities. We then tested this experimentally. We applied ouabain to poison the pump and in extracellular measurements in the rat retina we found that the spike was abolished, before the response amplitude was reduced. We shall present the details of the experiment and we shall also discuss our data from intracellular recordings in Bufo rods. From these it follows that the pump makes a significant contribution to the response.

T-PM-C9 THE EFFECT OF GEOMETRY ON THE EXCITATION OF NEURONS. F. A. Dodge, IBM T. J. Watson Research Center, P.O. Box 218, Yorktown Heights, NY 10598

When the geometry of a neuron and its input admittance (esp.the capacitance) are known with sufficient precision, computer modeling becomes a powerful tool for synthesizing diverse electrophysiological observations into quantitative specifications on the density and kinetics of the ionic channels in different regions of that neuron. A few (yet unproven) principles, which may facilitate new applications of this technique, have emerged from the study of particular cases. Conduction velocity is maximal when the ionic channels are uniformly distributed along an axon. Since conduction is only slightly slower for a periodic clustering, we can apply the physical laws established on the squid axon to predict the properties of mammalian nodes of Ranvier that are required to explain the observed ratio of conduction velocity to diameter. For a fixed geometry, membrane parameter values derived from the model converge to a unique set as more modes of excitation are optimally fit. A model of the spinal motor neuron is shown to be very robust; i.e., the final membrane parameter values do not depend on what initial values were assumed, and the uncertainty of the final values is no greater than the observed biological variability. We find that the membrane parameters depend strongly on the assumed geometry; but this is expected on the basis of cable theory, which tells us that the source impedance of excited cables and the electrical load of the unexcited cable vary inversely as the 3/2 power of the diameter. Partial spikes in excitable dendrites illustrate this point. A specialized site of impulse initiation requires a lower intrinsic threshold, geometrical inhomogeneity is not sufficient. Originally proposed to explain prior firing of the initial segment of the motor neuron, this point is confirmed on simplified models which show that a threshold difference is both necessary and sufficient.

T-PM-C10 A neural net model for the decay of short-term memory with human age.
P. A. Anninos and P. Argyrakis, Department of Physics, University of Crete, Iraklion, Crete-Greece.

A mathematical neural net model based on our previous studies (Anninos et al, J. Theo. Bio., 26,121 (1970), Anninos, Kybernetik, 10,165 (1972) is proposed here to show that the short-term memory of events decay with man age.
In particular, in this work we tried to explain why recent memories die out with age before the establishment of permanent memory. As it was shown, due to the loss of a large number of neurons with age, we lose some connections, and in our model this corresponds to a smaller hysterisis loop which according to our assumption represents the short-term memory of an event.
Thus we showed that if we decrease the number of connections even further the hysteresis loop will vanish to a single curve which according to Katchalsky and Oplatka (1969) corresponds to a memory-less system.

T-PM-C11 ANALYSIS OF SLOW WAVE FIELD POTENTIALS IN THE BRAINS OF SPONTANEOUSLY HYPERTENSIVE RATS. R. J. Morgan, T. N. Solie and C. C. Turbes*, Physiology and Biophysics Department, Colorado State University, Fort Collins, CO 80523 and *Anatomy Department, Creighton University School of Medicine, Omaha, NE 68178.

In studies of the Central Nervous System (CNS) control of hypertension in the rat, we found electrical activity of the Limbic System differs between normal and spontaneously hypertensive rats (SHRs). This suggests a central mechanism is "reset" to allow higher blood pressures in SHRs.

We implanted chronic electrodes in the amygdala (AMY), the pre-optic area (POA), and the arcuate nucleus (ARC) of normal and SHRs. After recovery from surgery, the CNS signals were recorded simultaneously for the first ten minutes of each half-hour, for eight hours, for four days of the normal estrous cycle. These records were analyzed using signal processing techniques drawn from communications theory. Crosscorrelogram maxima, delay times at which the maxima occurred and cross-spectral estimates were all studied for statistically significant differences between groups.

For animals studied to date (adult females) the crosscorrelogram maxima for the AMY-ARC signals from the SHRs differed by more than a standard deviation unit from the mean for normal rats, on all four days of the estrous cycle. This suggests that Limbic System electrical activity in the SHRs differs significantly from the controls.

T-PM-C12 EFFECT OF CYCLIC NUCLEOTIDES ON NERVE IMPULSE ACTIVITY AND ITS SIGNIFICANCE FOR INFORMATION PROCESSING. Michael Conrad, Department of Computer Science and Department of Biological Sciences, Wayne State University, Detroit, Michigan 48202.

E.A. Liberman, S.V. Minina, and N.E. Shklovsky-Kordy have shown that microinjection of cAMP causes depolarization in large neurons of the snail Helix lucorum. cGMP usually causes hyperpolarization or transient depolarization followed by hyperpolarization. I will report on collaborative work done with the Liberman group during a National Academy of Sciences Exchange visit to the Institute for Problems of Information Transmission in Moscow. Cyclic nucleotide mechanisms may be interpreted in a reaction-diffusion framework. It is possible to account for rhythmic activities of neurons and for differential neuronal response to different patterns of presynaptic input on the basis of cyclic nucleotide mechanisms. I will also report on the cross-correlation of the reaction-diffusion picture with formal neuron models, called enzymatic neurons, previously developed in the context of the evolutionary selection circuits model of learning. Both the reaction-diffusion interpretation of the cyclic nucleotide work and extensive computational experiments on the selection circuits model (in collaboration with R. Kampfner) suggest that single neurons may serve as analogs for effector cells which they control and that intraneuronal mechanisms are potentially more effective for adaptive pattern recognition and motor control than network processes.

T-PM-C13 X-RAY EVIDENCE FOR A COLLAGEN FIBRIL LATTICE STRUCTURE IN PERIPHERAL NERVE. H. Inouye and C.R. Worthington, Department of Biological Sciences, Carnegie-Mellon University, Pittsburgh, PA.

X-ray reflections other than those originating from the myelin sheath have been previously reported in peripheral nerve. Two orders of a 550 Å repeat was reported for frog sciatic nerve. These extra reflections were thought to arise from a two-dimensional array of filaments, the filament axes were parallel to the nerve fiber axis (S. Lalitha, B.W. Berringer and C.R. Worthington, these abstracts, 1973). In 1973 it was thought that these filaments might be microtubules. The possibility that they might be neurofilaments had not been considered at that time. However, a re-analysis of these extra reflections did not support a lattice of either neurofilaments or microtubules. A study of the electron micrographs of toad nerve (Dr. Alan Hodge, unpublished data) suggested a third possibility, namely, the collagen fibril arrays in nerve. The presence of collagen in peripheral nerve had been previously described using x-ray diffraction. New x-ray experiments were run using a camera with a long specimen-to-film distance. The low-angle x-ray diffraction data are in support of a collagen fibril lattice structure in nerve. The x-ray data provides information on the interfibrillar distance and on the diameter of the collagen fibrils. The first-order reflection varied from 440 to 550 Å for frog sciatic nerve and from 600 to 860 Å for rabbit and rat sciatic nerves depending on treatment. The "second-order" reflection was almost constant: 250 Å for frog, 320 Å for rabbit and 330 Å for rat.

T-PM-D1 EFFECT OF PHOSPHORYLATION ON THE ASSEMBLY OF AORTA MUSCLE MYOSIN. Kathleen M. Trybus, Ted W. Huiatt and Susan Lowey. Rosenstiel Center, Brandeis University, Waltham, MA 02254.

Smooth muscle myosin shows a more complex polymerization behavior (Megerman & Lowey, 1981) than does skeletal myosin (Josephs & Harrington, 1968). Since reports suggest that phosphorylation of the 20,000 dalton light chain affects the assembly of smooth muscle myosin (Suzuki et al., 1978), we have examined the equilibrium distribution and structure of filaments formed from phosphorylated or dephosphorylated aorta myosin. Filaments at 0.15 M KCl, pH 7.5 showed a 10S peak in equilibrium with two polymeric species of approximately 100S and 200S. Phosphorylation affected the relative amounts of the two polymeric species and the total amount of polymer formed, but did not change the sedimentation coefficient of the slow peak. The 10S species can be converted into 6S typical of myosin monomer by the addition of salt. Preliminary sedimentation equilibrium measurements of the 10S component suggest that a simple dimer is not an adequate model for this species. Addition of 1 mM MgATP to dephosphorylated filaments shifted the equilibrium distribution to >90% 10S component; phosphorylated filaments were also depolymerized, but to a lesser extent. Thus phosphorylation increases the amount of polymer formed, while MgATP as well as high salt and pH tend to destabilize the filament. Smooth muscle myosin can assemble into two types of filaments, bipolar and side-polar, which have different interactions between molecules within the filament (Craig & Megerman, 1977). We have shown by electron microscopy that both types of filaments are formed regardless of the state of phosphorylation, although phosphorylation appeared to favor formation of side-polar filaments. Since numerous factors affect the assembly of smooth muscle myosin, it is premature to speculate on the state of aggregation of myosin filaments in the in vivo system.

T-PM-D2 PROTEIN PHOSPHORYLATION DURING CONTRACTION OF CHICKEN SLOW AND FAST SKELETAL MUSCLES. Michael Bárány, Steven R. Hager, Kate Bárány and Fred L. Homa, Depts. of Biol. Chem. and Physiol. and Biophys., Univ. of Illinois, Medical Center, Chicago, IL 60612.

Protein phosphorylation was compared in various subfractions of chicken anterior latissimus dorsi (ALD) and posterior latissimus dorsi (PLD) muscles during tetanic stimulation. The phosphorylation was quantitated by incubating the muscles with $^{32}P_i$ and comparing the specific activities of ^{32}P-labeled proteins, isolated by one- or two-dimensional gel electrophoresis. In the case of myosin light chain, the phosphorylation was also quantitated by densitometry of the staining intensities of the phospho- and dephospho-light chains, separated by two-dimensional gel electrophoresis. Increased phosphorylation of the 19,000-dalton or the 18,000-dalton myosin light chain was invariably found upon tetanic stimulation of the slow ALD or fast PLD muscle, respectively. On the average, the [^{32}P]phosphate content of light chain was about 1.8-fold higher in contracting muscle than in the contralateral resting muscle. Similar differences were found by the densitometric technique. The extent of light chain phosphorylation was independent of the time of stimulation from 2-sec to 180-sec. In addition to myosin light chains, the phosphorylation of membrane proteins was also detected during contraction of ALD and PLD muscles. Furthermore, two proteins were phosphorylated in the sacroplasmic fraction of PLD as a result of contraction. In contrast, the [^{32}P]phosphate content of a large number of proteins remained the same during contraction as in resting ALD and PLD muscles. This work represents the first approach for simultaneous monitoring of protein phosphorylation in all subcellular fractions of contracting muscle. (Supported by NIH, CHA and MDA).

T-PM-D3 COOPERATIVITY AND THE REVERSIBLE PHOSPHORYLATION OF SMOOTH MUSCLE HEAVY MEROMYOSIN. James R. Sellers and Robert S. Adelstein, NHLBI, NIH, Bethesda, MD 20205.

Smooth muscle heavy meromyosin (HMM) prepared from turkey gizzard myosin is regulated by reversible phosphorylation of the 20,000-dalton light chains. (Sellers et al. J. Biol. Chem. 256, in press, 1981). To study the mechanism of activation, HMM was prepared at various levels of phosphorylation (from 0-2 mol P_i/mol HMM) and assayed for actin-activated MgATPase activity. A plot of % MgATPase activity vs. % phosphate incorporated is nonlinear and is consistent with a model in which both heads of an HMM molecule must be phosphorylated before the MgATPase activity of either head can be activated by actin. This agrees with the findings of Persechini and Hartshorne for myosin (Science 214, 1383, 1981). However unlike myosin, HMM shows no evidence of cooperativity during phosphorylation (i.e. the phosphorylation of one head by myosin kinase does not influence that of the second head).

When fully phosphorylated HMM is dephosphorylated by a smooth muscle phosphatase a linear relationship is obtained between % MgATPase activity and % phosphate remaining. This relationship is consistent with a number of models. To be consistent with the requirement that both heads be phosphorylated before either head is activated, the dephosphorylation data is best explained by a positive cooperative dephosphorylation of HMM. Therefore, although phosphorylation of HMM occurs in a random manner, dephosphorylation of the first head of HMM by the phosphatase may promote the dephosphorylation of the second head. (JRS was a fellow of the Muscular Dystrophy Association of America, Inc.)

T-PM-D4 SMOOTH MUSCLE PHOSPHATASES FROM TURKEY GIZZARDS. Mary D. Pato, Mary Anne Conti, and Robert S. Adelstein, NHLBI, NIH, Bethesda, MD 20205.

Two smooth muscle phosphatases (SMP-I and II) have been purified to apparent homogeneity. Both enzymes dephosphorylate the isolated 20,000-dalton smooth muscle myosin light chain (Specific Activity: SMP-I = 1.4; SMP-II = 4.1 μmol/min/mg) but not intact myosin. However, when SMP-I is dissociated by freezing and thawing in 0.2M 2-mercaptoethanol the free catalytic subunit is active against myosin. The catalytic subunit (M_r=38,000) can be separated from the other two subunits (M_r=60,000 and 55,000) by gel filtration. Characterization of the catalytic subunit reveals that it has the same pH optima (pH = 6.5) for dephosphorylation of both myosin and myosin light chains. ATP, ADP, AMP, pyrophosphate and NaF inhibit the activities of the catalytic subunit and the holoenzyme. Dephosphorylation of the myosin light chains by the holoenzyme and the catalytic subunit is inhibited by Ca^{2+} and Mg^{2+} while dephosphorylation of myosin by the catalytic subunit is not affected by these cations. In addition to SMP-I and II, we have isolated another phosphatase which preferentially dephosphorylates myosin compared to myosin light chains. This enzyme appears to be a unique phosphatase.

Dephosphorylation of myosin kinase by SMP-I was also studied. Myosin kinase is a substrate for cAMP-dependent protein kinase. In the absence of bound calmodulin two serine residues are phosphorylated resulting in a decreased affinity for calmodulin. Diphosphorylated myosin kinase is a substrate for SMP-I (S.A. = 0.7 μmol/min/mg) which restores its high affinity for calmodulin. In the presence of bound calmodulin one site on myosin kinase is preferentially dephosphorylated while in the absence of calmodulin both sites are dephosphorylated simultaneously.

T-PM-D5 EFFECT OF NUCLEOTIDE ANALOGS ON SKELETAL MUSCLE FIBERS: RELATIONSHIP OF LIGAND-INDUCED CHANGES IN RIGOR COMPLEX DENSITY TO COOPERATIVITY OF TRANSITIONS IN THE REGULATED ACTOMYOSIN ASSEMBLY. C.J. Ritz-Gold and R. Cooke, University of California, San Francisco, CA 94143

We are studying the effect of nucleotide analogs on skeletal muscle fibers using a maleimide spin probe rigidly bound to myosin heads at a specific orientation. The EPR spectrum of fibers in the rigor state indicates a largely ordered probe orientation; in this state, the heads are immobilized and form rigor complexes with actin. The spectrum of fibers in the ATP-relaxed state indicates a random probe orientation; in this state, the heads appear to be mobile and are either detached from actin or weakly attached with rapid equilibrium between attached and detached forms. We are looking at changes in probe orientation (ordered vs. random) as a function of [PPi] or [AMP-P(N)P] in the presence or absence of Ca++ (0 - 4 °C). As [PPi] is increased in the absence of Ca++, there is first a lag phase (zero or shallow slope), a steep transition phase with varying amplitude (midpoint ≃ 0.4 mM), and another shallow phase with the probe mostly random at 5 mM PPi. This suggests that cooperative interactions in the regulated actomyosin assembly are involved in the ligand-induced probe orientation changes. In all other cases, the transition phase was less steep - midpoints ≃ 0.06 mM (PPi + Ca++), ≃ 0.25 mM (AMP-P(N)P - Ca++), and ≃ 0.13 mM (AMP-P(N)P + Ca++) - suggesting diminished cooperativity in the ligand-induced probe changes. These results will be discussed in terms of a model of cooperative interactions in which state transitions of the tropomyosin-troponin complex are related to ligand-induced changes in rigor complex density. Supported by NIH HL07192 to C.J. R.-G. and by HL16683 to R.C.

T-PM-D6 BINDING OF S-1.ATP AND S-1.AMPPNP TO ACTIN. EVIDENCE FOR DIFFERENCES IN THE STRUCTURE OF THE TERNARY COMPLEXES. J.M. Chalovich, L.E. Greene and E. Eisenberg,NHLBI,NIH,Beth.,MD 20205

We have previously shown that, in the absence of Ca^{2+}, both S-1•ADP and S-1•AMPPNP bind cooperatively to the actin-troponin-tropomyosin complex (regulated actin), whereas S-1•ATP shows non-cooperative binding. This qualitative difference between the binding of S-1•ATP and S-1•AMPPNP (or S-1•ADP) to regulated actin could be due to structural differences between the S-1-nucleotide complexes; alternatively, it could simply be due to the fact that S-1•ATP binds much more weakly to actin than does S-1•AMPPNP or S-1•ADP. In the present study, we tested this latter possibility by directly comparing the binding of S-1•ATP and S-1•AMPPNP to regulated actin at ionic strengths where they bind with equal affinity: μ=0.018M for S-1•ATP and μ=0.18M for S-1•AMPPNP. We could use ionic strength to make the binding affinities equal because we first showed that changes in ionic strength have very little effect on the cooperative response of troponin-tropomyosin. We find that, at μ=0.18M, S-1•AMPPNP binds in a highly cooperative manner to regulated actin; at low levels of saturation $K=2.0\times10^{3}M^{-1}$, while at high levels of saturation $K=1.4\times10^{4}M^{-1}$. In contrast, at μ=0.018M, S-1 ATP binds non-cooperatively to regulated actin with a $K=1.3\times10^{4}M^{-1}$. Similar results are obtained with (A-1) S-1 which binds more strongly to F-actin than does S-1, thus allowing a higher saturation of the regulated actin with (A-1) S-1•ATP which, in turn, provides an even clearer demonstration that S-1•ATP does not bind cooperatively to regulated actin. We conclude that the non-cooperative binding of S-1•ATP to F-actin, in contrast to S-1•ADP and S-1•AMPPNP is due to some structural difference in the binding e.g. a difference in the angle of attachment of S-1•ATP compared to S-1•ADP and S-1•AMPPNP.

T-PM-D7 THE ROLE OF THE TROPONIN CA^{2+}-MG^{2+} SITES IN THE REGULATION OF MUSCLE CONTRACTION. Henry G. Zot and James D. Potter, Section of Contractile Proteins, Department of Pharmacology and Cell Biophysics, University of Cincinnati College of Medicine, Cincinnati, Ohio 45267.

We are currently attempting to extend other studies, in which actomyosin ATPase is reconstituted from purified components, using a model which retains some native structure, i.e., myofibrils. Extraction of myofibrils from rabbit skeletal muscle in the presence of EDTA was used to prepare myofibrils which exhibited a Ca^{2+}-independent loss in Mg^{2+}-ATPase. SDS gel electrophoresis confirmed an earlier report (Cox, J.A., et al. Biochem. J. 195, 205-211, 1981) that the primary myofibrillar component extracted with EDTA is TnC. Upon reconstitution with purified TnC, EDTA extracted myofibrils regained full activity; equal amounts of TnC added to control myofibrils had no effect. Maximal activation was restored to EDTA treated myofibrils, which retained about 30% of the original activity, with approximately 0.5 umol of TnC per g myofibrils. Since the TnC content of myofibrils has been estimated to be approximatly 0.6 umol/g myofibrils (Fuchs, F., Biochem. Biophys Acta 491, 522-531, 1977), the reconstitution appeared to be highly specific. This specificity holds for TnC and not calmodulin since as much as 2.6 umol of pure calmodulin per g myofibrils had no effect on the activation of EDTA treated myofibrils. By controlling the free Ca^{2+} and Mg^{2+} concentrations, Ca^{2+} or Mg^{2+} in the high affinity (Ca^{2+}-Mg^{2+}) sites and Ca^{2+} in the regulatory (Ca^{2+}-specific) sites were differentially controlled during the extraction process. The presence of Ca^{2+} or Mg^{2+} in the Ca^{2+}-Mg^{2+} sites was found to be sufficient to prohibit the removal of TnC, whereas Ca^{2+} in the regulatory sites was not required. Robertson et al. (Biophys. J. 34, 559-569, 1981) have shown that the in vivo Mg^{2+} concentration and Ca^{2+} transient during muscle contraction provide sufficient free metal to fill the Ca^{2+}-Mg^{2+} sites throughout the contraction cycle with either Ca^{2+} or Mg^{2+}. Since the Ca^{2+}-Mg^{2+} sites of TnC always contain either Ca^{2+} or Mg^{2+}, these results directly establish a structural role for the Ca^{2+}-Mg^{2+} sites in maintaining the integrity of the Tn complex. This work is supported by grants from the American Heart Association (78-1167) and NIH (HL 22619 3A, 3E).

T-PM-D8 EVIDENCE FOR A "SIX-STATE" KINETIC MODEL OF THE ACTOMYOSIN ATPASE. L. Stein, P.B. Chock, and E. Eisenberg, Laboratories of Cell Biology and Biochemistry, NHLBI, NIH, Beth., MD.

Recently, we showed that myosin does not have to detach from actin during each cycle of ATP hydrolysis; (Stein et al. (1981) PNAS 78, 1346). In the present study, using S-1(A1) we investigated the nature of the rate-limiting steps in the kinetic cycle. Our results show that, at 15° in very low ionic strength, K_{ATPase} determined from the double reciprocal plot of ATPase activity vs actin concentration is more than six times stronger than $K_{binding}$, determined by directly measuring the binding of S-1 to actin during steady-state ATP hydrolysis. A "four-state" kinetic model accounts for these data only if the rate-limiting step in the cycle is the acto-S-1 ATP hydrolysis step and the subsequent release of Pi is quite fast. However, this, in turn, predicts that the magnitude of the initial Pi burst should fall to very low levels as the actin concentration is increased. Using both fluorescence measurements and direct measurements of the Pi burst, we find that, when half of the S-1(A1) is bound to actin, the value of the initial Pi burst is about two-thirds the value obtained with S-1(A1) alone; and when 80% of the S-1(A1) is bound to actin, the value of the initial Pi burst is about one-half the value obtained with S-1(A1) alone. These values for the magnitude of the initial Pi burst in the presence of actin are much higher than those predicted by the "four-state" kinetic model. Therefore, a "six-state" kinetic model appears to be necessary to explain the actomyosin ATPase. In the "six-state" model proposed by Stein et al. the rate-limiting step (transition from the refractory to the non-refractory state) follows the ATP hydrolysis step, but preceeds the rapid release of Pi. This rate-limiting step may play a key role in determining the velocity of muscle contraction.

T-PM-D9 EVIDENCE FOR DIFFERENCES BETWEEN SUBFRAGMENT-1 ISOZYMES OF FAST-MUSCLE MYOSIN. K. George and P. Dreizen. Biophysics Program and Department of Medicine, State University of New York Downstate Medical Center, Brooklyn, New York 11203.

The role of light chains in the enzymatic properties of the subfragment-1 isozymes, S1(L1) and S1(L3), as isolated from rabbit fast-muscle myosin, has been ambiguous. At 25°C, actin activated ATPase and Ca-ATPase are both greater for S1(L3) than for S1(L1) at low ionic strength, but similar for the two isozymes at higher ionic strength. Reisler and associates (1981) have reported that S1(L1) denatures faster than S1(L3), based on turbidity measurements at temperatures above 34°C, raising the possibility that differences between the isozymes reflect selective denaturation. We confirm differences in heat-induced aggregation of the S1 isozymes; however, under the same conditions, rates of heat denaturation of Ca-ATPase and K/EDTA-ATPase are identical for the two isozymes, indicating that differences in ATPase between them cannot be attributed to selective denaturation. Further studies are reported elaborating the differences in ATPase between S1(L1) and S1(L3). (1) Arrhenius plots for K/EDTA-ATPase and Ca-ATPase are non-linear for both isozymes; specific activities for the isozymes are similar below 10°C, but diverge at higher temperature, indicating differences in thermal sensitivity of critical rate constants for the two isozymes. (2) Evidence is adduced from several sources showing that S1(L1) and S1(L3) exhibit differences in their interactions with Ca^{++} and Mg^{++}. (3) Fractions from the chromatographic peaks for S1(L1) and S1(L3) do not exhibit microheterogeneity in specific activity or subunit composition, so that the observed differences in ATPase cannot be attributed to a minor variant within either isozyme fraction. Supported by research grants from the US Public Health Service and the N.Y. Heart Association.

T-PM-D10 SH_1-SH_2 CROSS-LINKED MYOSIN SUBFRAGMENT-ONE (S-1): AN "ANALOG" OF S-1•ATP. L.E. Greene, J. Chalovich and E. Eisenberg, NHLBI, NIH, Beth., MD 20205.

The bifunctional thiol cross-linking reagent, N,N'-p-phenylenedimaleimide (pPDM) has been used by Wells and Yount (PNAS 76, 4966 (1979)) to trap MgADP at the active site of S-1 by cross-linking the SH_1 and SH_2 thiol groups. Based on the fluorescence of the pPDM-S-1, they have suggested that it is similar in conformation to the M•ADP state, but unlike M•ADP, they also found that ppDM-S-1 binds weakly at 0.1M KCl. In this study we examined the binding of pPDM-S-1 to actin both in the presence and absence of troponin-tropomyosin to determine whether it resembles M•ADP or M•ATP in its ability to bind to actin. The binding was measured by labeling S-1 with (^{14}C)-pPDM and then separating the free from the bound S-1 by centrifugation in an air driven centrifuge. We first found that ppDM-S-1 binds to actin about 1000-fold weaker than does S-1•ADP and 100-fold weaker than does S-1•AMPPNP. On the other hand, the binding of pPDM-S-1 to actin is only two-fold stronger than the binding of S-1•ATP or S-1•ADP•Pi when measured over a range of ionic strengths from 0.012M to 0.05M. Second, we find that in the presence of the troponin-tropomyosin complex, there is no inhibition of the binding of pPDM-S-1 to actin, although the troponin-tropomyosin complex causes marked inhibition of the binding of S-1, S-1•ADP and S-1•AMPPNP to actin. On the other hand, the troponin-tropomyosin complex does not inhibit the binding of S-1•ATP or S-1•ADP•Pi to actin. Therefore, cross-linking the SH_1 and SH_2 groups of S-1 in the presence of MgADP appears to induce a conformation which mimics the conformational change induced by the binding of ATP.

T-PM-D11 USE OF PHASE-MODULATION FLUORESCENCE LIFETIME ANALYSES TO DETERMINE SPATIAL RELATIONSHIPS IN MYOSIN SUBFRAGMENT ONE (SF1) BY ENERGY TRANSFER. J. Weiel, W. J. Perkins and R. G. Yount. Biochemistry/Biophysics Program and Dept. of Chem., Washington State Univ., Pullman, WA 99164.

Phase-modulation fluorescence spectroscopy using an SLM 4800 spectrofluorometer has been used to determine the fluorescence lifetimes of energy donors associated with myosin SF1 in the presence/absence of energy acceptors. Since donor/acceptor combinations usually result in a binary system with respect to donor lifetimes, several different mathematical treatments have been devised to solve for the two lifetimes present. All routines stem from considerations of phase-modulation theory of heterogeneous systems [G. Weber (1981) J. Phys. Chem. 85, 949-953]. The most successful routines use a "Monte Carlo best fit" in which the data from all three modulation frequencies are simultaneously utilized. This approach has been applied to measuring lifetimes of 1,5-AEDANS attached to the SF1 reactive thiol, SH1, in the presence of two acceptor ATP analogs: 2'(3')-O-(2,4,6-trinitrophenyl)ATP (TNP-ATP) and N(4-azido,2-nitroanilino)ethyl triphosphate (NANTP). In each case, the data are consistent with the presence of two lifetimes, about 20.6 ns for unquenched AEDANS-SF1 and 4.1 ns and 6.5 ns in the presence of TNP-ATP and NANTP, respectively. With TNP-ATP, this corresponds to an active site to SH1 distance of 32 Å at 5°C (R_0 = 40.3 Å). At 25°C, a longer lifetime (5.9 ns) indicates a distance of 35 Å. The results with NANTP indicate an active site to SH1 distance of 29 Å at both 5° and 25°C (R_0 = 32.8 Å). Thus, SH1 is too far away from the active site to be involved in either the binding or the cleavage of ATP by myosin, confirming the earlier epr studies of Bagshaw and Reed (J.B.C., 1976, 251, 1975-1983) and the recent single photon counting energy transfer results of Tao and Lamkin (Biochem., 1981, 20, 5051-5055).

T-PM-D12 INTERNAL FLEXIBILITY OF F-ACTIN: ANGULAR ROTATIONS AND AXIAL DISPLACEMENTS IN TWO F-ACTIN AGGREGATES. E.H. Egelman, D.J. DeRosier, N. Francis, Brandeis University, Waltham, MA.

We have been studying the structure of actin aggregates to shed light on how a single, highly conserved protein, actin, can bind with itself and at least 20 other proteins to produce a variety of different observed forms (i.e. filaments, bundles, sheets, etc.). Since the structure of the actin filament will determine how actin binds sterically and stoichiometrically with other proteins in many of these aggregates, we have examined the helical geometry of isolated F-actin. Image analysis of these filaments shows that a substantial angular disorder of subunit positions exists. The disorder takes the form of coupled, cumulative motions of subunits along the azimuthal orientation, while at the same time the axial rise per subunit in free filaments appears to be fairly constant. When actin filaments are assembled (in the absence of other proteins) into higher-order aggregates, deviations of the component filaments from helical symmetry can also be seen. Mg^{++} angle-layered aggregates can be described as sheets with two different classes of surfaces: those on the inside surface, where the actin subunit positions are ordered, and those surfaces on the outside, where subunits display a similar angular disorder to that found in free filaments. Mg^{++} paracrystals, formed at slightly higher Mg^{++} concentrations, can contain significant axial shifts of subunits in every filament, which appear as "forbidden" meridional reflection on the 6th layer line of the transforms. These shifts are imposed by interactions between neighboring filaments. We suggest that azimuthal and axial deviations of subunits in Mg^{++} paracrystals allow a greater number of interfilament bonds to be made than pure helical symmetry of filaments would allow.
(Supported by NIH grant #GM 21189 to D.J.D.)

T-PM-D13 THREE-DIMENSIONAL RECONSTRUCTION OF SCALLOP THICK FILAMENTS. Peter Vibert and Roger Craig, Rosenstiel Basic Medical Sciences Research Center, Brandeis University, Waltham, MA 02254.

Thick filaments isolated from the striated muscles of several scallop species retain key features of their native structure in negative stain (Castellani et al., this volume). Preliminary three-dimensional reconstruction from images of filaments from sea scallop (Placopecten magellanicus) reveals the myosin crossbridge array at a resolution of about 70 Å. The number of bridges at each level is 7, one of the possibilities indicated by earlier X-ray diffraction analysis (Wray et al., Nature 254, 561 (1975); Millman & Bennett, J. Mol. Biol. 103, 439 (1976)). The bridges appear as elongated units (probably representing unresolved pairs of heads) with most of their mass concentrated at one end, and run almost parallel to the filament axis. The filaments display an unusual pairing interaction between alternate levels of bridges, generating a 2x145 Å = 290 Å axial repeat that is most prominent near the bare-zone. The specialized design of this thick filament may be related to its highly sensitive regulatory response to Ca^{++} (Chantler et al., Biochemistry 20, 210 (1981)).

Supported by grants (to C. Cohen) from NIH, NSF and MDA. Peter Vibert is an Established Investigator of the American Heart Association.

T-PM-D14 STRUCTURE OF TROPONIN AND ITS INTERACTION WITH TROPOMYOSIN. Paula F. Flicker, George N. Phillips, Jr. and Carolyn Cohen, Graduate Program in Biophysics and Rosenstiel Center, Brandeis University, Waltham, MA 02254.

Some new features of the troponin complex have been revealed by electron microscopy of rotary shadowed molecules. Our results demonstrate that the troponin complex has both a globular and rod-like domain. The length of the entire complex is about 265±40Å and the tail about 165±25Å. Isolated troponin T has a shape and dimensions that correspond closely to those of the tail. These findings indicate that troponin I and C comprise most of the globular region of troponin. (The rather large dimensions observed for this part of the complex (about 100Å) suggest that it may be somewhat flattened.) When troponin is added to tropomyosin, the globular domain can be seen bound about 130A from one end of the tropomyosin molecules, but the direction of the troponin T tail cannot yet be distinguished. Often troponin can be seen periodically bound to end-to-end polymers of tropomyosin, and may indeed bind preferentially to such aggregates. In some cases two troponin complexes appear to bind directly across from each other on the same tropomyosin molecule. This finding supports the model for tropomyosin with two chains in register. The shape of the troponin complex--in particular the highly extended nature of troponin T--suggests that troponin may interact with tropomyosin over a considerable portion of its length. This picture of the regulatory complex may account for the variety of binding sites proposed for troponin on tropomyosin and clarifies also certain aspects of the motions of tropomyosin on actin.

Supported by grants from NIH, NSF and MDA. G.N.P. is a Medical Foundation Fellow.

T-PM-E1 DIFFERENTIAL SUPPRESSION OF FIBROBLASTS AND THE GROWTH OF EPITHELIOID CELLS FROM A SUSPENSION OF SINGLE RAT VENTRAL PROSTATE CELLS., M. Rubenstein, K.M. Anderson, Oncology Lab., Dept. of Medicine, Dept. of Biochemistry, Rush-Pres.-St. Luke's Med. Ctr., Chicago, Ill. 60637

Many efforts to culture epithelial cells are thwarted by an overgrowth of accompanying fibroblasts. We collagenase-digested ventral prostate from Sprague-Dawley rats and separated fibroblasts (band 2) and epithelial cell (band 4)-enriched fractions by centrifugation on isokinetic ficoll gradients (Endocrinology 106, 530, 1980). These fractions were cultured in RPMI-1640 containing 20% fetal calf serum, vitamin A, and insulin, under 95% air-5% CO_2. Fraction 2 yielded fibroblasts without evident epithelial clones, while fraction 4 contained numerous clones of epitheloid cells and scattered fibroblasts, which eventually encapsulated them. If a 10% extract (in PBS containing 0.1% Na_2 EDTA) from a Dunning R3327 rat prostate adenocarcinoma, subline G (Miami), carried in Copenhagen X Fisher rats, was included in the original incubation mixture, fibroblasts in fraction 2 were completely destroyed within 1-3 days. The same effect occurred in the absence of fetal calf serum. In fraction 4, no fibroblasts were evident, while epithelioid cells gradually grew out. These clones could be subcultured. Cholera toxin (0.01 ug/ml) appeared to help maintain their morphology. In summary, we report (1) growth on standard culture plates, of epithelioid clones from individual rat ventral prostate cells believed to be of epithelial origin; (2) transfer of these primary epithelioid clones with maintenance of their morphology; (3) differential cytotoxicity, by a mechanism that has not been established, of an EDTA-containing Dunning extract added to the incubation medium, , and (4) the advantage of prior cellular enrichment before culture in a selective medium. (Supported by grant CA-31105 from the National Prostatic Cancer Task Force to KMA.)

T-PM-E2 AMILORIDE INDUCES FLUCTUATIONS OF THE SHORT CIRCUIT CURRENT IN RABBIT URINARY BLADDER. D.D.F. Loo, S.A. Lewis[1], and J.M. Diamond. Dept. of Physiology, U.C.L.A. Medical School, Los Angeles, California 90024. [1]Dept. of Physiology, Yale University School of Medicine, New Haven, Connecticut 06510.

The reversible sodium blocker amiloride is known to decrease the transepithelial conductance and short-circuit current of rabbit urinary bladder when applied to the mucosal solution. In a modified Ussing chamber (tissue area, 2 cm^2), with NaCl-$NaHCO_3$ Ringer's solution bathing both the mucosal and serosal membranes, the power spectral density of the fluctuations in short circuit current has now been found to exhibit a Lorentzian component with a plateau value A_o and a corner frequency f_c. This Lorentzian spectrum depends on the amiloride concentration, studied in the range from 0 to 10^{-5} M. A_o, approximately 10^{-17} Amp^2/Hz, decreases with increasing amiloride concentration while concurrently f_c, varying in the range 10^0 - 10^2 Hz, increases. The density of sodium channels and the conductance of a single channel has been determined.

Supported by NIH grants GM 14772 and AM 17328.

T-PM-E3 THE ROLE OF MICROFILAMENTS IN ADH-INDUCED WATER FLOW ACROSS TOAD URINARY BLADDER. M.A. Hardy and D.R. DiBona*; Depts. of Physiology & Biophysics, Univ. of Miami School of Medicine, Miami, FL 33101 and *Univ. of Alabama in Birmingham, Birmingham, AL 35294.

Gravimetric methods were used to measure osmotic water flow across sac preparations of toad urinary bladder. With a mucosal medium diluted to 58 mOsm/Kg H_2O (with 233 mOsm/Kg H_2O Ringer's solution in the serosal bath), addition of ADH (Pitressin), 50 mU/ml, resulted in a measured osmotic permeability coefficient (P_f) of 190±12 μm/sec. When cytochalasin B (CB) ($2x10^{-5}$ M) was added to the serosal bath 40 min prior to ADH application, P_f was reduced to 138±6 μm/sec ($p<0.0005$; n=12). However, ADH-induced diffusional permeability to tritiated water, P_D, was enhanced by 17% with CB (from 6.5±0.3 to 7.6±0.4 μm/sec; n=6; $p<0.0125$). The toxin, which prevents polymerization of intracellular actin filament (microfilaments), caused a pronounced vacuolation in granular cells only when both ADH and an osmotic gradient were present. This led to experiments with brief glutaraldehyde (1%) fixation after addition of ADH or ADH + CB but before osmotic gradient imposition. Subsequent osmotic flow measurements yielded P_f values of 180±18 and 210±7 μm/sec for ADH and ADH + CB respectively (n=18, Δ=+17%, $p<0.0125$). Persistence of colchicine-inhibition of the ADH response with the fixation protocol suggested validity of this approach. We conclude that CB inhibition is through disruption of the intracellular portion of the pathway for osmotic flow rather than through interference with ADH-action on the mucosal membrane itself. These results cast some doubt on the significance of the particle aggregation phenomenon which is thought to indicate ADH-induced water channels but which is reported to be precluded by cytochalasin B treatment.

T-PM-E4 ADH–INDUCED MEMBRANE CAPACITANCE AND WATER PERMEABILITY IN TOAD URINARY BLADDER

L.G. Palmer and M. Lorenzen. Dept. of Physiology, Cornell Univ. Med. College, New York, N.Y. 10021

Antidiuretic hormone (ADH) increased the electrical capacitance of the apical membrane of the toad bladder; this effect was modulated by the osmotic gradient across the tissue. Capacitance was measured from the transepithelial voltage response to current pulses, using bladders depolarized with high-K serosal solution to reduce basal-lateral membrane resistance. Addition of ADH (20 mU/ml) increased capacitance by 28 ± 9% over basal levels (mean ± SD) in the absence of an osmotic gradient, and by 8 ± 3% in the presence of a gradient (200 mOsm, mucosal side hypotonic). With bladders stimulated in the absence of an osmotic gradient, rapidly imposing a gradient resulted in a peak rate of water flow which declined to 40% of the peak value after 15-20 minutes. ADH-dependent capacitance also decreased, with a similar time course. Removal of ADH reversed the capacitance change ($t_{1/2}$ = 10-15'), but the reversal was slower than the decline in water flow to basal levels ($t_{1/2} < 5'$). These results suggest that ADH-induced capacitance reflects an increase in membrane area, possibly brought about by fusion of cytoplasmic structures with the apical membrane. The decrease in capacitance in the presence of osmotic water flow indicates that the rates of addition and/or retrieval of membrane to the apical surface are altered, resulting in a decreased water permeability. (Supported by PHS AM27847, B.R.S.C. 80-11-10 from CUMC).

T-PM-E5 INTRACELLULAR CHLORIDE ACTIVITY IN NECTURUS GALLBLADDER IS INDEPENDENT OF EXTERNAL pH.

J.F. Garcia-Diaz and W. McD. Armstrong, Dept. of Physiology, Indiana University School of Medicine, Indianapolis, IN 46223

Open-tip and Cl^- selective (Corning 477315) microelectrodes were used to study the effect of external pH on Cl^- accumulation by epithelial cells of Necturus gallbladder. The Ringer's solutions contained, in mM, 100.0 NaCl, 2.5 KCl, 1.0 $CaCl_2$ and were buffered to pH 7.2 or 8.2 with 5 mM imidazole-Cl or Tris-Cl. Increasing the pH from 7.2 to 8.2 in the mucosal, the serosal, or in both solutions simultaneously, hyperpolarized the apical membrane potential (V_a = -60 ± 5 mV) by about -6, -10 and -17 mV, respectively, without a significant change in transepithelial potential (V_T = 0.3 ± 0.5mV). The same hyperpolarizations were recorded with Cl^- selective microelectrodes, even 40 min after the change in external pH, indicating that intracellular Cl^- activity (a^i_{Cl} = 12 ± 2 mM) remained essentially constant. The fractional resistance of the apical membrane (FR_a) decreased when mucosal pH was raised, and increased when serosal pH was raised. The changes in transepithelial resistance (R_T) were in the opposite direction to those in FR_a.

The changes in V_a and FR_a are due, at least in part, to a pH-dependent K^+ conductance of the cell membrane (Reuss et al., J. Memb. Biol. 59:211, 1981). The constancy of a^i_{Cl}, despite significant increases in V_a, indicates that apical membrane Cl^- conductance (g_{Cl}) is virtually zero or decreases, with increased external pH, in a way that compensates for the increased driving force for Cl^- exit. Supported by USPHS AM 12715, HL 23332.

T-PM-E6 CYTOPLASMIC VESICLE FUSION ALTERS THE PERMEABILITY PROPERTIES OF THE APICAL MEMBRANE OF THE RABBIT URINARY BLADDER EPITHELIUM.

S.A. Lewis and J.L.C. de Moura*. Dept. of Physiology, Yale University, New Haven, CT 06510. *Dept. of Urology, University of Lisboa, Lisboa, Portugal. (Intr. by M. Ifshin).

The cation selectivity of the apical membrane in urinary bladder has been shown to be dependent on the ionic balance of the animal. When the plasma is depleted of Na^+ the amiloride sensitive channel has a greater selectivity to Na^+ over K^+, compared to control animals. In light of the phenomenon of intracellular vesicle fusion with the apical membrane, a number of possible explanations for the altered apical membrane properties can be excluded by investigating the permeability properties of newly inserted vesicles. Cytoplasmic vesicles were fused by a rapid compression of the cells (punching). Such compression resulted in a rapid loss of epithelial resistance and voltage (typically from some 20,000 Ω cm^2 to 40 mV to 400 Ω cm^2 and 1-3 mV). The resistance nearly recovered and the potential recovered to values greater than control. This indicates that new membrane is fused into the apical surface and that this membrane has a greater Na^+ transporting ability (by a factor of 4) as determined by amiloride inhibition of Na^+ transport. The new pathways had a much higher selectivity than the control membranes. We developed a method for estimating the apical surface area to that of the cytoplasmic pool of vesicles. This ratio is in the order of 1:3.4.

This data suggests that amiloride sensitive Na^+ pathways exposed to the urine lose selectivity to Na^+ and are ultimately removed from the membrane. Expansion of the bladder results in membrane fusion that contain new channels with greater selectivity.

Supported by grant AM 20851 to S.A.L.

T-PM-E7 CYTOPLASMIC VESICLES FUSE WITH THE APICAL MEMBRANE OF RABBIT URINARY BLADDER EPITHELIUM.

S.A. Lewis. Department of Physiology, Yale University, New Haven, CT 06510.

During a filling cycle of the urinary bladder the cells change from goblet shape to an oblate spheroid. Such a dramatic alteration in cell geometry implies that the apical membrane must increase its surface area by the addition of membrane from a cytoplasmic pool. (Lewis and Diamond (J. Membr. Biol. 28: 1, 1976) and Minsky and Chlapowski (J. Cell Biol., 1978)). Vesicles were inserted by bathing both apical and basolateral membranes in a Ringers of 1/2 molarity. This causes, after 70 minutes, a 74 ± 8% (n=8; S.E.M.) increase in apical capacitance, which is reversed to within 10% of control 30 minutes after returning the bathing solutions to control osmolarity. To study the control of this system, a microtubule antagonist (colchicine, 10^{-4} Molar) and a microfilament disrupting agent (cytochalasin B 5 x 10^{-5} M) were placed in both bathing solutions for 90 to 180 minutes respectively. Colchicine did not alter the response. Cytochalasin B did not cause any change in control capacitance but completely eliminated the change induced by hypo-osmotic solutions. Swelling the cells and then treating with cytochalasin B for 90 minutes caused no change in the increased capacitance. Returning the epithelium to control Ringers caused the capacitance to return (more slowly) to near control levels. If this protocol was followed by another exposure to hypo-osmotic solutions there was no increase in capacitance.

This data indicates that fusion of vesicles is dependent on microfilaments for insertion. Removal under the conditions described is independent of microfilaments but relies on the close apposition of the vesicles for removal.

Supported by grant AM 20851. W. Alles' technical assistance was flawless.

T-PM-E8 OUABAIN EFFECT ON K FLUX ACROSS THE BASOLATERAL MEMBRANE OF FROG SKIN. Thomas C. Cox and Sandy I. Helman. Dept. of Physiology and Biophysics, University of Illinois, Urbana, IL 61801

The effects of ouabain on ^{42}K fluxes across the basolateral membranes of isolated epithelia of frog skin (Rana pipiens) were examined using a Cl-free (SO_4) Ringer. K uptakes into the tissue were examined at 10 minutes. Under control conditions, K uptake was 3.1 ± 0.09 nmoles/cm^2min. 10^{-3} M ouabain decreased this by 97 ± 1% to 0.09 ± 0.03 nmoles/cm^2min (N=3). For washout studies, epithelia were loaded with isotope for four hours and then mounted in flux chambers. The appearance of isotope in the basolateral solution (short-circuited conditions) was measured at one minute intervals. The efflux was relatively stable over the time intervals (minutes) of the experiments. When 10^{-3} M ouabain was added to the basolateral solution, short-circuit current decreased from 17.4 ± 3.4 μA/cm^2 to 11.5 ± 2.0 μA/cm^2 at 5 minutes with a corresponding increase of K efflux of 53 ± 13% over control values (N=11). In nontransporting skins (10^{-4} M amiloride for 20 minutes), ouabain caused a 35 ± 4% decrease in K efflux in 2-3 minutes. We conclude that > 95% of K uptake occurs through a ouabain sensitive mechanism. The post-ouabain increase in K efflux in Na transporting tissues may be due to the depolarization of the basolateral membrane caused by ouabain. The inhibition caused by ouabain in nontransporting tissues was unexpected because ouabain also depolarizes the basolateral membrane under nontransporting conditions. This result suggests that under these conditions K may in part be extruded by a ouabain sensitive pump. (Supported by USPHS AM 16663 and GM 07357.)

T-PM-E9 Assembly of the occluding junctions in a transporting epithelium Carlos A. Rabito (Intro. by Alexander Leaf) Renal Unit, Massachusetts General Hospital, Boston, MA 02114

The present study explores the ability of isolated LLC-PK_1 cells to re-assemble the occluding junctions during the reconstruction of the epithelial membrane in tissue culture conditions. LLC-PK_1, an epithelial cell line from a normal pig kidney, was removed by trypsin-EDTA treatment and plated on collagen coated Nucleopore filters. After plating the filters were removed periodically from the culture medium and placed between two Lucite chambers to determine the electrical resistance across the monolayer (R). R increases from 9.5 ± 0.19 Ω cm^2 (n=9) at 2 hs to 411 ± 7.5 Ω cm^2 (n=9) at 20 hs after plating. Forty hours after plating, however, this value decreases to 178 ± 3 Ω cm^2 (n=9). Simultaneous measurements show that the DNA content per cm^2 of monolayers increases from 2.90 ± 0.10 μg (n=9) at 16 hs to 5.19 ± 0.11 μg (n=9) at 48 hs after plating. The decrease in R observed 40 hs after plating can be avoided by blocking the cell division with 10 mM thymidine. The effect of cell density on R was further investigated in monolayers plated at different cell densities in which the cell division was blocked with thymidine. The results show that there is an inverse correlation between cell density and R. In addition, cells obtained from cultures in exponential growth show a delay in the development of R as compared with cells obtained from confluent arrested cultures. Synchronization of the exponential growing cells, however, abolish this delay. From these studies we concluded that changes in cell density and synchrony, modulated the density and the participation of the occluding junctions in the transepithelial electrical resistance.

T-PM-E10 K^+ SELECTIVITY, K^+ ACTIVITY AND MORPHOLOGY OF INSECT MIDGUT CELLS. D.F. MOFFETT, R.L. Hudson, S.B. Moffett and R.L. Ridgway. Zool. Dept., Washington St. Univ., Pullman WA 99164.

Isolated perfused preparations of the K^+-transporting posterior midgut of the tobacco hornworm (Manduca sexta)were penetrated with single-barrelled electrodes for measurement of transbasal electrical potential (V_b), double-barrelled electrodes for simultaneous measurement of V_b and intercellular K activity ($(K^+)_i$), or double-barrelled electrodes for measurement of V_b and iontophoretic injection of fluorescent Lucifer yellow CH dye. Intraepithelial voltages ranged from +8 mV to -48 mV; in standard bathing solution there is a direct relationship between intraepithelial voltage and K^+ activity such that K^+ is seldom far from electrochemical equilibrium. Changes of bathing solution K^+ concentration resulted in large Nernstian changes in V_b and small, slow changes in $(K^+)_i$ if V_b under standard conditions was more negative than about -20 mV. For impalements with less negative voltages, intraepithelial K^+ activity rapidly approached the new external value and voltage changes were small. When epithelial regions more negative than -20mV were dye-marked, the dye was clearly localized in single cells or small groups of adjacent cells and both major cell types (columnar and goblet) were marked. When marking of less negative regions was attempted, no dye marks were found. These results suggest that K^+ distribution across the basal cell membrane is passive and that V_b of -20mV to -48 mV and $(K^+)_i$ of 80 mM to 160 mM are typical of intact midgut cells: less negative values of V_b and lower values of $(K^+)_i$ are probably recorded from damaged cells or extracellular sites. These studies failed to confirm reports of midgut cells with very low V_b values. Supported by NIH GM 26287.

T-PM-E11 MEASUREMENTS OF CYTOSOLIC CALCIUM ACTIVITY IN MONKEY KIDNEY CELLS USING THE HOST METHOD OF AEQUORIN INCORPORATION. K.W. Snowdowne and A.B. Borle, Department of Physiology, University of Pittsburgh, School of Medicine, Pittsburgh, PA 15260.

Cultured monkey kidney cells (LLC-MK2) can be exposed to a hypoosmotic medium at 4°C for 2 minutes (hypoosmotic shock treatment or HOST) and regain completely their normal biological properties when replaced in physiological media. HOST cells can transport and incorporate ^{3}H-leucine, exclude the dye trypan blue, exclude succinate, reestablish normal ionic gradients of Na and K, and if returned to culture, grow at the same rate as control cells. The intracellular Ca pools and Ca fluxes measured by the kinetic analysis of steady state ^{45}Ca movements and the total cell Ca content are not altered by the procedure. The HOST procedure also provides a method by which aequorin can be incorporated into mammalian cells. Aequorin is a photoprotein which emits photons in the presence of calcium ions. When placed in a light gathering apparatus, the aequorin containing cells provide sufficient luminescence to permit a continuous measurement of the intracellular calcium activity. Using the Allen-Blinks calibration method we estimate that the intracellular calcium activity of kidney cells is in the range of 40 nM (35.7±12 (N=9)). We have also observed that the signal is increased by exposure of the cells to media containing no substrate and saturated with N_2 or by the addition of the calcium ionophore A23187. Both effects are fully reversible, suggesting that HOST cells are capable of reestablishing a normal low cytosolic calcium activity. (Supported by NIH grant AM 07869)

T-PM-E12

DIRECT DETERMINATION OF THE CHYMOTRYPSINOGEN CONTENT OF INDIVIDUAL ZYMOGEN GRANULES. Edmund A. Mroz and Claude Lechene, Department of Physiology and Biophysics, and National Biotechnology Resource in Electron Probe Microanalysis, Harvard Medical School, Boston, MA.

We have used micromanipulation techniques and a picoliter-scale fluorescence assay to determine the content of chymotrypsiogen in individual pancreatic zymogen granules. Knowing the contents of enzymes in individual granules will clarify the dispute over "parallel secretion" by the exocrine pancreas, and will help studies of secretion from individual cells. Zymogen granules were prepared by differential centrifugation of an homogenate of a single rat pancreas. A suspension of granules in sucrose was then sprayed onto a siliconized glass cover slip so that dried droplets, some containing individual granules, were obtained. The cover slip was placed on an inverted microscope and covered with light paraffin oil. Granules in the dried droplets could be seen with Nomarski differential interference optics. A microhook controlled with a micromanipulator was used to dislodge individual dried droplets containing a known number (0-2) of granules, and to move them to a region of the cover slip suitable for performing microfluorometric assays. After treatment with 100 pl of a trypsin solution to activate chymotrypsinogen, the chymotryptic activity of each droplet was determined with an NADH-coupled fluorometric assay that we have developed. The reaction was carried out in calibrated droplets of less than one nanoliter under oil; fluorescence was determined directly from the droplets with a microscope-fluorometer. Early studies indicate about 0.3 attomol (10^{-18}mol) of cymotrypsinogen per zymogen granule, a value in close agreement with that expected on the basis of bulk chymotrypsinogen content and zymogen granule size. Similar combinations of micromanipulation and picoliter-scale fluorescence assays should find wide application in studies of metabolites and enzymes in single cells and in single subcellar organelles.

This research was supported in part by grant AM 26488 from the National Institutes of Health.

T-PM-E13 MEASUREMENTS OF CELL WATER OSMOTIC PERMEABILITY P^c_{os} IN EPITHELIA: SOURCES OF ERROR.

Paola Carpi-Medina, E. González & G. Whittembury. Instituto Venezolano de Investigaciones Científicas, IVIC, POBox 1827, and Escuela de Medicina Vargas, UCV, Caracas 1010A, Venezuela.

To measure P^c_{os} in epithelia, an osmotic difference ΔC must be instantaneously applied across the cell membrane under study. The ensuing water movement per unit area, J_v, leads to the calculation of $P^c_{os} = \int J_v \, \Delta C$. However, thick unstirred layers, δ, slow changes of solutions with high viscosity, slow diffusion coefficient, D, of test solutes and excessively large ΔC may affect these measurements because of non-linear relation and rectification between J_v and ΔC which falsify P^c_{os}. These sources of error have been evaluated in proximal convoluted (PCT) and proximal straight (PST) tubules dissected out of the rabbit kidney. Solution is changed in < 0.1 s. Cell volume changes can be evaluated from continuous records of tubule diameter (which can be detected with a precision of 10 pl/mm tubule using an image splitter) as a function of time (time resolution 0.2 s). ΔC as small as 2 - 3 mOsmolar can be detected; δ = 70-100 μm when NaCl ($D = 1.6 \times 10^{-5} cm^2/s$) is used. Linearity of a plot of J_v vs ΔC is observed with $\Delta C \leq$ 20 mOsmolar and $\leq$ 30 mOsmolar for PCT and PST respectively. ΔC induced by solutes with smaller D increases the non-linearity. The use of $\Delta C >$ 50 mOsmolar leads to rectification effects. It is concluded that to avoid undesirable errors, P^c_{os} should be measured as a function of small ΔC and the data extrapolated to $\Delta C = 0$. With this method P^c_{os} values are 41.6 $\pm$ 3.5 and 25.1 $\pm$ 2.3 in units of $10^{-4} cm^3/s.Osmolar$ per cm^2 of basal surface area for PCT and PST, respectively.

Supported by PNUD/UNESCO RLA 78/024 and CONICIT. G.W. is Professor of the Instituto Internacional de Estudios Avanzados.

T-PM-F1 ON THE DYNAMICS OF EXCITED STATE PROCESSES IN VISUAL PIGMENTS. Toshiaki Kakitani, Hiroko Kakitani and Barry Honig, Department of Biochemistry, Columbia University, New York, NY 10032.

Photochemical cis-trans isomerization of the 11-cis chromophore of visual pigments occurs very rapidly. It is important to understand the factors that lead to such a fast process both from a physico-chemical point of view and also to better understand the biochemical role of the photoisomerization. In this presentation a number of the dynamical properties of rhodopsin in its excited state are discussed.

An important observation that is not generally appreciated is the absence of any observed fluorescence in rhodopsin. Thus the quantum yield for fluorescence must be less than 10^{-5}. The intrinsic fluorescence lifetime can be estimated to be about 5 nsec based on absorption data and the theoretical result that the absorbing state is the lowest excited singlet. These values indicate that rhodopsin escapes from the Franck-Cordon state in less than .05 psec which is two orders of magnitude faster than the upper limit for photoisomerization (6psec) determined from psec data.

The .05 psec limit for vibrational relaxation provides a possible explanation for two puzzling phenomena: a) The 11-12 torsional mode of rhodopsin is not Raman active despite a large ground-excited state deformation. b) The absorption spectrum of rhodopsin shows no evidence of vibrational structure. The rapid relaxation time also provides an important criterion for evaluating specific models for the photoisomerization of the visual chromophore.

Supported by NIH grant GM30518 and NSF PCM 81-18088.

T-PM-F2 POSSIBLE ROLE OF POSITIONAL ISOMERIZATION IN THE CONVERSION OF RHODOPSIN TO BATHORHODOPSIN. P. E. BLATZ, Department of Chemistry, University of Missouri-Kansas City, Kansas City, Missouri 64110.

The conversion of the retinylic cation to the anhydroretinylic cation is an acid-base induced positional isomerization of the double bonds. Spectroscopic and structural properties of these cations were examined by theoretical methods, and the results were shown to be in agreement with those from experiment. The isomerization process is responsible for shifting the λ_{max} from 588nm to 620nm for the cations derived from all trans retinol. The isomerization is accomplished by proton elimination from carbon four of the ionone ring producing the intermediate anhydroretinol, which undergoes proton addition at carbon fifteen to yield the anhydroretinylic cation. A similar set of events may be postulated to occur within visual pigments, and the mechanism is in agreement with current evidence indicating proton transfer. The newly formed positional isomer, bathorhodopsin, whould be similar to the anhydroretinylic cation, and its predicted wavelength and molar absorptivity would be close to the known values.

T-PM-F3 A COMPARISON OF THE BATHORHODOPSIN INTERMEDIATES FROM 11-CIS AND 9-CIS RHODOPSIN, M. L. Applebury, Dept. of Biochemical Sciences, Princeton Univ., Princeton, NJ 08544, P. M. Rentzepis, A. H. Reynolds, J. D. Spalink, Bell Laboratories, Murray Hill, NJ 07974, and W. Sperling Institut für Neurobiologie, KFA Jülich, D-517 Jülich, West Germany

Bathorhodopsin-rhodopsin difference spectra of native 11-cis rhodopsin and regenerated 9-cis rhodopsin were measured with a double beam laser spectrophotometer following excitation at 532 nm. Technical attention to obtaining highly purified samples, to improving signal to noise in amplitudes measured and to avoiding multiphoton events allows us to carefully compare the difference spectra generated from these visual pigments. A detailed analysis of data obtained at 85 ps suggests the 11-cis bathorhodopsin and 9-cis bathorhodopsin are different in their extinction coefficients and that the λ max are shifted by about 10 nm. The ratio of quantum yields for photochemical production of 9-cis Bathorhodopsin to 11-cis Bathorhodopsin is $\sim$0.5-1.0. These results question the classical argument that the first photochemical intermediate is the same all-trans intermediate whether generated from an 11-cis or 9-cis retinal-opsin chromophore and imply that the early photochemical process in vision are more complex than previously considered.

T-PM-F4 COMPARATIVE ^{13}C NMR STUDIES OF LABELLED RETINAL IN RHODOPSIN AND BACTERIORHODOPSIN. D. D. Muccio, W. G. Copan, E. W. Abrahamson, and G. D. Mateescu.[1] Department of Chemistry, Case Western Reserve University, Cleveland, Ohio 44106, U.S.A.

In continuation of our NMR studies of the structure and conformation of visual pigments and related systems, we present the results of a ^{13}C NMR study of rhodopsin and bacteriorhodopsin in which the retinylidene chromophore was incorporated with 95% ^{13}C enrichment at position 13. The enriched proteins were obtained by the regeneration of the apoproteins with the labelled retinals. ^{13}C NMR spectra were obtained on the octylglucoside-solubilized proteins. The [13-^{13}C]-rhodopsin preparation yielded a resonance at 168.1 ppm from TMS. The dark-adapted [13-^{13}C]-bacteriorhodopsin exhibited two absorptions at 168.9 ppm and at 165.1 ppm, assigned to the all-trans isomer and the 13-cis isomer, respectively, on the basis of a study of model retinylidene imines. The similarity of the chemical shifts observed for both rhodopsin and bacteriorhodopsin suggests a similarity of the environments of the carbon position 13 in each protein. These findings are not consistent with the recently proposed model by Nakanishi, et al.[2] which suggests different electron densities at these sites.

1 Address correspondence to this author. Work supported by NIH Grant EY 02998.

2. K. Nakanishi, et al., J. Am. Chem. Soc., 1980, 102, 7945.

T-PM-F5 A RHODOPSIN DERIVATIVE LACKING THE FULL CYCLOHEXYL RING OF RETINAL. Rosalie K. Crouch, Medical University of South Carolina, Charleston, S.C. 29425.

The retinal derivative, 3,7-dimethyl-10-ethyl-2,4,6,8-dodecatetraenal, structure 1. has been synthesized which is lacking the C-3 of the retinal structure and hence the closed six membered ring.

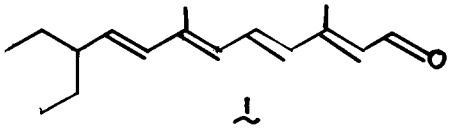

1

The structure of 1 was established by ir, absorption and mass spectra. The cis isomer corresponding to the 11-cis isomer of retinal forms a photosensitive pigment with bovine opsin in good yield with a λ_{max} at 454 nm, somewhat blue shifted from that of native rhodopsin. The rate of pigment formation was about 3 times slower for this analogue as compared with native rhodopsin but the yield of pigment was approximately the same. The pigment analogue is photobleachable and is stable to the addition of both 11-cis retinal and hydroxylamine. These results demonstrate that the cyclohexyl ring is not essential for pigment formation with bovine opsin.

Funded by grant #BNS 8011563 from the National Science Foundation.

T-PM-F6 RESONANCE RAMAN MICROSCOPY: STUDIES OF SINGLE PHOTORECEPTOR. B.A. Barry and R. Mathies Department of Chemistry, University of California, Berkeley, CA 94720

We have constructed a resonance Raman microscope which has enabled us to perform comparative vibrational spectroscopy on the visual pigments of single photoreceptor cells. The laser is focused on the outer segment of the cell (77 K, glycerol glass) through the epi-illumination system of a light microscope. Raman scattering is collected by the objective and dispersed by a monochromator on a dry-ice cooled intensified vidicon detector. This microscope system has enabled us to obtain spectra of outer segments as small as 1 x 10μ.

We have studied the primary photochemistry in pigments from toad (Bufo marinus) and goldfish (Carassius auratus). Raman spectra of 500 nm toad rod pigments have demonstrated that species-to-species variation in protein sequence (or in protein folding) affects the conformation of the chromophore in the first photointermediate. The intensity of the 875 cm^{-1} line ($C_{10}H$ wag) of toad bathorhodopsin is greater than the intensity of 875 cm^{-1} line of bovine bathorhodopsin; therefore the proteins of the two pigments exert a different influence on the C_{10} center during chromophore isomerization. Our studies of the goldfish photoreceptors are the first Raman spectra of A_2 pigments. Comparison of the fingerprint lines of the goldfish rod steady-state mixture with the fingerprint lines of A_2 model compounds indicates that a red-shifted, "trans" intermediate is produced on illumination of the pigment. However, the composition of the steady-state of the goldfish rod differs from the composition observed in bovine and toad pigments at comparable probe wavelengths. We have also used the Raman microscope to obtain vibrational spectra of two of the cone pigments of the goldfish. Comparative vibrational studies of color pigments are now feasible.

T-PM-F7 ANISOTROPY OF THE INFRA-RED LIGHT-SCATTERING CHANGES INDUCED BY ILLUMINATION OF ORIENTED RETINAL ROD OUTER SEGMENTS (ROS). Marc Chabre, Minh Vuong*, and Lubert Stryer, Department of Structural Biology, Sherman Fairchild Center, Stanford University School of Medicine, Stanford, CA 94305.

The fast scattering changes observable in the near IR upon weak flash illumination of ROS disc membranes arise from reactions between photoexcited rhodopsin (R*) and transducin (T), the GTP-binding protein (Kühn, Bennett, Michel-Villaz, and Chabre, PNAS, Nov. 1981). The long axes of magnetically-oriented ROS were at 45° to the 900 nm incident light beam. The relative changes in the scattered light intensity at 90° (left) and 270° (right) were measured. The "binding" signal observed in the absence of GTP, which monitors the formation of a stable R*-T-GDP complex, is highly anisotropic. In the presence of GTP, the main "dissociation" signal (a decrease in scattering) is isotropic. This change probably results from the release of a subunit of T-GTP from the ROS into the solution. In addition, an earlier and highly anisotropic GTP-dependent signal was observed. The latter signal disappears upon sonication, whereas the other two signals become isotropic. The anisotropic nature of these light-scattering changes may provide insight into their structural bases and the detailed mechanism of the cyclic nucleotide cascade. Marc Chabre was on leave from CNRS and CENG Grenoble and supported by a grant from DGRST. This work was supported by the National Eye Institute.

T-PM-F8 ELECTRON MICROSCOPE AND LOW-ANGLE X-RAY DIFFRACTION STUDIES ON THE RETINAL PHOTORECEPTOR STRUCTURE OF SQUID. C.R. Worthington, A.R. Worthington and A.R. Czeto, Department of Biological Sciences, Carnegie-Mellon University, Pittsburgh, PA and A.J. Hodge, Laboratory of Biophysics, NINCDS, NIH, Marine Biological Laboratory, Woods Hole, MA.

We have studied the molecular structure of the invertebrate rhabdomeric visual cells of squid by electron microscopy and low-angle x-ray diffraction. It is known from previous x-ray studies (in 1976) that x-ray patterns can be recorded from squid retina after fixation with glutaraldehyde while in later work (in 1980) x-ray patterns were obtained from intact, untreated strips of squid retina. In order to interpret the x-ray intensities from squid retina it was proposed that the observed intensity transform profile came from a pair of membranes (C.R. Worthington and A.R. Czeto, Biol. Bull. Abstracts, 1981). This implied that the membranes of the adjacent microvilli adhere together to form a membrane pair. The previously published electron micrographs of squid photoreceptors while showing the elegant hexagonal packing of microvilli did not reveal the fine structure of the microvilli array. New electron micrographs of squid eyes have been now obtained. The squid eyes were fixed in glutaraldehyde-EGTA-sucrose buffer IIIB (A.J. Hodge and W.J. Adelman, J. Ultrastruct. Res. 70: 220, 1980) and treated with osmium tetroxide before dehydration and embedding. It is clear from these micrographs that the walls of the neighboring microvilli are to a larger extent pressed together to form a double membrane structure. This was true for unstained sections and for sections stained with uranyl acetate and lead acetate. Further, combined electron microscope and x-ray diffraction experiments using different specimen preparations are in progress.

T-PM-F9 ELECTRICAL CABLE OR DIFFUSION PROCESSES CAN ACCOUNT FOR INVERTEBRATE PHOTORESPONSE DYNAMICS. by L.L. Odette and P.H. Hartline (Intr. by H.K. Hartline)
Eye Research Institute of Retina Foundation, Boston, MA 02114

Our experiments show that the sinusoidal steady state dynamics of the invertebrate photoresponse are well described by a time and space dependent physical process with the dispersion relation: $\kappa = (1 + j\omega\tau)^{1/2}/\lambda$ where κ and ω are the wave number and frequency, and τ and λ are the system characteristic time and length, respectively. We analyze two candidates for a physical process with the required dispersion relation.

(1) Diffusible Transmitter model: We assume that absorption of light by the photopigment results in a transient local increase in the concentration of a transmitter. Transmitter diffuses to a membrane site that increases conductance in proportion to transmitter concentration at the site. By a constant rate inactivation or uptake mechanism, transmitter concentrations relax to base levels after photon absorption. System characteristic time and length are functions of the transmitter diffusion coefficient (D) and the uptake rate (R): $\tau = 1/R$, $\lambda = (D/R)^{1/2}$.

(2) Electrical Cable model: We assume that absorption of light causes a local increase in membrane conductance. In the invertebrate photoreceptor, most of the photopigment is located in the membranes of the tightly packed microvilli composing the rhabdom. Decremental conduction of local responses through the restricted extracellular space between microvilli has the dispersion relation required to account for our observations. The characteristic time and length are determined by membrane electrical properties (membrane conductance G_m mho/cm^2, capacitance C_m F/cm^2, and the geometry and electrical properties of the extramicrovillar space (combined in a surface conductivity, σ_s mho): $\tau = C_m/G_m$, $\lambda = (2\sigma_s/G_m)^{1/2}$.

Mechanisms (1) or (2) or both convolved could give the photoresponse its dynamics.

T-PM-G1 CHANGES IN RED CELL MEMBRANE MECHANICAL PROPERTIES ASSOCIATED WITH IN VIVO AGEING. G.B. Nash and H.J. Meiselman, Department of Physiology and Biophysics, University of Southern California School of Medicine, Los Angeles, California 90033.

Using micropipette and flow channel techniques, we have compared the membrane mechanical properties of age-separated human erythrocytes. Micropipette aspiration measurements show that the membrane shear elastic modulus does not alter during ageing. However, the time constant for shape recovery of elongated cells is greater for older erythrocytes. Ageing is accompanied by increased cell hemoglobin (Hb) concentration and hence increased internal viscosity. When young cells were shrunk in hypertonic media only relatively small increases in recovery time were induced, bearing out the theoretical prediction that at physiologic Hb concentrations energy disipation takes place mainly in the cell membrane. Observations of red cell ghosts from young and old fractions showed the importance of the membrane in determining erythrocyte recovery rates, thus implying that membrane surface viscosity increases during ageing. Altered Hb binding to the membrane might play a part in causing these changes. Preliminary data from experiments on ghosts prepared at various pH suggest that Hb-membrane interactions influence membrane properties. Viewed collectively, these data suggest that altered membrane mechanical properties, particularly membrane surface viscosity, may affect the rate of transit through the reticuloendothelial system and thus influence in vivo cell survival.

Supported by NIH Grants HL15722 and HL15162 and by AHAGLAA Award 5371G5.

T-PM-G2 ELECTRICAL AND CHEMICAL PROPERTIES OF RED BLOOD CELL-MEMBRANE SYSTEMS. Howard C. Mel & Steven J. Peros, Department of Biophysics & Medical Physics and Donner Laboratory, Lawrence Berkeley Laboratory, University of California, Berkeley, California 94720.

This study reports on the interactive effects of high electric fields, the fixative glutaraldehyde (GA), and the detergent Triton X-100 on red blood cells (RBC). The experimental results are derived from resistive pulse spectroscopy (RPS) measurements of apparent cell size and kinetics of size change, analogously to our previous study on the kinetics of GA fixation (Yee and Mel, Blood Cells 4, 485-97, 1978). Using combinations of differing electric fields and concentrations of GA and Triton, it is possible to "look at" both membrane and cytoplasmic properties, independently. Since the nonionic detergent removes lipids, glycolipids and glycoproteins from membrane systems, treatment of RBC fixed by the protein cross-linking agent GA, yields a protein-cytoskeletal object (which maintains gross morphological and structural integrity). In the experiments reported here we varied the electrical field strength across the RPS orifice up to a maximum value of 2.7 kV/cm, and monitored apparent (electrical) size changes over a one hour period. New results include: (1) RBC only fixed with GA are essentially insensitive to electrical breakdown of their membranes, whereas unfixed RBC display breakdown above about 1 kV/cm; (2) fixed cells treated with the detergent show both a field-strength-dependent and a Triton-concentration-dependent conductivity; (3) at higher field strengths the fixed-Tritonized cells achieve a plateau of constant electrical resistivity sooner than for lower fields. These and related results are discussed in terms of membrane and cytoplasmic properties of the RBC.

T-PM-G3 TEMPERATURE DEPENDENCE OF THE YIELD SHEAR RESULTANT AND THE PLASTIC VISCOSITY COEFFICIENT OF RED BLOOD CELL MEMBRANE. R.E. Waugh. University of Rochester Medical Center, Rochester, N.Y. 14642.

Structural failure of the red blood cell membrane in shear deformation occurs when the maximum shear resultant (force/length) exceeds a critical value, the yield shear resultant. When the yield shear resultant is exceeded the membrane flows with a rate of deformation characterized by the plastic viscosity coefficient. The temperature dependence of the yield shear resultant and the plastic viscosity coefficient have been measured over the temperature range 10-40°C. Over this range the yield shear resultant does not change significantly (+ 15.0 percent), but the plastic viscosity coefficient changes exponentially from a value of 1.3×10^{-2} surface poise (dyn sec/cm) at 10°C to a value of 6.2×10^{-4} surface poise at 40°C.

The different temperature dependence of these two parameters is not surprising, since they characterize different molecular events. The yield shear resultant depends on the number and strength of intermolecular connections within the membrane skeleton whereas the plastic viscosity depends on the frictional interactions between molecular segments as they move past one another in the flowing surface. From the temperature dependence of the plastic viscosity, η_p, a temperature-viscosity coefficient, E, can be calculated (η_p = const. x exp(-E/RT). This quantity is related to the probability that a molecular segment can "jump" to its next location in the flowing network. The temperature-viscosity coefficient for red cell membrane above the elastic limit is calculated to be 18 kcal/mole, which is similar to coefficients for other polymeric materials; e.g., for polyisobutylene, E = 21.1 kcal/mol.

T-PM-G4 FRACTURES ALONG THE HYDROPHILIC SURFACES OF MAMMALIAN LENS FIBER CELL MEMBRANES. M.J. Costello, H.P. Ting-Beall and J.D. Robertson. Department of Anatomy, Duke University Medical Center, Durham, N.C. 27710

Although the fracture patterns of most biological membranes can be explained in terms of the propagation of the fracture planes along membrane hydrophobic interiors, fractures of membranes in lens fiber cell junctions can occur along the hydrophilic surfaces revealing square crystalline arrays of protein subunits in the plane of the membranes. Such crystalline arrays cover extensive surfaces in unetched freeze-fracture images of junctions isolated from bovine lenses (Zampighi et al., 1981) and also from junctions in fragments of rat lenses taken from the deep cortex. Several features of these membrane pair fracture patterns are unusual. Four unique fracture surfaces are observed and none of the surfaces show intramembrane particles or pits typical of other junctions such as the gap junctions ocassionally seen between lens fiber cells. A key factor is that there is no EF-to-PF fracture step. Instead a step commonly seen is from the surface displaying the square array to the surrounding ice and is the thickness of one membrane (7nm). In addition the fracture surface showing the square array sometimes grades into a smooth surface without a fracture step. Because this occurs independently of the angle or the amount of metal deposited, it is not characteristic of a hydrophobic fracture face. This textural variation is probably due to a thin layer of ice, of continuously varying thickness, covering the crystalline surface.

Zampighi, G., Simon, S.A., Robertson, J.D., McIntosh, T.J. and Costello, M.H. (1981) On the Structural Organization of Isolated Bovine Lens Fiber Junctions. J. Cell Biol. (in press).

T-PM-G5 EFFECTS OF PHOTO-CROSSLINKING ON BIOMEMBRANE DYNAMICS. M.J.Pringle, D.Chapman and P.J. Quinn. Biochemistry Dept., Royal Free Hospital School of Medicine, London WC1N 1BP, UK.

Inactivation of cellular function by photo-labile compounds is attracting interest as a potential therapy against neoplastic cells. In this context, we have studied membrane perturbations induced by the bi-functional agent 4,4'-dithiobisphenylazide, using sarcoplasmic reticulum (SR) vesicles as a model membrane system. This compound can be photo-activated to produce a highly reactive bis-nitrene which, in erythrocytes, causes crosslinking of membrane proteins (Mikkelsen,R.B. and Wallach D.F.H. (1976) J.Biol.Chem. 251, 7413-6). Purified SR vesicles were incubated with photolabel (6-33 mole% with respect to membranelipid) and then irradiated in ice with a uv lamp (15W,λ_{max}350nm). After irradiation, Ca^{2+}-ATPase activity was reduced by 50%. The inhibition was prevented by addition of 2mM dithiothreitol. The rotational motion of membrane-bound Ca^{2+}-ATPase was studied by laser-induced dichroism using the covalent triplet probe erythrosin isothiocyanate. Irradiation in the presence of 4,4'-dithiobisphenylazide produced a 15-fold increase in τ_2 of the double exponential decay of phosphorescence anisotropy, suggesting a marked reduction in rotational diffusion. Freeze-fracture electron microscopy showed particle aggregation which is consistent with photo-crosslinking of enzyme proteins. To assess the role of membrane lipids, we measured the steady-state fluorescence polarisation of diphenylhexatriene in SR vesicles. The photo-label itself produced a 25% increase in fluorescence polarisation at 37°C, which could be prevented or reversed by 2mM dithiothreitol. However, in both cases, the fluorescence polarisation after subsequent irradiation was 11-15% higher than in untreated samples. The data are discussed in terms of the interaction between DTT and photolabel and protein-lipid interactions.Supported by Cancer Research Campaign.

T-PM-G6 DEUTERIUM NMR OF BIOLOGICAL MEMBRANES. Ian C.P. Smith, Harold C.Jarrell, Mark Rance, Keith W. Butler, Andrew R. Byrd, and Alexander P. Tulloch, Division of Biological Sciences, National Research Council, Ottawa, Canada K1A OR6

Recent developments in spectrometer hardware, acquisition techniques, and data analysis have made deuterium NMR an ideal way to study the dynamics and spatial ordering of lipid components in live whole cells. Our efforts have concentrated on the lipid acyl chains of Acholeplasma laidlawii, Escherichia coli, and Lactobacillus plantarum. Studies have been done with saturated, unsaturated, and cyclopropane fatty acids, all specifically-deuterated. The profiles of molecular ordering versus position, once corrected for geometric variables such as the cis double bond are remarkably similar. By use of avidin in the growth medium of A. laidlawii, enrichments of up to 95% in a particular fatty acid may be obtained, circumventing earlier ambiguities due to mixed fatty acid composition. Whole cells yield results very similar to those derived earlier from lysed and freeze-dried membranes. The use of moment techniques, and "de-Pakeing" to isolate multiple splittings, yields much greater detail on molecular ordering. T_1 and T_2 values yield rates of molecular motion, which vary little down the chains. The influence of proteins is largely confined to changes in component linewidth rather than in quadrupole splittings, suggesting the presence of slower acyl chain motions due to protein-lipid interaction.

T-PM-G7 THREE DIMENSIONAL IMAGE RECONSTRUCTION OF A PHOTOSYNTHETIC MEMBRANE
Kenneth R. Miller, Division of Biology and Medicine, Brown University, Providence, Rhode Island. (Introduced by Robert P. Davis).

The photosynthetic membranes of Rhodopseudomonas viridis are organized in the form of a regular hexagonal lattice with unit cell dimensions of 100 Å. The membrane is composed of a total of seven polypeptides, including three polypeptides associated with the photosynthetic reaction center, and two involved in the binding of light-harvesting bacteriochlorophyll. Preliminary studies on the membrane [Miller, PNAS 76: 6415 (1979)] illustrated its suitability for analysis by Fourier transform techniques. Starting with electron micrographs of the membrane in negative stain taken at various tilt angles in the microscope, we have used Fourier mapping techniques to develop a three dimensional image of the membrane. Images from tilts as high as 60 degrees were used for the reconstruction. The missing cone of meridional data around the 0,0,Z transform line was partially filled from two dimensional transforms of edge-on views of folded membranes in negative stain. The reconstructed structure displays six peripheral lobes of density around a central core which protrudes slightly from each side of the membrane. A model for the integration of the photosynthetic process in the structure has been developed and will be discussed. [supported by NIGMS grant GM28779].

T-PM-G8 CARBON-13 NMR T_1 AND NOE STUDIES OF RHODOPSIN-LIPID INTERACTION IN THE NATIVE RETINAL ROD OUTER SEGMENT DISK MEMBRANE.
A.J. Deese, E.A. Dratz,† and M.F. Brown, Dept. of Chemistry. Univ. of Virginia, Charlottesville, VA 22901 and †Dept. of Chemistry, Univ. of Calif., Santa Cruz, CA 95064

We have recently completed a series of natural abundance ^{13}C T_1 relaxation time and nuclear Overhauser effect (NOE) studies of retinal rod outer segment (ROS) disk membranes and bilayers of their total extracted phospholipids. The samples consist of sonicated vesicles $\sim 10^3$ Å in diameter,[1] and the studies were carried out under conditions where the ROS phospholipids are in the lamellar phase.[2] The ^{13}C T_1 and NOE measurements were made at 15, 25, 45, 50, and 90 MHz as a function of temperature. For the saturated and polyunsaturated phospholipid acyl chain resonances and N^+Me_3 headgroup resonance, the ^{13}C T_1 relaxation rates are singly exponential. The presence of rhodopsin in the ROS disk membrane results in a significant reduction in the T_1 times and NOE values. The T_1s of the ROS membrane and ROS phospholipid vesicles increase with increasing temperature, suggesting that the lipid motions responsible for the temperature dependence, i.e. high frequency trans-gauche isomerizations, are in the fast motional regime, and our data further indicate that one effect of rhodopsin is to reduce the frequency of these types of fluctuations. In contrast to the T_1 results obtained for the ROS phospholipid vesicles, the T_1 times and the NOE values for the native ROS membranes do not show a strong relaxation frequency dependence. Therefore, it appears likely that rhodopsin may damp out any relatively slow lipid motions responsible for the relaxation frequency dependence, postulated elsewhere[3] to arise from collective bilayer excitations, i.e. director fluctuations. (Supported by NIH Grants RO1 EY03754 and RO1 EY00175). 1) M.F. Brown et al., FEBS Lett. 70, 56(1976), 2) A.J. Deese et al., FEBS Lett. 124, 93(1981). 3), M.F. Brown and J.H. Davis, Chem. Phys. Lett. 79, 431(1981).

T-PM-G9 TRANSLATIONAL DIFFUSION OF BACTERIORHODOPSIN AND OF A LIPID ANALOGUE IN ARTIFICIAL BILAYER MEMBRANES.
R. Peters and R.J. Cherry (intr. by K. Jacobson). Max-Planck-Institut für Biophysik, D-6000 Frankfurt 70, Germany; Eidgenössische Technische Hochschule, Laboratorium für Biochemie, CH-8092 Zürich, Switzerland.

Fluorescence Microphotolysis has been applied to large multilamellar vesicles reconstituted from eosin-labeled bacteriorhodopsin (BR), the fluorescent lipid analogue diO-C18(3) and dimyristoylphosphatidylcholine. Translational diffusion coefficients D of BR and of diO-C18(3) have been determined at various lipid:protein (L:P) molar ratios and temperatures. At L:P≅140 $D/\mu m^2 s^{-1}$ is:

	12.5	17.0	20.0	21.5	23.0	24.5	28.5	32.0 T/°C
BR	<0.0005	0.0045	0.044	0.15	0.33	1.10	1.80	2.30
diO-C18(3)	<0.0005	0.0037	0.094	0.21	0.70	1.40	3.30	4.30

Inserting D of BR into eq.10 (Saffman, P.G. and Delbrück, M.(1975) Proc.Natl.Acad.Sci.USA 72, 3111-3113) and using 16.4 Å as the molecular radius a and 45 Å as the molecular height h yields an effective membrane bulk viscosity μ = 4.3 poise at 24.5°C, 2.4 poise at 28.5°C and 1.8 poise at 32°C, respectively. D of the lipid analogue together with a = 4.0 Å and h = 22.5 Å yields μ/poise = 8.0 (24.5°C), 3.1 (28.5°C) and 2.3 (32°C). These values are in good agreement with membrane viscosity as determined for the same system from BR rotational diffusion (Cherry, R.J. and Godfrey, R.E. Biophysical J., in press). As the first rigorous experimental test our studies suggest that the hydrodynamic model employed by Saffman and Delbrück correctly describes translational and rotational diffusion of integral proteins in fluid bilayer membranes.

T-PM-G10 LATERAL DIFFUSION OF A LIPID ANALOG AND THE b-c_1 COMPLEX IN THE MITOCHONDRIAL INNER MEMBRANE: A FLUORESCENCE RECOVERY AFTER PHOTOBLEACHING STUDY.
Arthur E. Sowers, Mathias Hoechli, Luzia Hoechli, Zenon Derzko, Kenneth Jacobson, and Charles R. Hackenbrock. Laboratories for Cell Biology, Department of Anatomy, School of Medicine, University of North Carolina at Chapel Hill, Chapel Hill, N.C. 27514.

The fluorescence recovery after photobleaching technique (FRAP) was used to study the lateral diffusion of dihexadecylindotricarbocyanine (diI), a lipid analog, and the b-c_1 complex in the bilayer of the mitochondrial inner membrane. A fluorescein isothiocyanate conjugated monospecific rabbit IgG was used to label the b-c_1 complex. FRAP was carried out on mitochondrial inner membranes which were fused by calcium into large membrane structures of 20-50 μm. Solutions containing the fluorescent lipid analog or the fluorescent labeled IgG were passed over these large membranes in order to add the lipid analog to the bilayer or label the b-c_1 complex. Lateral diffusion coefficients were in the low 10^{-9} cm^2/sec range for both the diI and the bc_1-complex. Thus the lateral diffusion coefficients for these two components were of the same order of magnitude. The diffusion coefficient for the b-c_1 complex, an integral protein complex, is consistent with the diffusion coefficient determined for intramembrane particles in the mitochondrial inner membrane using the electrophoretic-freeze fracture electron microscopy technique reported recently (Sowers & Hackenbrock, P.N.A.S., 78, 6246, 1981; Sowers & Hackenbrock, J.C.B., 91, 264a, 1981). Supported by NSF grant PCM 7910968 to C.R.H. and NIH grants GM 28704 to C.R.H and GM29234 to K.J. K.J. is an AHA established investigator.

T-PM-G11 H-$2K^k$ AND VSV-G PROTEINS ARE NOT EXTENSIVELY ASSOCIATED IN RECONSTITUTED MEMBRANES RECOGNIZED BY T CELLS. G. S. Cartwright, L. M. Smith and H. M. McConnell, Department of Chemistry, Stanford University, Stanford, CA 94305, and E. W. Heinzelmann, M. J. Ruebush and J. W. Parce, Departments of Microbiology and Immunology, and Biochemistry, Bowman Gray School of Medicine, Winston-Salem, NC 27103.

Fluorescein-conjugated murine histocompatibility antigen (H-$2K^k$) and/or G protein of vesicular stomatitus virus have been reconstituted into cell-size liposomes by a new technique. It is shown that these liposomes can elicit H-2 restricted, syngeneic, anti-viral cytotoxic T cells, as assayed by ^{51}Cr release from appropriate virally infected target cells. Fluorescence recovery after photobleaching was used to measure the lateral diffusion coefficients of fluorescein-conjugated H-$2K^k$ or fluorescein-conjugated G protein in the presence or absence of unlabeled G or H-$2K^k$, respectively. The same rate of lateral diffusion ($D \sim 1 \times 10^{-8}$ cm^2/sec at 37°C in 25% cholesterol and 75% dimyristoylphosphatidylcholine) was obtained in every case. Both proteins, fluorescent as well as non-fluorescent, could be patched using specific antibodies. When G was patched with antibody, FITC-H-$2K^k$ did not copatch. When H-$2K^k$ was patched with antibody, FITC-G did not copatch. These diffusion and patching measurements rule out the possibility that these proteins undergo extensive oligomeric associations or have strong specific pairwise associations. These results place restraints on models of H-2 restricted recognition of virus-infected cells by pre-cytotoxic T cells.

This work has been supported by National Institutes of Health Grant Nos. 5R01 AI13587 (HMMcC) and 1R01 AI 16810 (JWP), and by National Science Foundation Grant No. PCM 79-22937 (JWP).

T-PM-G12 COMPARATIVE IMMUNOLOGICAL STUDIES OF TRANSVERSE TUBULE MEMBRANE FROM RABBIT SKELETAL AND CARDIAC MUSCLES. Mario S. Rosemblatt. Department of Muscle Research, Boston Biomedical Research Institute, Boston, Ma. 02114

Specific antibodies prepared against purified T-tubule membranes from rabbit skeletal muscle (Rosemblatt et al., JBC, 256, 8140, 1981) have been used as a tool for identifying a T-tubule membrane fraction obtained from cardiac muscle. Microsomes prepared from rabbit left ventricle were separated into four fractions by centrifugation in a discontinuous sucrose density gradient. Results obtained using a quantitative immunoassay (ELISA) showed that the lightest fraction (Fr. IV) ($d \leq 1.09$) but not the others (e.g. SR) cross-reacts significantly with the anti-skeletal T-tubule antibodies. Immunoabsorbant affinity column chromatography followed by SDS polyacrylamide gel electrophoresis showed that of the several (5-7) protein antigens recognized in the skeletal T-tubule membrane three are also present in Fr. IV of the rabbit cardiac microsomes. Similar results have been obtained from a comparative analysis of the protein antigens from various skeletal and cardiac fractions after transfer of the protein bands from SDS polyacrylamide gels onto nitrocellulose sheets. Detection of the cross-reacting antigens has been accomplished by indirect immuno-staining using a lactoperoxidase coupled antibody. These results suggest that we have isolated a membrane fraction from cardiac muscle (Fr. IV) highly enriched in membranes of T-tubule origin and that the T-tubule membranes from both skeletal and cardiac muscles share some common protein components. Further studies directed at characterizing the cross-reacting antigens are being pursued with the use of monoclonal antibodies prepared against the skeletal T-tubule membrane. (Supported by HL-27229)

T-PM-Po1 IMPEDANCE PROPERTIES OF THE RABBIT DESCENDING COLON. N. Wills and C. Clausen*. Dept. of Physiology, Yale Univ., New Haven, Ct. and *Dept. of Physiology and Biophysics, S.U.N.Y. Stony Brook, Stony Brook, N.Y.

Impedance studies were performed on isolated segments of colon to investigate K^+ transport mechanisms in this epithelium.Impedance was measured by injecting a binary pseudo-random current signal and measuring the voltage response. The data were digitized and subjected to Fourier analysis with the aid of a laboratory computer. The data were best fitted by a morphologically-based distributed model which takes into account the geometry of colonic crypts. To permit calculation of individual membrane resistances and areas, junctional resistance was measured using an independent method. Estimated values for five tissues bathed on both sides with control Ringer's solution ($NaCl-HCO_3$) were as follows: apical membrane resistance (R_a)= 510± 170 ohm cm^2, basolateral membrane resistance (R_{bl})=97± 18 ohm cm^2, apical membrane capacitance (C_a)=17±3.9 $\mu F/cm^2$, basolateral membrane capacitance (C_{bl})= 9.4 ±1.4 $\mu F/cm^2$, and crypt series resistance =17± 0.7 ohm cm^2. After replacement of the mucosal bath with K_2SO_4 Ringer's solution, R_a increased to only 940± 250 ohm cm^2 (n=5), suggesting that the apical membrane has a significant potassium conductance in addition to its known Na^+ permeability. These findings are compared to available microelectrode data and discussed in relation to potassium transport mechanisms in this epithelium.(Supported by N.I.H. grants # AM29962 to N.K.W. and AM28074 to C.C.)

T-PM-Po2 CHLORIDE TRANSPORT IN THE GLANDS OF THE FROG SKIN Ian G. Thompson & John W. Mills (Intr. by Alexander Leaf) Renal Unit, Massachusetts General Hospital, Boston, MA 02114

Ion transport in the glands of the frog skin has been studied using conventional short-circuit current (SCC) and isotope exchange techniques. After inhibition of the epithelial Na^+ transport with amiloride (10^{-4}), a small current signal equal to 7.0 ± 0.5 μA/cm was elicited by the addition of isoproterenol (9 x 10^{-7}M) to the serosal side. That this SCC is due to transport events occurring in the glands is suggested by observations on gland-free preparations (glands removed by enzymatic splitting of the skin) in which the isoproterenol (ISO) induced SCC is absent. We have shown that this glandular SCC is Na^+-dependent, Cl^--dependent, and inhibitable by ouabain (Thompson & Mills, Am. J. Physiol. in press). In the present study the effects of varying external Cl^- concentration, addition of exogenous cAMP, and furosemide on SCC were examined. The relationship between extracellular Cl^- concentration and SCC conformed to simple Michaelis-Menton kinetics with K_m = 34.4 mM and V_{max} = 14.4 μA/cm . The addition of dibutyryl cAMP (0.1 mM) and IBMX (0.25 mM) to the serosal side increased the glandular SCC from 1.9 ± 0.6 to 12.3 ± 1.9 $\mu A/cm^2$ mimicking the action of ISO. Furosemide (1 mM) added to the serosal side blocked the ISO induced increase in SCC. The bidirectional fluxes of Na^+ and Cl^- were also examined in the frog skin glands. ISO elicited net serosa-to-mucosa fluxes of both Na^+ and Cl^- equal to 0.19 ± 0.05 and 0.57 ± 0.05 μeq/cm^2/hr respectively. The residual ion flux (Cl^- flux minus Na^+ flux) of 0.38 ± 0.05 μeq/cm^2/hr closely approximates the ISO stimulated SCC of 0.30 ± 0.04 μeq/cm^2/hr. Furosemide inhibited the net fluxes of both Na^+ and Cl^-. We conclude that an active Cl^- transport mechanism is responsible for the ISO induced SCC in the glands of the frog skin.

T-PM-Po3 ANOMALOUS PATTERNS IN CULTURED CELL MONOLAYERS,E.M.Adler,L.J.Fluk, and J.M. Mullin,(Intr. by A. Kleinzeller),University of Pennsylvania School of Medicine Department of Physiology,Philadelphia,Pennsylvania 19104

Grid-like patterns of differing cell density were observed in evenly seeded cell monolayers, with areas of heavy cell growth surrounding patches of low cell density. The pattern of cell growth corresponded to the structure of the incubator tray on which the culture dishes had been placed during incubation, with the areas of low density corresponding to holes in the tray and the areas of higher density corresponding to the metal framework. The phenomenon appears to involve small transient temperature differences between the metal portion of the tray and the holes. These were detected by means of sheets of thermophotochromic liquid crystals, temperature sensitive in the range of 30-40°C, placed on the incubator tray. The time course of pattern appearance (less than one hour) implicates attachment or sedimentation rather than cell growth as the critically affected factor. Patterning appears to be independent of specific growth substratum, type of culture vessel, ans specific incubator and/or tray design. Patterns were observed in five cell lines (LLC-PK_1, LLC-RK_1, MDCK, RK_{13}, and primary hamster embryo fibroblasts) of six tested, suggesting widespread occurrence. The unsuspected presence of such patterning could have significant impact on various aspects of cell culturing. Support by NIH grant AM12619-13 (to A.K.) NIH fellowships HL07027-07 (to J.M.) & PHS 2T32GM07229-07 (to E.A.) and the Whitehall Foundation (to A.K.).

T-PM-Po4 SPONTANEOUSLY FLUCTUATING K^+ CHANNELS IN THE APICAL AND BASOLATERAL MEMBRANES OF THE COLON. N. Wills, W. Van Driessche* and W. Zeiske*. Dept. Physiol., Yale Univ., and * Lab. voor Fysiologie, K.U.L., Leuven, Belgium.

Two sources of K^+ channel noise were identified in the rabbit descending colon using current fluctuation analysis. The first source was seen in the presence of transepithelial potassium gradients. The spectral density revealed a Lorentzian-type noise (corner frequency, f_c= 16± 0.9 Hz and plateau value, S_o= 7.0×10^{-20}± 2.94×10^{-20} A^2s/cm^2) and a steep low frequency component below 5 Hz (slope=1.5± 0.94). S_o values responded to changes in the net driving force for potassium and were depressed by mucosal addition of the K^+ channel blocking agents Cs^+ and TEA. Reduction of the apical membrane resistance by mucosal addition of nystatin abolished the Lorentzian component; serosal addition had no effect. These data suggest the existence of spontaneously fluctuating K^+ channels in the apical membrane in parallel with the Na^+ transport pathway. A second Lorentzian was seen after further increasing the nystatin concentration at the apical membrane. This Lorentzian showed a f_c=201± 59 Hz and S_o= 3.1×10^{-21}± 1.40×10^{-21} A^2s/cm^2. S_o was decreased after serosal addition of Ba^{2+}. This signal appears to arise from the basolateral membrane. Comparison of apical and basolateral membrane K^+ channels may reveal new information concerning the different roles of these two membranes in transepithelial ion transport. (Supported by N.I.H. grant #AM29962 to N.K.W.)

T-PM-Po5 IDENTIFICATION OF THE CELL TYPES OF THE ELECTRICAL POTENTIAL PROFILE IN THE FROG SKIN EPITHELIUM. R.L. Duncan* and J.T. Blankemeyer, Dept. of Physiological Sciences, Oklahoma State University, Stillwater, OK. 74078.

The electrical potential profile of the frog skin epithelium has been studied by many investigators but most agree that there are only two potential steps when impaling from the pond side of the tissue. The first step is highly negative when referenced against the pond side bathing solution while the second step is a positive step (W. Nagel, Pflugers Arch. 365; 1976). Voute and Hanni (Transport Mechanisms in Epithelia. Copenhagen: Munksgaard, 1973), however, have shown four cellular layers in this epithelium by using light and electron microscopy.

A histological identification was made of cell types based on their cellular membrane potential utilizing microelectrodes backfilled with Lucifer Yellow CH dye and KCl. The dye was iontophoretically injected into a cell which exhibited a particular membrane potential. Using this technique three cell types were found. When impaling from the pond side of the tissue, the first step is -4 to -10 mV with the dye being observed in the region of the stratum corneum. The second step ranges from -47 to -80 mV with the dye being observed in the region of the stratum granulosum. The third step is positive and ranges from +5 to +25 mV. The dye has been observed to be in the region corresponding to the stratum spinosum, although the line of demarcation between the spinosum and the germinativum layers is unclear.

T-PM-Po6 MEMBRANE POTENTIALS AND CONDUCTANCE RATIOS IN FROG SKIN. W. Nagel and A. Essig, Depts. of Physiology, University of Munich, W. Germany, and Boston University, Boston, MA 02192.

Previous studies in anuran epithelia have shown that after clamping the transepithelial voltage in symmetrical sequences for 4-6 minutes there is near-constancy of the rate of active Na transport and the associated oxidative metabolism, with a near-linear potential-dependence of both. We have here investigated in frog skin cellular electrophysiological events associated with voltage-clamping (V_t ≡ inside-outside potential). Increase and decrease of V_t produced converse effects, related directly to the magnitude of V_t. Hyperpolarization resulted in prompt decrease in inward transepithelial current I_t and increase in fractional outer membrane resistance fR_o and in outer membrane potential V_o. Overshoot of V_o was followed by relaxation to a quasi-steady state in minutes. Changes in fR_o were progressive, with half times of some 2-10 sec. Changes in transepithelial conductance g_t, evaluated by small and brief superimposed perturbations of V_t, were more variable, usually preventing precise evaluation of the outer and inner cell membrane conductances g_o and g_i. Nevertheless, it was shown that g_o is related inversely to V_t and V_o. Presuming insensitivity of g_i to V_t, the dependence of g_o on V_o in the steady state much exceeds that predicted by the constant field equation. Apparent inconsistencies with earlier results of others may be attributable to differences in protocol and the complex dependence of g_o on V_o and/or cellular current. In contrast to previous findings in tight epithelia at open circuit, differences in V_t were associated with substantial differences in fR_o and inner membrane potential V_i. Hyperpolarization of V_t over ranges commonly employed in studies of active transport and metabolism appears to increase significantly the electrochemical work per unit rate of Na transport.

T-PM-Po7 EFFECTS OF CYTOCHALASIN B ON SODIUM AND FLUID TRANSPORT, PASSIVE PERMEABILITY PROPERTIES AND STRUCTURE OF RAT JEJUNUM. M. M. Cassidy, M. Dinno and G. Vahouny. The George Washington University Medical Center, Washington, DC and the Univ. of Mississippi, Oxford, MS.

The relationship of certain cytoskeletal components to normal salt and water absorptive processes was studied in an in vivo perfused jejunal preparation utilizing Cytochalasin B (CB) as a microfilament disruptive agent. Labelled polyethylene glycol (MW=4000) and erythritol were used to monitor fluid, and passive permeability characteristics respectively. Sodium movement was determined by flame photometric analysis of luminal perfusates. 10^{-5} M CB, dissolved in DMSO, in the mucosal fluid, reduced steady state fluid absorption from 80±4.1 to 48±5.2 µl/min/g dry wt. and that of sodium from 18+6±6.2 to 9 6±4.7 µmol/min/g dry wt. The DMSO vehicle, per se, had a small effect in reducing absorptive rates. Inhibition of absorption was evident at 30 minutes following exposure and was maximal at 60 minutes. The degree of inhibition was more pronounced when 28 mM glucose was present in the balanced electrolyte perfusate. Passive permeability characteristics, as measured by erythritol loss from the mucosal fluid, was significantly enhanced at 60 minutes after exposure to CB. At this time, electron microscopy of the jejunal microsurface revealed mild disarray of the microfilaments within the brush-border, significant abnormal widening of the enterocyte junctional regions and the presence of thread-like structures on the mucosa with dimensions characteristic of microfilaments. These results suggest a role for microfilaments in intestinal absorptive function. The effects appear to be both intracellular and paracellular in nature but the observed inhibition cannot be apportioned between transcellular and paracellular transport pathways because of the experimental design.
(Supported by ONR Contract # N00014-79-C-0603).

T-PM-Po8 SODIUM AND AMILORIDE COMPETITION IN APICAL MEMBRANE CHANNELS: A 3-STATE MODEL FOR NOISE. S. Machlup, T. Hoshiko, Case Western Reserve Univ., and E. Frehland, Univ. Konstanz. (Intr. by Ronald C. Rustad.)

The corner frequency of the Lorentzian spectrum of amiloride or triamterene-induced fluctuations in sodium current through frog skin falls with increasing [Na] [Hoshiko and Van Driessche (1981) Arch. Internat. Physiol. Biochim. (In press)]. This suggests a mechanism in which entry of the blocker is inhibited by the presence of Na in the Na-selective channel: i.e., they compete for binding sites. The simplest open/closed model for the channel noise thus considers 3 states of the channel: empty/one sodium inside/amiloride-blocked. The full DC current is assumed to stop flowing only when the channel is amiloride blocked. The corner frequency of the Lorentzian spectrum predicted by such a model increases linearly with amiloride concentration A with a slope which is a decreasing function of [Na]: $f_c = f_{co}[1+a/(1+s)]$, where $a=A/K_A$ and $s=[Na]/K_S$. The predicted noise power goes as $a(1+s)^2/(1+a+s)^2$. It peaks at $a=\frac{1}{2}(1+s)$. Values of K_A and K_S obtained from steady-state current measurements [Cuthbert and Shum (1974) Naunyn-Schmiedeberg's Arch. Pharmacol. 281, 261-269] are roughly consistent with the noise data. To explain the observed saturation of the channels at high [Na] (sodium self-inhibition) one can postulate that two sodium ions in the channel can trigger "channel clogging" lasting several seconds. The noise spectrum predicted by such a 4-state model is scarcely different from that of the 3-state model for frequencies of interest (1 to 1000 Hz).

Supported in part by NIH Grant AM05865-13.

T-PM-Po9 CURRENT FLUCTUATIONS IN FROG SKIN ARE DUE TO APICAL SODIUM CHANNELS: MORE EVIDENCE. T. Hoshiko and W. Van Driessche. Dept. of Physiology, Case Western Reserve University, School of Medicine, Cleveland, OH 44106 and Labo, voor Fysiologie, Campus Gasthuisberg, K.U.L. B-3000 Leuven, Belgium.

Amiloride and triamterene-induced fluctuations vary with voltage-clamp level. These effects were studied in abdominal skin of R. temporaria and provide further evidence that they arise from a Na channel mechanism at the apical membrane (cf. Lindemann and Van Driessche, Science (1977) 195: 292; Nature (1979) 282:519). Skins bathed in NaCl Ringer's were treated with 1 µM amiloride in 20 or 40 mM NaCl. Steady-state currents and Lorentz-type spectra were obtained. The spectra for a given preparation showed very little change in the corner frequency but the plateaus (S_O) were dependent upon the current. Lorentzian spectra were rarely obtainable when the clamp level resulted in reversal of the current. Under such conditions, low frequency noise predominated. Log-log plots of the plateaus versus the clamp currents were examined and the slopes averaged to 1.74. A carrier model predicts a slope of unity, whereas a channel model predicts a slope of 2. These data therefore provide further evidence that the amiloride-blockable apical sodium permeation pathway involves a channel mechanism. The simple two-state blocking-unblocking model of amiloride action on a pore predicts that the low frequency plateau (S_O) should peak at a blocking agent concentration equal to one-half the inhibition constant (K_I). Such a maximum has been observed in trianterene-induced current fluctuations (Hoshiko and Van Driessche (1981) Arch. Internat. Physiol. Biochim. (in press)), again bolstering the channel model of apical sodium permeation. (Supported by grants from the Onderzoeks fonds. K.U.L. and PHS AM 05865).

T-PM-Po10 IONIC CONDUCTIVITY OF THE GASTRIC MUCOSA WITH HYPEROSMOTIC SECRETORY MEDIA.
Villegas, L. (Introd. by Sananes, L.) Centro de Biofísica y Bioquímica, IVIC, Apartado 1827, Caracas 1010A, Venezuela.

In isolated frog gastric mucosa the unidirectional water diffusion fluxes are significantly reduced by the use of hyperosmotic secretory solution at the mucosal surface with isosmotic nutrient solution at the serosal surface. In the absence of solute/solvent interaction able to develop a driving force responsible for these changes, an effect is required in the total water conductivity across the mucosa. Ionic conductivity of the serosal and the mucosal surfaces of the main cell types were explored by measuring the intracellular potential changes induced by transmucosal current flow. In mucosae maintained in nutrient and secretory isosmotic solutions (220 mOsm/Kg water) the ratio of the mucosal-to-serosal potential changes produced by transmucosal current flow were 2.2 ± 0.3 (22) in the epithelial cells and 4.0 ± 0.3 in the oxyntic cells. When the tonicity of the secretory solution was increased to 416 mOsm/Kg water, by adding 200 mmol of glucose, the ΔV ratios obtained were 2.9 ± 0.3 (24) and 4.4 ± 0.3 (20) for the epithelial and oxyntic cells respectively. The same 100 $\mu A/cm^2$, 1 sec, current pulses used for these measurements induced transmucosal potential changes of 26 ± 1 and 32 ± 1 mV across the mucosa when isosmotic and hyperosmotic secretory solutions were used. This significant ($P < 0.001$) reduction in the total ionic conductivity, simultaneous with the reduction in water conductivity, is the result of changes in both surfaces of the main cell types. Use of hyperosmotic secretory solution does not produce a significant change in the ratio of the mucosal-to-serosal potential changes induced by transmucosal current flow.

T-PM-Po11 DIFFERENCES IN BIOLOGICAL AND CHEMICAL PROPERTIES AMONG TUBULIN SUBSPECIES. Deborah J. Field. Dept. of Biochemistry, St. Louis University School of Medicine, St. Louis, Mo. 63104.

Purified calf brain tubulin can be resolved into at least 17 individual subspecies when subjected to isoelectric focusing (IEF). This polymorphism appears to be conserved regardless of the source of brain tissues tested, eg., calf, lamb, rabbit, dog, rat. The distribution of these tubulin subspecies in several brain sections were studied. Results from IEF experiments show that all 17 subspecies found in whole brain are qualitatively represented in cerebrum, cerebellum, medulla and caudate nucleus but that the mass distribution of these subspecies is dependent upon the brain region. The distribution and identity of tubulin subspecies from non-neuronal tissues were also studied. Results show that tubulin from lamb liver, kidney and spleen contain 9-11 subspecies. Furthermore, they demonstrate the same isoelectric points (pI) as some of those from the brain. The chemical identity of these subspecies with the same pI was tested by two dimensional tryptic peptide maps.

The functional significance of these subspecies was tested by using a colchicine affinity column. An apparent difference in binding affinity among these subspecies has been detected.

T-PM-Po12 THE STRUCTURE OF THE LEUKOCYTE CYTOSKELETON AND PURE CYTOSKELETAL PROTEIN GELS
R. Niederman. Harvard School of Dental Medicine and the Mass. Gen. Hosp., Boston, MA.

Sol-gel transitions in cortical cytoplasm may be important for cell movement. I therefore evaluated the structure of polymorphonuclear leukocyte (PMN) cytoskeleton, and gels formed from purfied cytoskeletal proteins. Cells and gels were examined with the transmission EM.

In stationary PMNs, a lattice (gel) of short, highly branched, actin filaments is observed. In motile PMNs three actin configurations are observed: (1) a highly branched actin lattice; (2) actin bundles; and (3) a combination of both. Few free filament ends are observed.

Previous work has demonstrated that actin and actin binding protein occur in the leukocyte cytoplasm in a mole ratio of 50:1 (A:ABP), and that they form a rigid gel in-vitro. I therefore examined pure actin and ABP in a mole ratio of 50:1. This protein mixture exhibits a highly branched lattice. The lattice is formed of single short actin filaments with a spacing of 250-500 nm between branch points. Few free filaments ends are seen. This array is strikingly similar to cortical cytoplasm. At higher concentrations of ABP (A:ABP=25.1) the mixture forms an array of branching and bundling actin filaments. These bundles contain from 5 to >10 actin filaments. Again, these bundles are strikingly similar to cytoplasmic bundles. Actin alone at similar concentrations does not form this lattice. Instead, pure actin forms long unbranched filament meshes of undetermined length.

These results: (1) provide the first three dimensional visualization of cytoplasmic protein gels; (2) provide a basis for the development and testing of hypothesis regarding sol-gel transformations which may effect cell motility; and (3) allow us to test the polymer gel theory of Flory as it relates to cytoplasmic gels.

T-PM-Po13 A SPIN LABEL STUDY OF THE MEMBRANE FLUIDIZATION OF HUMAN ERYTHROCYTE IN DISCOCYTE-STOMATOCYTE TRANSFORMATION. S. NOJI, T. TAKAHASHI, and H. KON, NIADDK, National Institutes of Health, Bethesda, MD 20205.

A normal human erythrocyte has a biconcave shape (discocyte), which is easily transformed into a cup form (stomatocyte) by addition of various cationic amphiphilic agents. Sheetz and Singer (Proc. Natl. Acad. Sci. U.S.A., 71, 4457 (1974).) proposed the bilayer couple hypothesis as an explanation of the stomatocyte formation. However, Brailsford et al. (J. Theor. Biol., 86, 531 (1980).), in their theoretical studies, found that the stomatocyte formation could not be explained by the bilayer couple hypothesis, but that the stomatocyte would result from a loss of bending resistance of the membrane caused by a sliding of the inner and outer leaflets of the lipid bilayer over one another. Then, they predicted that the action of stomatocytogenic substances such as chlorpromazine should be to increase the fluidity of the hydrophobic interior of the lipid bilayer so that the sliding becomes facilitated. In the present study, we attempt to see if their prediction of the fluidity increase as a step in the discocyte-stomatocyte transformation has an experimental support. Using a spin-label ESR method, we measured the change in the membrane fluidity of stomatocytes induced according to the five qualitatively different methods reported in the past: (1) addition of cationic agents; (2) addition of non-ionic agents; (3) lowering the pH; (4) depleting the membrane cholesterol; (5) treatment with an enzyme phospholipase C. The results appear to support the theoretical prediction proposed by Brailsford et al. Based on the present experimental results as well as their theoretical model, we discuss plausible mechanisms for the discocyte-stomatocyte transformation.

T-PM-Po14 MAINTENANCE AND TURN-OFF OF ADH-INDUCED WATER FLOW: ROLE OF MICROFILAMENTS, R.H. PARSONS, R.J. BRADY, L.M. COLUCCIO, BIOL. DEPT. R.P.I., TROY, N.Y. 12181

The ADH-induced water flow was shown to be stable (no flow attenuation, i.e., turn-off, occurred) in the absence of a trans-tissue osmotic gradient during pressure treatment or ADH washout (hormone removal). In the presence of a trans-tissue osmotic gradient however, the ADH-induced water flow was unstable; a significant and rapid attenuation of water flow occurred during pressure treatment or washout. In the presence of an osmotic gradient, a reparable pressure-sensitive element (6,000 psi produced less of a flow attenuation than 8,000 psi) was necessary to maintain the ADH-induced water flow. Simultaneous application of pressure treatment (8,000 psi) and ADH washout caused only a modest slowing of turn-off. Sequential application of pressure and ADH washout caused a complete, transient, inhibition (8,000 psi) or slowing (6,000 psi) of turn-off. These data support a model for ADH turn-off which incorporates an active step-the dismantling of a stabilizing element, possibly microfilaments, - and a passive step-the dissipation of water flow sites, very likely aggregates of intramembranous particles.

T-PM-Po15 SPECIFIC LOCALIZATION OF SCALLOP GILL EPITHELIAL CALMODULIN IN CILIA. E. W. Stommel, R. E. Stephens, H. R. Masure, and J. F. Head, Marine Biological Laboratory, Woods Hole, MA 02543 and Department of Physiology, Boston University School of Medicine, Boston, MA 02118.

Calmodulin has been isolated and characterized from the gill of the bay scallop Aequipecten irradians. Quantitative electrophoretic analysis of epithelial cell fractions shows most of the calmodulin to be localized in the cilia, specifically in the detergent-solubilized membrane-matrix fraction. Calmodulin represents 2.2 ± 0.3% of the membrane-matrix protein or 0.41 ± 0.05% of the total ciliary protein. Its concentration is at least 10^{-4} M if distributed uniformly throughout the matrix. Extraction in the presence of calcium suggests that the calmodulin is not bound to the axoneme proper. The ciliary protein is identified as a calmodulin on the basis of its calcium-dependent binding to a fluphenazine-Sepharose affinity column and its co-migration with bovine brain calmodulin on alkaline-urea and SDS polyacrylamide gels in both the presence and absence of calcium. Scallop ciliary calmodulin activates bovine brain phosphodiesterase to the same extent as bovine brain and chicken gizzard calmodulins. The amino acid composition is typical of known calmodulins but it is less acidic, in agreement with an observed isoelectric point approximately 0.2 units higher than bovine brain calmodulin. Comparative tryptic peptide mapping indicates over 75% coincidence of major peptides. ATP-reactivated gill cell models are not affected by calcium in the micromolar range but ciliary arrest will occur at calcium levels in excess of 150 μM. Since calmodulin usually functions in the micromolar range, its role in this system is unclear. It may be involved in the direct regulation of tubule sliding or it may serve some coupled calcium transport function but, at 10^{-4} M, it must at least act as a calcium buffer.

T-PM-Po16 SPECIFICITY FOR CHEMOTACTIC RESPONSIVENESS IN CARCINOSARCOMA CELLS John A. Wass, James Varani and Peter A. Ward. Department of Pathology, University of Michigan Medical School, Ann Arbor, Michigan 48109

A large data base has accumulated concerning the nature of the interaction between chemotactic factors and the cell surface receptors in polymorphonuclear leukocytes (PMNs) but very little analagous data has been collected for non-leukocytic cells. As part of our ongoing studies concerning the responsiveness of Walker 256 carcinosarcoma cells to chemotactic factors we have examined the specificity of the chemotactic peptides which elicit these responses. The leukocyte chemotactic peptide n-formyl-methionyl-leucyl-phenylalanine (f-met-leu-phe) has been found to elicit a variety of biologic responses in these tumor cells as well as in PMNs. We have examined 11 peptides that possess structural similarity to the parent compound. Responsiveness was measured in four assays: chemotaxis, cell swelling, foreign surface adherence and lectin-receptor mobility. The responses of the tumor cells were found to be highly specific for f-met-leu-phe as only one of the analogs (n-formyl-methionine) had any effect in any of the assays, and this response was greatly diminished compared to that of the parent compound. Correlation between responsiveness (or lack of) was excellent between the four systems. These results suggest the presence of a receptor for the chemotactic peptide and furthermore infer a high degree of specificity. This work was supported in part by NIH grants CA29550 and CA29551

T-PM-Po17 THE TERMINAL PIECE OF CIONA SPERM FLAGELLA. Charles J. Brokaw and Charlotte K. Omoto, Division of Biology, California Institute of Technology, Pasadena, CA. 91125.

Light and electron microscope observations of the terminal piece at the distal end of the Ciona sperm flagellum indicate an abrupt transition from the 9+2 axoneme to a much thinner terminal piece, with uniform diameter over most of its length of about 7 μm. The internal structure in many cases appears to be a simple extension of the two central pair microtubules, surrounded by a membrane. These observations suggest that the bending resistance of the terminal piece should be approximately an order of magnitude less than that of the 9+2 axoneme. On the other hand, the hydrodynamic drag on a cylinder is only a slowly varying function of diameter.

Photographs showing the shapes of bends at the distal end of a swimming Ciona spermatozoan do not show any obvious discontinuity in curvature at the junction between the terminal piece and the 9+2 axoneme. Computer simulations in which the bending resistance of the terminal piece is 1/10 of the bending resistance of the 9+2 axoneme show behavior that is obviously different from the photographs. Computer simulations in which the bending resistance of the terminal piece decreases gradually from the transition region to the tip come closest to reproducing the observed movement, but this graded bending and resistance appears to be inconsistent with our ultrastructural observations. (Supported by GM 18711, GM 21931, and F32-GM07445.)

T-PM-Po18 NEW GAP JUNCTION STRUCTURAL FEATURES REVEALED BY LOW-IRRADIATION ELECTRON MICROSCOPY. T.S. Baker, C. Hollingshead, D.L.D. Caspar, Rosenstiel Basic Medical Sciences Research Center, Brandeis University, Waltham, MA, and D.A. Goodenough, Harvard Medical School, Department of Anatomy, Boston, MA.

Micrographs of negatively-stained mouse liver gap junctions, recorded using low and normal irradiation procedures, and processed by Fourier techniques, reveal new substructural features not previously observed in other gap junction preparations. The typical "high-dose" image reconstruction shows large connexons usually with little evidence of substructure except for the prominent central staining region. The connexons have circular or hexagonal profiles with a diameter about 70Å. The Fourier averaged reconstructions of images recorded with "minimal" exposure consistently reveal connexons with smaller outer dimensions (~60Å), clearly resolved six-fold substructure and significant amounts of stain-excluding matter on the crystallographic three-fold position of the unit cell. In high-dose images, the matter at the three-fold positions disappears or is obscured by stain that has migrated to this area. A three-dimensional reconstruction from tilted and minimally irradiated specimens will provide a clearer understanding of the nature of these new gap junction structural features. (Supported by Charles A. King Trust Fellowship to T.S.B. and NIH grant CA15468 to D.L.D.C.)

T-PM-Po19 REVERSIBLE GAP JUNCTION CRYSTALLIZATION AND ELECTRICAL UNCOUPLING BY HEPTANOL. Giovanni Bernardini, Camillo Peracchia, and Lillian L. Peracchia. Department of Physiology University of Rochester, Rochester, New York.

An increase in tightness and crystallinity of gap junction particle packing has been shown to parallel cell-to-cell electrical uncoupling (Peracchia. Int. Rev. Cytol. 66:81, 1980). The junctional changes and electrical uncoupling are believed to be mediated by a calmodulin-like protein (Peracchia, et al., J. Cell,Biol. 91:124a, 1981). Recently Johnston, et al. (Nature. 286:498, 1980) have shown that heptanol and other similar molecules reversibly uncouple crayfish axons. To test whether or not gap junction crystallization closely parallels heptanol uncoupling, membrane resistance and coupling ratio were measured in Xenopus embryo cells superfused with Ringer solutions with or without 3.5 mM heptanol. A sharp decrease in coupling ratio occurred 10-15 min after the beginning of heptanol treatment and full recovery occurred 15 min after heptanol removal During heptanol treatment the membrane potential decreased slightly. After recoupling, the cells had normal electrical properties including their usual sensitivity to CO_2 uncoupling. The gap junctions of several vertebrate tissues were studied by freeze-fracture electron microscopy after 5, 10, 15, 20 min of heptanol treatment and 15 min after heptanol removal. The junctional particles became closely packed into small crystalline domains at the onset of uncoupling (~10 min)and became disordered, like controls, when electrical recoupling was complete (15 min after heptanol removal). The heptanol effect may be indirect (Ca++-mediated ?) because isolated lens junctions do not crystallize in heptanol-EDTA solutions at pH 7.4, although these junctions crystallize in intact lenses upon incubation in the presence of heptanol. (Supported by NIH grant GM 20113).

T-PM-Po20 CONTROL OF INTERCELLULAR COMMUNICATION BY VOLTAGE DEPENDENCE OF JUNCTIONAL CONDUCTANCE, A.L. Harris, D.C. Spray and M.V.L. Bennett, Div. Cellular Neurobiol., Dept. Neuroscience. Albert Einstein Col. Med., Bronx, N.Y. 10461.

We have recently described and characterized under voltage clamp the voltage dependence of the conductance of gap junctions between amphibian blastomeres (Spray et al., J. Gen. Physiol. 77: 77, 1981; Harris et al., ibid. 77: 95, 1981). In these cells, junctional conductance is a steep function of transjunctional voltage, being maximal at zero transjunctional voltage and decreasing symmetrically with transjunctional voltages of either polarity. Current clamp experiments and mathematical modelling using parameters obtained under voltage clamp show that voltage dependence of junctional conductance can give rise to regions of negative slope and bistability in the current-voltage relations of pairs of coupled cells, and that current transients (applied or intrinsic) can evoke regenerative and sustained changes in coupling under appropriate conditions. Boundaries of coupling within a population of cells may be altered by changes in intrinsic or applied current. Properties of nonjunctional membrane (e.g., resistance, ionic selectivity, electrogenic pump activity) can alter the voltage-current relations of coupled cells, and thus the thresholds for and stability of the changes in coupling, as well as the width of the region of bistability. Under specific conditions, cells can be coupled uniformly, coupled as small groups, or isolated from one another depending on the passive and active properties of the junctional and nonjunctional membranes. The plasticity of coupling allowed by voltage dependence of junctional conductance may be important in determination, differentiation and development of embryonic tissues in amphibia.

T-PM-Po21 INCREASE OF PERMEABILITY IN CELL JUNCTION BY HORMONE STIMULATION. Aurelian Radu* and Werner R. Loewenstein, Department of Physiology and Biophysics, University of Miami School of Medicine, Miami, FL 33101.

Elevation of the endogenous cyclic AMP concentration (by supplying cells with cAMP or inhibiting their phosphodiesterase) promotes new cell-to-cell channel formation and hence increase in junctional permeability in various mammalian cell types (1). Thus, in cells with receptors (r) linked to the adenylate cyclase system so as to produce elevation of [cAMP] upon hormone (s) binding, one would expect an increase in junctional permeability according to the scheme:

$$s + r \rightarrow \uparrow [cAMP] \rightarrow \uparrow \text{ number of cell-to-cell channels (2).}$$

We show here that this scheme, indeed, applies to a cell system with β-adrenergic receptors, the rat glioma line C6: treatment with isoproterenol (7 or 100 μM; cell density constant), within 6.75 and 9 hours, leads to increase in cell-to-cell transfer of fluorescent mono- or diglutamate (lissamine rhodamine B-labelled).

(1) Flagg-Newton, J.L., Dahl, G., Loewenstein, W.R. J. Membr. Biol. 63:105-121, 1981
(2) Loewenstein, W.R. Physiol. Rev. 61:829-913, 1981

*Fulbright-Hays International Research Scholar

T-PM-Po22 KINETICS OF INTRACELLULAR AND CELL-TO-CELL (TRANSJUNCTIONAL) DIFFUSION OF FLUORESCENT TRACERS. A. L. Zimmerman & B. Rose. Dept. of Physiol. & Biophys., U. of Miami Sch. Med., Miami, FL 33101.

We have analyzed the kinetics of fluorescent tracer diffusion within and among cells of Chironomus salivary glands by monitoring fluorescence intensity simultaneously at two locations, using a dual-wavelength microfluorometer. We measured fluorescence intensity of two different tracers simultaneously, both at the site of injection and in an adjacent cell or at the opposite edge of a single cell. The tracers included lissamine rhodamine B (LRB), carboxy-fluorescein (CO-F), and peptides labelled with LRB or FITC. For a single cell, the decay of fluorescence intensity of a given tracer at the site of injection was well described by the sum of two exponentials: a rapid component, presumably representing intracellular diffusion, with a time constant on the order of tens of seconds; and a slow component, presumably representing loss from the cell, with a time constant on the order of tens of minutes. For a cell pair or whole gland, the decay of fluorescence intensity at the injection site included a third exponential component with an intermediate time constant on the order of one to a few minutes. The values of these time constants differed for the various tracers used; for example, for CO-F (MW 376) all three components were about twice as fast as for LRB-GluTyrGlu (MW 982). Membrane depolarization, which reduces junctional conductance in these cells, reversibly abolished the intermediate component as well as the rise in fluorescence intensity in the adjoining cell. Thus, this component seems to represent the transjunctional flux and, for a given tracer and junction, its changes would reflect changes in junctional permeability.

T-PM-Po23 THREE-DIMENSIONAL STRUCTURE OF GAP JUNCTIONS. Lee Makowski, Dept. of Biochemistry, College of Physicians and Surgeons of Columbia University, N.Y., N.Y., 10032, D.L.D. Caspar and W.C. Phillips, Rosenstiel Basic Medical Sciences Research Center, Brandeis University, Waltham, Mass., 02254, and D.A. Goodenough, Dept. of Anatomy, Harvard Medical School, Boston, Mass. 02115.

X-ray diffraction patterns have been obtained from oriented specimens of gap junctions isolated from mouse livers with a protocol that uses the detergent Brij 58 and requires no exogenous proteases. The lattice constant of the two-dimensional hexagonal array of connexons varies between 74-84 A in junctions isolated with this protocol. Several specimens have been produced with sufficiently good orientation to allow measurement of diffraction data along lattice lines to 30A resolution using angular deconvolution. A three-dimensional electron density map was calculated from these intensities and the phase choice which produced the electron density map most consistent with the results of electron microscopy and the known bilayer structure of the membrane lipids. In this map the aqueous channel through the center of the connexon can be seen extending most of the way from the center of the gap to the cytoplasmic surface. The channel may not extend entirely through the junction to the cytoplasm. Analysis of diffraction patterns from isolated gap junctions in 50% sucrose shows that the sucrose fills the extracellular gap but fails to enter the channel. It is possible that the channel is closed at both cytoplasmic surfaces, excluding sucrose. This suggests that the isolated junctions are in a high resistance state.

T-PM-Po24 THE EFFECT OF PROTEIN REAGENTS ON THE GAP JUNCTIONS OF CRAYFISH SEPTATE AXONS.
A. Campos de Carvalho*+ and Fidel Ramón. Department of Physiology, Duke University Medical Center, Durham, N.C. 27710

Gap junctions contain hydrophilic channels that open or close as a result of conformational changes in the proteins that form them. Data from other channels suggest that specific groups in the proteins may be involved in those changes. To investigate the involvement of such specific groups, we tested the effects of protein reagents on gap junctions of crayfish axons. Experiments were conducted on intact septate axons of the crayfish abdominal nerve cord. The junctional resistance was measured using three, and sometimes four, microelectrodes; one for passing current pulses and the remaining for voltage recordings at both sides of the septum. Three types of drugs were used: sulfhydryl, amino and carboxyl group reagents. The sulfhydryl group reagents N-ethylmaleimide and p-chloromercuribenzoate produced uncoupling. Three other reagents in this group had no effect on junctional parameters, as well as three amino group reagents tested. Among the four carboxyl group reagents tried, only N-ethoxy carbonyl-2-ethoxy-1,2 dihydroquinoline produced uncoupling. The effects of the same drugs on closed channels were also tested by applying them to previously uncoupled axons. The results suggest that two essential groups, probably sulfhydryl and carboxyl in nature, are involved in closure of gap junctional channels through protein conformational changes.

(+Fellow of the CNPq, Brazil. This work was supported by NIH Grant HL22767.)

T-PM-Po25 IMPROVED ELECTRICAL COUPLING IN SMOOTH MUSCLE IS ASSOCIATED WITH INCREASED AREA OF GAP JUNCTION CONTACT.
Sims, S.M., E.E. Daniel and R.E. Garfield. Dept. of Neurosciences, McMaster Univ. Hamilton, Ontario. Canada. L8N 3Z5.

Cable properties of uterine smooth muscle were studied to determine if the appearance of large numbers of gap junctions at parturition was associated with improved cell-to-cell coupling. Tissues from pregnant animals before term exhibited a length constant (λ) of 2.6 ± 0.8 mm (SD, n= 17). Tissues from delivering animals had λ = 3.8 ± 1.0 mm (n=16, $p<.05$). The basis of the increased λ at parturition was a 46% increase in membrane resistance and a 33% decrease in internal resistance of the tissue. The internal resistance of a syncytium such as uterine smooth muscle is composed of both myoplasmic resistance and junctional resistance between cells. We interpret the decreased internal resistance to indicate improved cell-to-cell coupling in delivering tissues. Quantitative thin section electron microscopy was performed on some of the same samples of muscle. Both the frequency and fractional area of gap junctions (GJ's) were larger in delivering samples (5.0 GJ's/1000 μm membrane; fractional area of junctional membrane 0.22%) than those before term (0.66 GJ's/1000 μm membrane; fractional area of junctional membrane 0.008%). Therefore, improved coupling was associated with increased area of gap junction contact between smooth muscle cells. Supported by MRC (Canada).

T-PM-Po26 POTASSIUM ION AND DICHLOROFLUORESCEIN MOVE THROUGH THE NEXUS IN A HYDRATED STATE.
P. R. Brink, V. Verselis, M. M. Dewey. Department of Anatomical Sciences, SUNY at Stony Brook, Long Island, NY 11794.

The potassium ion conductance and dye permeability were measured in D_2O saline at various temperatures and compared to experiments done in H_2O. K^+ conductance of the nexus was measured via the method of Brink and Barr (J. Gen. Physiol. 69:517) (1977). Permeability was measured by the method of Brink and Dewey (1978). Both conductance and permeability showed greater temperature dependence in D_2O than in H_2O which is an indicator of solvent isotope effects (i.e. larger hydration radii). Junctional conductance was reduced 25% at 20°C in D_2O saline and showed a 51% reduction from 5° to 20° while in H_2O the reduction was 40% over the same range. The permeability of dichlorofluorescein showed a 42% reduction at 25° in D_2O saline vs H_2O and a 54% reduction at 10°. In D_2O, the dye showed a 72% reduction in permeability from 10° to 20° and in H_2O the reduction was 61%. These data indicate that the dye moves through the junction in a hydrated form but is influenced by a hydrogen deuterium exchange. If solvency only were involved, the reduction of permeability in D_2O vs H_2O at 25° would be expected to be 20%, much like the reduction for K^+ ion, not 42%. The greater temperature dependence in D_2O indicated increased hydration radii in D_2O. Thus K^+ and the dye pass from one cell to another in a hydrated form. Because of the dyes larger size in its hydrated form it was affected by a hydrogen-deuterium exchange which further enhanced its reduced velocity through the junction.

T-PM-Po27 CHEMICAL SIGNAL SYSTEMS IN ORGANISMS. Alfred T. Kornfield
Biosearch Co. Phila., Pa. 19103

Development of CSS theory requires several conceptual studies: derivations of analogs from several fields, eg (neuro)endocrine, morphogenic, immunologic, parasitic & invasive processes, toxicology, phytohormone & pheromone; a telecommunications model, with component processes of: Emitter (synthesis and release site of information-encrypted signal carriers), SC (formatted messages, source & target addresses, controls for switching, modulation, error protection), Translink (drive forces, media, paths from Angst.-Kilom.), Receptor (surveillance, recognition, acceptance, transduction/across membrane/cell, signal conditioning, command message extraction), Action-Effecter (message acceptance, go-decision, kinetic and metabolic action spread from unit events to pleiotropes). Common processes here include: interface transport, (de)crypting, signal complements, (un)binding, budgets/fluxes for CS-related energy and materials needs. Overall organization of CSS signal, movement, and chemical mechanisms must consider: coordination, eg orchestration (CS time/space mixes & patterns) of repertoires of signals, etc), programming, feature analyses, control in and across CS channels, and of CS links into organism homeostatic systems (and their loops, response dynamics, signals flow); overall performance, eg in/out dynamic responses, operating variable arrays, transfer and coupler functions; reliability-limits, fallbacks, fault sources, correction; structure, hierarchy & cascades, connectivity, position arrays and transforms in overall organism architecture

T-PM-Po28 STRUCTURAL STUDIES ON PILI ISOLATED FROM Pseudomonas aeruginosa USING X-RAY DIFFRACTION, HYDRODYNAMIC AND COMPUTER MODELLING TECHNIQUES. T.H. Watts and W. Paranchych, Department of Biochemistry, University of Alberta, Edmonton, Canada T6G 2H7 and D.A. Marvin, European Molecular Biology Laboratory, Postbox 10.2209, 6900 Heidelberg, West Germany.

Bacterial pili are filamentous, non-flagellar appendages that mediate adhesion, twitching motility, bacteriophage adsorption and in some cases bacterial conjugation. Pili isolated from Pseudomonas aeruginosa are made up of a single protein subunit, pilin, arranged in a helix with four 18,000-dalton subunits per turn of 41Å pitch (1).

The pilus can be dissociated into subunits using the non-ionic detergent octyl-glycoside. Studies on the pilin/detergent complex using classical hydrodynamic techniques in combination with x-ray diffraction data obtained from fibers of intact pili suggest an axial ratio for the pilin subunit of between 3:1 and 5:1 (2).

A computer model building approach was used in an attempt to define the orientation of the subunit in the supramolecular assembly as well as the orientation of the helical portions of the subunit with respect to the pilus axis. While this approach is useful in determination of the helix direction, the precise subunit orientation could not be determined because tight packing of the structure gives rise to indistinguishable transforms for a variety of models at low resolution.

(1). Folkhard, W., Marvin, D.A., Watts, T.H. and W. Paranchych (1981), J. Mol. Biol. 43: 79-93.
(2). Watts, T.H., Kay, C.M. and W. Paranchych, (1981) manuscript submitted.